



2011

MATHEMATICAL MODELING OF *CLOSTRIDIUM THERMOCELLUM*'S METABOLIC RESPONSES TO ENVIRONMENTAL PERTURBATION

Bless Adotey

University of Kentucky, blessadotey@yahoo.com

[Click here to let us know how access to this document benefits you.](#)

Recommended Citation

Adotey, Bless, "MATHEMATICAL MODELING OF *CLOSTRIDIUM THERMOCELLUM*'S METABOLIC RESPONSES TO ENVIRONMENTAL PERTURBATION" (2011). *Theses and Dissertations--Biosystems and Agricultural Engineering*. 1.
https://uknowledge.uky.edu/bae_etds/1

This Doctoral Dissertation is brought to you for free and open access by the Biosystems and Agricultural Engineering at UKnowledge. It has been accepted for inclusion in Theses and Dissertations--Biosystems and Agricultural Engineering by an authorized administrator of UKnowledge. For more information, please contact UKnowledge@lsv.uky.edu.

STUDENT AGREEMENT:

I represent that my thesis or dissertation and abstract are my original work. Proper attribution has been given to all outside sources. I understand that I am solely responsible for obtaining any needed copyright permissions. I have obtained and attached hereto needed written permission statements(s) from the owner(s) of each third-party copyrighted matter to be included in my work, allowing electronic distribution (if such use is not permitted by the fair use doctrine).

I hereby grant to The University of Kentucky and its agents the non-exclusive license to archive and make accessible my work in whole or in part in all forms of media, now or hereafter known. I agree that the document mentioned above may be made available immediately for worldwide access unless a preapproved embargo applies.

I retain all other ownership rights to the copyright of my work. I also retain the right to use in future works (such as articles or books) all or part of my work. I understand that I am free to register the copyright to my work.

REVIEW, APPROVAL AND ACCEPTANCE

The document mentioned above has been reviewed and accepted by the student's advisor, on behalf of the advisory committee, and by the Director of Graduate Studies (DGS), on behalf of the program; we verify that this is the final, approved version of the student's dissertation including all changes required by the advisory committee. The undersigned agree to abide by the statements above.

Bless Adotey, Student

Dr. Sue E. Nokes, Major Professor

Dr. Dywane Edwards, Director of Graduate Studies

MATHEMATICAL MODELING OF *CLOSTRIDIUM THERMOCELLUM*'S METABOLIC
RESPONSES TO ENVIRONMENTAL PERTURBATION

DISSERTATION

A dissertation submitted in partial fulfillment of the
requirements for the degree of Doctor of Philosophy in the
College of Engineering
at the University of Kentucky

By

Bless Adotey

Lexington, Kentucky

Director: Dr. Sue E. Nokes, Professor of Biosystems & Agricultural Engineering

Lexington, Kentucky

2011

Copyright © Bless Adotey 2011

ABSTRACT OF DISSERTATION

MATHEMATICAL MODELING OF *CLOSTRIDIUM THERMOCELLUM*'S METABOLIC RESPONSES TO ENVIRONMENTAL PERTURBATION

Clostridium thermocellum is a thermophilic anaerobe that is capable of producing ethanol directly from lignocellulosic compounds, however this organism suffers from low ethanol tolerance and low ethanol yields. *In vivo* mathematical modeling studies based on steady state traditional metabolic flux analysis, metabolic control analysis, transient and steady states' flux spectrum analysis (FSA) were conducted on *C. thermocellum*'s central metabolism. The models were developed in Matrix Laboratory software (MATLAB® (The Language of Technical Computing), R2008b, Version 7.7.0.471)) based on known stoichiometry from *C. thermocellum* pathway and known physical constraints. Growth on cellobiose from Metabolic flux analysis (MFA) and Metabolic control analysis (MCA) of wild type (WT) and ethanol adapted (EA) cells showed that, at lower than optimum exogenous ethanol levels, ethanol to acetate (E/A) ratios increased by approximately 29% in WT cells and 7% in EA cells. Sensitivity analyses of the MFA and MCA models indicated that the effects of variability in experimental data on model predictions were minimal (within $\pm 5\%$ differences in predictions if the experimental data varied up to $\pm 20\%$). Steady state FSA model predictions showed that, an optimum hydrogen flux of $\sim 5\text{mM/hr}$ in the presence of pressure equal to or above 7MPa inhibits ferredoxin hydrogenase which causes NAD re-oxidation in the system to increase ethanol yields to about 3.5 mol ethanol/mol cellobiose.

KEYWORDS: Metabolic Flux Model, *Clostridium thermocellum*, Steady state, Transient state, Sensitivity analyses.

BLESS ADOTEY

Student's Signature

Date

MATHEMATICAL MODELING OF *CLOSTRIDIUM THERMOCELLUM*'S METABOLIC
RESPONSES TO ENVIRONMENTAL PERTURBATION

By

Bless Adotey

Dr. SUE E. NOKES

Director of Dissertation

Dr. DYWANE EDWARDS

Director of Graduate Studies

RULES FOR THE USE OF DISSERTATIONS

Unpublished dissertations submitted for the Doctor's degree and deposited in the University of Kentucky Library are as a rule open for inspection, but are to be used only with due regard to the rights of the authors. Bibliographical references may be noted, but quotations or summaries of parts may be published only with the permission of the author, and with the usual scholarly acknowledgments.

Extensive copying or publication of the dissertation in whole or in part also requires the consent of the Dean of the Graduate School of the University of Kentucky.

A library that borrows this dissertation for use by its patrons is expected to secure the signature of each user.

Name

Date

ACKNOWLEDGEMENTS

This dissertation is more than a catalog of my academic exploits. Each page is imbued with the generous and inspiring spirits of people I have met throughout my graduate studies. While the list maybe lengthy, I deeply appreciate each contribution made towards my evolving into a scholar and a well-equipped person:

To my advisor Dr. Sue Nokes: for providing me tremendous support and opportunities throughout the course of my research. I am also particularly thankful for her gracious mentorship, exemplary leadership, and priceless guidance in helping me become a competent and confident engineer, and inculcating in me that the true value of scholarship is the translation of academic privileges into beneficial social change.

To my committee members: Dr. Joseph Taraba, Dr. Fred Payne and Dr. Robert Molzon for insightful suggestions, thoughtful criticisms and comments which greatly contributed to the quality and completion of this work.

To my external examiner: Dr. Mark Coyne, thank you for accepting to serve on my committee for my dissertation defense.

Special appreciation to Dr. Michael Flythe, Dr. Bert Lynn, Dr. Barbara Knutson, Hsin-Fen Li and Matthew Ruwaya for their support with experiments and whose efforts, expertise and interaction deepened my critical thinking skills and provided complementary insight and perspective for the completion of my graduate work and dissertation.

To my parents Eunice Adotey and Sam Adotey who have been extremely instrumental in completing this work through their support and encouragement at every stage of my life. I dedicate this work to their never ending love and care, which has been my motivation to pursue and attain the goals I set for myself throughout my life. I am also truly grateful to my brothers for their continued love, encouragement, motivation, and moral support. They are my true engineers.

It would not have been possible to complete this work without the invaluable assistance from Francisco Llaneras of AI2, Universidad Politécnica de Valencia in Spain. He generously gave necessary MATLAB information and resources for implementing the flux interval approach to metabolic modeling.

I am grateful to Gaspard Lequeux in the Biochemical and Microbial biotechnology department of Ghent University, Belgium for patiently taking the time to address various concerns regarding dynamic MFA (transient metabolic modeling).

I also thank the department of Biosystems and Agricultural Engineering (BAE) for offering me financial support throughout my Ph.D. studies. I also wish to express gratitude to all BAE staff, especially Jayne White, Julie Tolliver and Dustin Mattingly for addressing my academic and administrative concerns so that I always felt at home. All faculty and fellow students of BAE who assisted in various forms during my entire studies are also appreciated.

I am very grateful to my priceless network of friends and colleagues for their contagious enthusiasm and joie de vivre. Special thanks to Michael Danquah, Michael Chibuike Egbuka and Blessing Chijioke Kanu whose wisdom and advice supported and enlightened me throughout this graduate work.

Importantly, I wish to thank my dear husband Michael Omane-Achamfuor for being a pillar of support, a voice of reason and his abundant patience throughout my studies. To Naa Omane-Achamfuor, my lovely daughter and gem of my life: whose smile and adoration gives me the impetus to keep on through the challenging times of this research.

Finally, I thank God for my life, for making all things possible and being my source of strength, peace and good health. He is my Alpha and Omega.

TABLE OF CONTENTS

CHAPTER 1	INTRODUCTION	1
1.1	General Background	1
1.2	Literature Review	2
1.3	<i>Clostridium thermocellum</i>	7
1.3.1	Wild Type <i>Clostridium thermocellum</i> Cells	9
1.3.2	Ethanol Adapted <i>Clostridium thermocellum</i> Cells	10
1.4	Metabolic Modeling	10
1.4.1	Metabolic Flux Analysis.....	11
1.4.2	Metabolic Control Analysis	13
1.4.3	Whole Cell Modeling.....	15
1.4.4	Errors/Sensitivity Analyses Applications.....	22
1.5	Objectives	24
1.6	Thesis Organization	24
CHAPTER 2	METABOLIC FLUX AND CONTROL ANALYSES OF WILD TYPE AND ETHANOL ADAPTED CLOSTRIDIUM THERMOCELLUM CELLS.....	26
2.1	Synopsis	26
2.2	Introduction	27
2.2.1	Motivation for Lignocellulose Degradation	27
2.2.2	Organism Selection	28
2.3	Experimental Data And Statistical Analysis	33
2.4	Modeling Methods	34
2.4.1	Metabolic Flux Analysis.....	34
2.4.2	Flux Control Coefficient (FCC) and Concentration Control Coefficient (CCC)	37
2.4.3	Statistical Analyses.....	41
2.5	Results and Discussion	43
2.5.1	Carbon Flux Distribution	45
2.5.2	Flux and Concentration Control Coefficients.....	51
2.6	Conclusion	58
CHAPTER 3	SENSITIVITY ANALYSIS OF <i>CLOSTRIDIUM THERMOCELLUM</i> METABOLIC FLUX MODEL.....	59
3.1	Synopsis	59

3.2	Introduction	60
3.3	Methods	62
3.3.1	Sensitivity Analysis by Introducing Error into the Measured Data	62
3.3.2	Sensitivity Analysis by Chi-Square Tests	62
3.3.3	Sensitivity by Monte Carlo Simulation.....	64
3.4	Results and Discussion	65
3.5	Conclusion	78
CHAPTER 4 STEADY STATE MODELING OF DISSOLVED HYDROGEN GAS EFFECT ON THE METABOLISM OF WILD TYPE CLOSTRIDIUM THERMOCELLUM CELLS		80
4.1	Synopsis	80
4.2	Introduction	81
4.3	Materials and Methods	84
4.3.1	Experimental Data	84
4.3.2	Central Metabolic Network of <i>Clostridium thermocellum</i>	85
4.3.3	Metabolic Flux Analysis Using Flux Spectrum Approach	86
4.4	Results	94
4.4.1	Redox Balance.....	95
4.4.2	Effect of Pressure	95
4.4.3	Effect of Dissolved Hydrogen Gas.....	97
4.4.4	Predicted Combined Effect of Hydrogen and Pressure	98
4.5	Discussion	100
4.6	Conclusion	102
CHAPTER 5 TRANSIENT STATE MODELING OF DISSOLVED HYDROGEN GAS EFFECT ON THE METABOLISM OF WILD TYPE CLOSTRIDIUM THERMOCELLUM CELLS.....		104
5.1	Synopsis	104
5.2	Introduction	105
5.3	Materials and Methods	106
5.3.1	Experimental Data	106
5.3.2	Central Metabolic Network of <i>Clostridium thermocellum</i>	110
5.3.3	Metabolic Flux Estimation over Time Using Flux Spectrum Approach	111
5.4	Results and Discussion	117
5.5	Conclusion	129

CHAPTER 6 FUTURE DEVELOPMENTS	130
APPENDIX A - CHAPTER 2	131
A.1 Example MATLAB code used for MCA (Wild type).....	131
APPENDIX B - CHAPTER 3	134
B.1 MFA And MCA Estimates From Model	134
B.2 MFA And MCA Estimates From Monte Carlo Simulation.....	135
APPENDIX C - CHAPTER 4	136
C.1 Flux calculations.....	136
C.2 Example MFA for Generating Stoichiometric matrix	136
C.3 vspectrumC_Opt function to calculate the flux spectrum	145
C.4 vspectrumCb_Opt function to calculate the flux spectrum	146
C.5 Example Steady State FSA code using Llaneras function vspectrumCb_opt.....	147
APPENDIX D - CHAPTER 5.....	149
D.1 SAMPLE MATLAB CODE ODE FOR SOLUTION TO GIVEN DATA.....	149
D.2 Function FSADYNAMICFUNC3	151
D.3 Example Dynamic State FSA code using function vspectrumCb_opt.....	155
D.4 Llaneras' et al., 2007 function vspectrumCb_opt	157
D.5 Llaneras' et al., 2007 function vzpectrumC_opt.....	158
BIBLIOGRAPHY	160
VITA.....	172

LIST OF TABLES

Table 2-1: Two-way ANOVA for WT flux distribution	45
Table 2-2: Two-way ANOVA for EA flux distribution.....	45
Table 2-3: Paired T-tests evaluated within WT	45
Table 2-4: Paired T-test evaluated within EA.....	45
Table 2-5: Two-way ANOVA for WT flux control coefficients.....	52
Table 2-6: Two-way ANOVA for EA flux control coefficients.....	52
Table 2-7: Flux control coefficients (FCCs) for wild type and ethanol adapted strains at each reaction stage.....	52
Table 2-8: Concentration control coefficients (CCCs) for wild type and ethanol type strains at each reaction stage.....	53
Table 3-1: Fluxes of measured extracellular and predicted key metabolites (WT 0% ETOH).....	75
Table 3-2: Fluxes of measured extracellular and predicted key metabolites (EA 0% ETOH)	75
Table 4-1: Selected experimental data (measured concentrations of metabolites) on pressurized continuous culture growth of <i>C. thermocellum</i> on cellobiose from literature (Bothun et al. 2004)	85
Table 4-2: Predicted ethanol and acetate fluxes versus their measured fluxes for 0.05hr ⁻¹ at 0.1MPa ...	94
Table 4-3: Predicted ethanol and acetate fluxes versus their measured fluxes for 0.05hr ⁻¹ at 7MPa	94
Table 4-4: Predicted ethanol and acetate fluxes versus their measured fluxes for 0.05hr ⁻¹ at 17MPa	95
Table 4-5: Fermentation equation balance, hydrogen balance and carbon recovery estimates	95
Table 4-6: Predicted fluxes of NADH consumed for hydrogen production by hydrogenase compared with fluxes of NADH consumed by lactate and alcohol dehydrogenases at all pressures over dilution rates (hr ⁻¹).....	97
Table 5-1: Selected experimental data on pressurized continuous culture growth of <i>C. thermocellum</i> on cellobiose from literature [38]	107

LIST OF FIGURES

Figure 1-1: Simplified <i>Clostridium thermocellum</i> catabolic network.....	8
Figure 1-2: Schematic metabolic pathway (Fell and Sauro 1985)	14
Figure 1-3: E-cell model user-interface (Tomita et al. 1999)	16
Figure 1-4: DBsolve (Goryanin et al. 1999)	19
Figure 2-1: Overview of MFA and MCA methods.....	34
Figure 2-2: Simplified <i>C. thermocellum</i> Central Metabolic Pathway	35
Figure 2-3: Schematic of simple linear pathway	37
Figure 2-4: Six key pathway steps and intracellular metabolites identified for MCA model development	40
Figure 2-5: Predicted carbon flux distribution in a simplified model of <i>C. thermocellum</i> 's central pathway (units in meC/g cell h) – Wild type (a- WT0%, b-WT0.5% and c-WT1%)	46
Figure 2-6: Flux Distribution in WT cells (a - WT0%, b -WT0.5%, c - WT1%) shown for key pathway steps. The first number in each triad represents the carbon flow in the WT0% treatment, the second and third number represents the WT0.5% and WT1% respectively.	47
Figure 2-7: Carbon Flux Distribution in the simplified <i>C. thermocellum</i> central pathway (units in meC/g cell h) – Ethanol Adapted (a-EA0%, b-EA1% and c - EA5%)	49
Figure 2-8: Flux Distribution in EA cells (d - EA0%, e -EA1%, f - EA5%) shown for key pathway steps. The first number in each triad represents the carbon flow in the EA0% treatment, the second and third number represent the EA1% and EA5% respectively.	50
Figure 2-9: Central Metabolic Pathway of <i>Clostridium thermocellum</i>	55
Figure 3-1: Predicted ethanol flux response to 5% (yellow), 10% (blue) and 20% (red) decreases in only lactate for exogenous ethanol treatments of 0%, 0.5% and 1% on wild –type (WT). Error bars showing sensitivity of predicted ethanol fluxes to possible errors.....	67
Figure 3-2: Predicted ethanol flux response to 5% (yellow), 10% (blue) and 20% (red) decreases in only acetate for exogenous ethanol treatments of 0%, 0.5% and 1% on wild –type (WT). Error bars showing sensitivity of predicted ethanol fluxes to possible errors in acetate.	67
Figure 3-3: Predicted ethanol flux response to 5% (yellow), 10% (blue) and 20% (red) decreases in only cellobiose for exogenous ethanol treatments of 0%, 0.5% and 1% on wild –type (WT). Error bars showing sensitivity of predicted ethanol fluxes to possible errors in cellobiose.	68
Figure 3-4: Predicted ethanol flux response to 5% (yellow), 10% (blue) and 20% (red) decreases in only lactate for exogenous ethanol treatments of 0%, 0.5% and 1% on ethanol adapted (EA). Error bars showing sensitivity of predicted ethanol fluxes to possible errors in lactate.	68
Figure 3-5: Predicted ethanol flux response to 5% (yellow), 10% (blue) and 20% (red) decreases in only acetate for exogenous ethanol treatments of 0%, 0.5% and 1% on ethanol adapted (EA). Error bars showing sensitivity of predicted ethanol fluxes to possible errors in acetate.....	69
Figure 3-6: Predicted ethanol flux response to 5% (yellow), 10% (blue) and 20% (red) decreases in only cellobiose for exogenous ethanol treatments of 0%, 0.5% and 1% on wild –type (WT). Error bars showing sensitivity of predicted ethanol fluxes to possible errors in cellobiose.	70
Figure 3-7: Ethanol to acetate ratio (E/A) response to 5% (yellow), 10% (blue) and 20% (red) decreases in only lactate for exogenous ethanol treatments of 0%, 0.5% and 1% on wild –type (WT). Error bars showing sensitivity of predicted ethanol fluxes to possible errors in lactate.....	70
Figure 3-8: Ethanol to acetate ratio (E/A) response to 5% (yellow), 10% (blue) and 20% (red) decreases in only acetate for exogenous ethanol treatments of 0%, 0.5% and 1% on wild –type (WT). Error bars showing sensitivity of predicted ethanol fluxes to possible errors in acetate.....	71
Figure 3-9: Ethanol to acetate ratio (E/A) response to 5% (yellow), 10% (blue) and 20% (red) decreases in only cellobiose for exogenous ethanol treatments of 0%, 0.5% and 1% on wild –type (WT). Error bars showing sensitivity of predicted ethanol fluxes to possible errors in cellobiose.....	71
Figure 3-10: Ethanol to acetate ratio (E/A) response to 5% (yellow), 10% (blue) and 20% (red) decreases in only lactate for exogenous ethanol treatments of 0%, 0.5% and 1% on ethanol adapted (EA). Error bars showing sensitivity of predicted ethanol fluxes to possible errors in lactate.....	72

Figure 3-11: Ethanol to acetate ratio (E/A) response to 5% (yellow), 10% (blue) and 20% (red) decreases in only acetate for exogenous ethanol treatments of 0%, 0.5% and 1% on ethanol adapted (EA). Error bars showing sensitivity of predicted ethanol fluxes to possible errors in acetate.....	72
Figure 3-12: Ethanol to acetate ratio (E/A) response to 5% (yellow), 10% (blue) and 20% (red) decreases in only cellobiose for exogenous ethanol treatments of 0%, 0.5% and 1% on ethanol adapted (EA). Error bars showing sensitivity of predicted ethanol fluxes to possible errors in cellobiose.....	73
Figure 3-13: Normal probability plot for predicted ethanol fluxes - WT	76
Figure 3-14: Normal probability plot for predicted ethanol fluxes - EA.....	77
Figure 3-15: A comparison between experiments and Monte Carlo simulations by normal distribution curve in WT.....	77
Figure 3-16: A comparison between experiments and Monte Carlo simulations by normal distribution curve in EA.....	78
Figure 4-1: Simplified glycolytic pathway of <i>C. thermocellum</i> . J_{UPT} : Cellobiose available for uptake (Cellobiose_out), Intracellular cellobiose (J_{CBP} : consumed; Cellobiose_in), Hydrogen inside cell (environment; J_{H2Dsol}), Extracellular production of acetate, ethanol and lactate denoted by J_{EXTACE} , J_{EXTETH} and J_{EXTLAC} respectively.	86
Figure 4-2: A hypothetical metabolic network for illustrating the FSA method	88
Figure 4-3: Plot of results for above example – the intervals denoted by blue represents measured inputs and the intervals denoted by magenta represent predicted fluxes of Met C and Met E.	91
Figure 4-4: Flux spectrum analysis results for predicted ethanol and acetate fluxes at $0.05hr^{-1}$ dilution rate. The predicted flux interval estimates are shown in bands with triangles for ethanol and circles for acetate. The corresponding measured fluxes are denoted in bands with crossbars and stars respectively. The numbering on the x-axis corresponds to each metabolite at a certain pressure where, "1" denotes ethanol at 0.1MPa, "2" denotes ethanol at 7MPa, "3" denotes ethanol at 17MPa, "4" denotes acetate at 0.1MPa, "5" denotes acetate at 7MPa, "6" denotes acetate at 17.3MPa.....	96
Figure 4-5: Relationship between Hydrogen flux and NADH consumption by lactate and alcohol dehydrogenases (NADH _{cell}), and NADH consumption by hydrogenase	98
Figure 4-6: Effect of both pressure and hydrogen flux on mean predicted J_{nadh} flux	99
Figure 4-7: Effect of both pressure and hydrogen flux on mean predicted ethanol yields	99
Figure 4-8: Effect of both pressure and hydrogen flux on mean predicted acetate yields.....	100
Figure 5-1: Modified glycolytic pathway of <i>C. thermocellum</i> . Cellobiose uptake (Cellobiose_out), Intracellular cellobiose (consumed; Cellobiose_in), Hydrogen transport across cell membrane as a function of hydrogen outside cell (environment; $H_{2,out}$) and Hydrogen inside cell (environment; J_{H2Dsol}), Extracellular production of acetate, ethanol and lactate denoted by J_{EXTACE} , J_{EXTETH} and J_{EXTLAC} respectively.....	110
Figure 5-2: A hypothetical metabolic network for illustrating the FSA method	112
Figure 5-3: Resulting flux (mM/hr) (both predicted and inputs) over time using FSA	115
Figure 5-4: Amount of Cellobiose (mM) remaining over 24hr	118
Figure 5-5: Amount of Cellobiose (mM) remaining over 120hr (input to model)	118
Figure 5-6: Cellobiose consumption fluxes for $0.05hr^{-1}$ (x) and $0.32hr^{-1}$ (+) at atmospheric pressure (predicted by model)	120
Figure 5-7: Cellobiose consumption fluxes for $0.05hr^{-1}$ (x) and $0.32hr^{-1}$ (x) at 7MPa pressure (predicted by model)	121
Figure 5-8: Cellobiose consumption fluxes for $0.05hr^{-1}$ (x) and $0.32hr^{-1}$ (+) at 17MPa pressure (predicted by model)	122
Figure 5-9: Predicted ethanol flux (mM/hr) over time @ $0.05hr^{-1}$ compared between 0.1MPa,	125
Figure 5-10: Predicted ethanol yield (mol ethanol/mol cellobiose consumed) over time @ $0.05hr^{-1}$	125
Figure 5-11: Predicted acetate flux (mM/hr) over time @ $0.05hr^{-1}$ compared between 0.1MPa,.....	126
Figure 5-12: Predicted acetate yield (mol acetate/mol cellobiose consumed) over time @ $0.05hr^{-1}$	126
Figure 5-13: Predicted dissolved hydrogen gas flux (mM/hr) over time @ $0.05hr^{-1}$ compared between 0.1MPa,	127

Figure 5-14: Predicted NADH consumption flux (mM/hr) over time @ 0.05hr⁻¹ compared between 0.1MPa, 127

CHAPTER 1 INTRODUCTION

1.1 GENERAL BACKGROUND

Lignocellulosic biomass made of lignin, hemicelluloses and cellulose has been identified over the years as a relatively feasible and economical way for producing ethanol fuel with the help of microbial cells made of enzyme complex [1-5]. However, the complex nature of the composition and structure of microbial cells cause the cells, behavioral characteristics that are difficult to understand. An appropriate description or interpretation of cell behavior will depend upon the extent to which the cell's metabolism is understood. A better understanding of the cell's metabolism is expected to enhance the ability to establish a definite relationship between the cell's environment, membrane and cytoplasm (genotype and phenotype). The genotypic and phenotypic components of the cell are characterized by individual processes that take place in the cell's metabolism known as the "metabolic pathway". Given that the metabolic pathway provides sequential connection between the metabolic reactions of the cell, computer simulation and mathematical modeling have been established as underlying methods for formulating steady state and dynamic metabolic models of the cell as an engine. Metabolic models have been successfully developed for steady and dynamic states of cellular subsystems. However, metabolic modeling approaches by incorporating relevant cell properties influenced by statics and dynamics have been identified as a more realistic way of capturing metabolism of the "whole cell", such as predicting cellular behavior, proposing efficient optimal metabolic control and design for metabolic network processes, and determining the functional properties of genome-scale metabolic networks. Many conceptual models combining experimental data with modeling have been proposed to help broaden the understanding of cell behavior [6, 7]. Whole cell modeling aims to determine the relationship between the desired phenotype and

genotype or particular environmental factors. This study focuses on applying the fundamental principles of whole cell modeling to investigate responses of the end-products of *Clostridium thermocellum* glycolytic metabolism to exogenous ethanol level, dissolved hydrogen gas and hydrostatic pressure during continuous culture fermentation. *C. thermocellum* was chosen because of the thermophilic and anaerobic characteristics coupled with a solid enzyme system (cellulose) it possesses which enable the bacteria to directly degrade abundantly lignocellulosic substrate (preferable cellobiose) into ethanol.

1.2 LITERATURE REVIEW

A microbial cell can be viewed as a self-contained bioreactor because the cell membrane separates the cell from its environment. Compounds that enter the cell through the membrane are termed substrates while compounds that exit the cell across the membrane are termed products. The conversion of substrates to products in the cell is called metabolism. Bio-chemicals formed inside the cell while remaining in the cell to be converted to other compounds are intracellular metabolites. The cell is influenced by the external environment in which it is contained, including the concentrations of extracellular chemicals, pressure, pH, temperature, and agitation of the fermenter [8, 9]. As a bioreactor, the cell can take up different amounts and types of substrates, and depending on the processing of these substrates, produce different types and amounts of products. The cell represents a dynamic system, capable of adjusting its metabolic response to various changing environmental conditions and inputs that may result in shifts in products, product ratios, and/or product concentrations. The complete set of potential pathways in an organism is referred to as the cell's metabolic genotype [10].

The particular set of pathways used under a given set of environmental and chemical conditions is termed the metabolic phenotype [9].

Cells control their metabolism by regulating enzyme concentrations and activities, which affect material flows through different pathways. Breakdown of macromolecules such as proteins, carbohydrates and lipids into subunits such as amino acids, simple sugars, and fatty acids and glycerol, respectively occur in the cytosol. These are further broken down into simple molecules accompanied by the production of energy, a process known as catabolism. The carbohydrate product undergoes glycolysis to produce pyruvate and acetyl CoA, which are also degradation products of amino acids. Fatty acid degradation produces only acetyl CoA. ATP and NADH are released as by-products/co-factors. Acetyl CoA undergoes oxidative phosphorylation to produce water, carbon dioxide and more ATP. ATP is often utilized as source of energy in the synthesis of cell constituents from simpler molecules such as organic and/or inorganic precursors through anabolism [11, 12].

Limited petroleum-based fuels are becoming an increasing concern as the world's industrialization and motorization grow. This has prompted the need to research and develop alternative fuels that can be produced from abundant renewable natural resources. Ethanol produced from renewable resource has been recognized as a potential alternative to fossil fuels [13-15] because of its beneficial greenhouse effect due to negligible release of unwanted gases into the atmosphere. Eventually, the agricultural economy will be improved as well as providing employment avenues and a greater scope of energy source will be sustained [13, 15, 16]. Efforts to produce fuel from abundantly available and renewable lignocellulosic biomass is one of the promising goals to encourage bioethanol production [16, 17] but research has shown limitations in developing and implementing effective techniques for utilizing biomass within economic means [18, 19]. "Highly effective cellulases and hemicellulases", "efficient and robust

fermentative microorganisms” and “low-cost thermochemical pretreatment” are comprehensive measures that are being employed for biomass conversion into fuels and chemicals [18]. However, it has been discovered that fermentation conditions for producing high ethanol yield require the application of inhibitor-tolerant strains of microorganisms to metabolize all sugars (substrates) into ethanol as the major product [20]. Various microorganisms have been employed to explore such desirable properties.

Saccharomyces cerevisiae (traditional yeast) for ethanol production has been the most commonly used microorganism in conventional fermentation [21]. Yeast cannot metabolize pentose sugars, but another fungus *Trichoderma reesei* was discovered by Palmqvist and coworkers to be capable of fermenting hemicelluloses (mostly dominated by pentoses), removing toxins from the fermentation process and eliminating product inhibitors [22]. Even though *Saccharomyces cerevisiae* and *Trichoderma reesei* are usually favored fermentative strains for ethanol production, they are incapable of degrading lignocellulosic biomass because they are not configured with enzyme complexes like some bacteria possess. Yeast also produces inferior ethanol yields compared to bacteria [20, 23-25]. Dien and Co noted that *Escherichia coli*, *Klebsiella oxytoca*, and *Zymomonas mobilis* have shown the most successful ethanol-only production [20]. Although *E. coli* and *K. oxytoca* easily ferment various sugars they require a lot of work (hydrolysis of sugar, fermentation and addition of enzymes at high costs) to selectively produce ethanol. *Zymomonas mobilis* on the other hand produces high ethanol yields but ferments only glucose and fructose [20].

It has been determined that cellulase and hemicellulase production can occur simultaneously with hydrolysis and fermentation of pentose and hexose sugars in a single step called consolidated bioprocessing. Consolidated bioprocessing (CBP) is a highly efficient and low cost process considered to be advantageous over conventional ethanol production [26]. The nature of CBP suggests the benefits of increasing ethanol

production from possible high hydrolysis rates when thermophiles of enzyme-microbe synergy and complex cellulase system are involved [26]. Thermophilic bacteria, such as *Thermoanaerobacter ethanolicus*, *Thermoanaerobacter thermohydrosulfuricus*, *Thermoanaerobacter thermosaccharolyticum* and *Clostridium thermohydrosulfuricum* have been investigated for hemicellulosic ethanol production [25]. *Thermoanaerobacter ethanolicus* and *Thermoanaerobacter mathranii* have also demonstrated the ability to ferment sugar polymers into high ethanol yields at elevated temperatures and are relatively highly tolerant of ethanol [25, 27]. Others have also demonstrated the potential of genetically engineered microorganisms (using recombinant DNA technology) to enhance ethanol production and yield [25, 28]. Thermophilic bacteria such as *C. thermocellum*, *C. thermosaccharolyticum* and *C. thermohydrosulfuricum* (have shown the promise to achieve direct microbial conversion of lignocellulosic biomass into ethanol (CBP) [21, 29].

The presence of the enzyme complex (cellulase) in the anaerobic thermophile, *C. thermocellum* characterized as gram positive bacteria enables the bacteria to readily break down complex polysaccharides into simple sugars and ferment the sugars into ethanol. The microorganism has been used by Cardona and Co to demonstrate the usefulness of CBP which showed a substrate conversion of 31% higher than *T. reesei* and *S. cerevisiae* [23]. Previous studies have suggested that *C. thermocellum* is easier to work with for fermenting lignocellulose into ethanol than yeast [30]. Recent studies have sought to perform fermentation in the absence of oxygen (anaerobic conditions) due to the expense of supplying oxygen [31]. Therefore it is advantageous to work with an organism that is an obligatory anaerobe such as *C. thermocellum*.

With *C. thermocellum*, cooling costs are reduced because the organism grows at a temperature of 60°C, which is optimal for the purposes of a simple cooling system, pure fermentation process, and easy ethanol extraction. A high percentage of the

substrate goes toward product formation because the fermentative activity of *C. thermocellum* results in low cell yields [32]. Unfortunately, this microorganism has shown characteristics of ethanol inhibition and thus gives relatively low ethanol yield. Emerging technologies such as organism genetic modifications and environmental manipulations have been identified as feasible techniques for improving biomass conversion to ethanol [26, 33]. With regards to the fact that Department of Energy reported in 2004 that *C. thermocellum* genome sequencing is complete, this study proposes to focus on adjusting the organism's environment (by regulating pressure in a continuous culture system as this is expected to affect acetate and ethanol production) to demonstrate its metabolic pathway responses to identify and predict phenotypes that maximize ethanol-only production. This type of fermentation control has been previously identified to greatly influence the metabolic selectivity of *C. thermocellum* [34-38]. Adjusting or manipulating the microbial environment results in metabolic responses like changes in product yields, product ratios, and product concentrations. The organism's metabolic response represents its phenotype while the complete metabolic pathway forms its genotype. The phenotype is a subset the genotype [39].

The National Academy of Science in 1999, recommended advanced models using optimization techniques in process engineering methods such as metabolic modeling to improve bioethanol production [23]. The importance many researchers place on making valuable products (for example, ethanol, butanol and hydrogen) available to the global market have resulted in the need to implement engineering tools (the design and application of mathematical models) for more exploration of cell metabolism because mathematical models can be used as simplifying abstractions for the relationship between phenotypes and genotypes to collect quantitative information on a microorganism and predict the desired outcomes that are transformed into biological insight [40-42].

1.3 CLOSTRIDIUM THERMOCELLUM

The use of thermophilic bacteria in industrial processes offers great promise and has potential benefits including: higher reaction rates at elevated temperatures, increased mass transfer, greater thermo-stability of enzymes and catalytic pathways, and less potential for contamination by other organisms [31, 43]. More importantly, thermophilic anaerobes are found in various habitats and are capable of providing thermodynamically feasible processes in the degradation of organic matter [43, 44]. *Clostridium thermocellum* is one of the most extensively studied anaerobic thermophiles with high cellulose degradation into cellobiose and cellodextrins and subsequently to ethanol production [36, 45, 46]. Cellobiose is then converted by the microorganism to its final end products of ethanol, lactate, acetate, CO₂ and H₂ [31]. A simplified pathway of the catabolic process of *C. thermocellum*'s metabolism is presented in Figure 1-1.

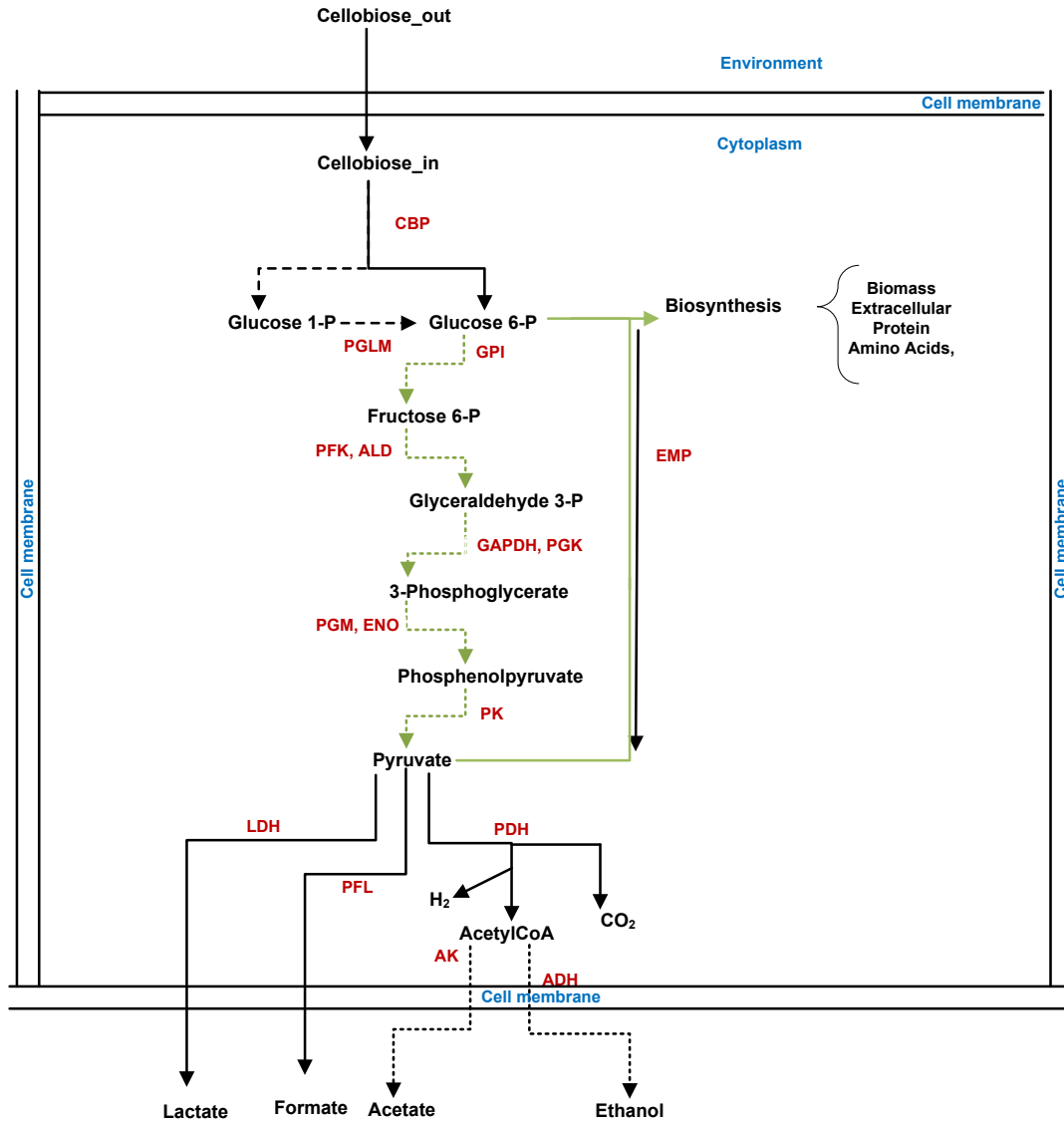


Figure 1-1: Simplified *Clostridium thermocellum* catabolic network

Clostridium. thermocellum is sensitive to low concentrations of ethanol and produces low ethanol yield as a result of organic acid such as lactate and acetate, formation. The organism's response to relevant environmental perturbations has shown preference for cellobiose over glucose in continuous cultures but otherwise in batch cultures; increases in ethanol to acetate ratios due to increased dissolved hydrogen gas concentrations at elevated hydrostatic pressures compared to atmospheric pressure

conditions; cell growth unaffected by different substrate concentrations ; potential for hydrogen production as bio-fuel [38, 47-49]. The results of genetic manipulation and natural adaptation of *C. thermocellum* have primarily been interpreted from end product concentrations, and the expression of RNA [50]. However, major interest in *C. thermocellum* lies in the potential to provide large scale ethanol production from cellulosic biomass especially due to its stability at high temperatures [26, 51-53]. With the availability of complete genomes and sufficient bioinformatic resources (which are substantial to understanding the microorganism's metabolic activities), enhanced biomass conversion by *C. thermocellum* can be achieved by developing mathematical models to predict the cellular phenotype and also create the platform for relevant genetic manipulation.

1.3.1 Wild Type *Clostridium thermocellum* Cells

The growths of cells that thrive on cellobiose or avicel have a well structured cellulase system made of a polypeptide composition. While cellobiose grown cells form compacts of protuberant structures, corridor-like structures have been observed for growth on avicel (or cellulose) [54, 55]. Optimal growth temperature for the cells varies and activation energy is higher compared to mutant strains as verified by its anisotropic measurements. Fast growth rates accompanied by high cell yields are observed in wild type cells in the absence of exogenous ethanol. The cells are highly inhibited at low ethanol concentrations. Sensitivity to low ethanol concentrations occur beyond 1%v/v [56-58]. Cell membranes are highly permeable and thus relatively more fluid compared to its mutant, ethanol adapted cell [52, 57]. A high percentage short fatty acid chains (less than 16:0) exist in the membrane. However, carbohydrate levels are believed to be

about 5 times less than mutant, ethanol adapted cells. Membrane fluidity increases in the presence of exogenous ethanol as a result of interruption of protein function [57].

1.3.2 Ethanol Adapted *Clostridium thermocellum* Cells

These are anteiso-branched, modified wild type cells that are ethanol tolerant but with a more rigid membrane caused by the presence of high percentage long-chained fatty acids. Fatty acid chain lengths exceed 16:0 in the membrane under similar environmental conditions to wild types but with fewer amounts of total lipid contents (56 μ g/mg dry cell weight hr) compared to wild type's 82 μ g/ mg dry cell weight hr. Ethanol adapted cells are capable of withstanding the inhibition by low ethanol concentration beyond optimal conditions. Ethanol tolerance is as high as 8%v/v [56-58]. Anisotropy of cells is less affected by temperature variations compared to wild type cells. Fatty acid phase transitions occur at higher temperatures relative to wild type cells. Higher percentages of plasmalogen compounds exist in ethanol adapted cell membranes compared to wild type cells. In the absence of exogenous ethanol, lower growth rates are observed in ethanol adapted cells [57]. A relatively low amount of protein expression associated with carbohydrate transport are found in ethanol adapted compared to wild types. Due to down regulated cellulosomes in ethanol adapted cells, lignocellulose degradation by these cell is relatively lower compared to wild type cells [58].

1.4 METABOLIC MODELING

Microbial cells are capable of adapting/adjusting their metabolic response to a various environments, which may result in shifts in products, product ratios, and/or product concentrations. Metabolic modeling forms the platform on which computational

or mathematical methods are used to quantify and interpret cell behavior based on information available on genotypes and phenotypes from experimental measurements. Deterministic or stochastic models based on static or dynamic principles may be developed depending on the microbial metabolic process of interest [59, 60]. Deterministic models provide numerical solutions that derive from differential equations. Stochastic models provide random (unpredictable) solutions based on statistical analysis [59]. Predictions from deterministic models come from the mean of variables. A model is static when it is used to develop the future state of an object given its current state. A dynamic model predicts the behavior of a system at each time point. Each of these has its own advantages and disadvantages. However, for a particular problem, the modeler is responsible for implementing the appropriate method (modeling approach) to suit the problem.

1.4.1 Metabolic Flux Analysis

Metabolic Flux Analysis (MFA) is one of the powerful tools used in modeling microbial systems for interpreting the channeling of their metabolic network towards desired metabolite production. Information derived from this method may be based on steady state and dynamic *in vivo* analysis [12, 61]. Mass balances are applied around key intracellular metabolites in central metabolic pathways to calculate intracellular fluxes from measured fluxes. Metabolic reactions are represented by a set of mathematical equations. Based on the number of measurements available for estimating the unknown variables, modeling may require stoichiometric constraints or appropriate objective functions to solve the problem. The system is often underdetermined [62, 63]. Limitations to metabolic flux analysis occurs from having singularities in the stoichiometric matrix when cyclic, bidirectional and parallel reactions exist in the

metabolic network under study [12, 62]. Most of metabolic flux analysis applications include predicting product yields, identifying the effects of substrate types, determining possible adaptations of metabolites to environmental perturbation, and implementing new measures if any to improve cellular properties [12, 62].

Steady-state metabolic flux analyses have been done on many clostridia organisms [64]. The specific growth rate is fixed for the steady state conditions to make flux estimates relatively easy to determine. However, this may prevent detailed analysis of the kinetic information in metabolic regulation of the microbe. To account for any missing transient responses, time profiles of growth rate and metabolite concentrations are predicted from metabolic models using the flux analysis concept [65, 66].

In transient metabolic flux analysis the metabolic behavior of the microorganism is accounted for over time step intervals to monitor any dynamic property of the microbe. An approximated derivative of species concentration with respect to time is estimated from experimental measurements using Euler methods or polynomial fitting [67-69]. The approximated derivative is then substituted into a rate of consumption or production equation from which the corresponding metabolite flux is estimated as shown in equation (1) below, where D is the dilution rate (hr^{-1}), C_{in} is the feed concentration (g/L), C is the measured concentration of extracellular metabolite (g/L), r_p is the corresponding flux of metabolite (g/L/hr), and $\frac{dC}{dt}$ is the approximated change in concentration of metabolite over time [70]. Once the measured fluxes are determined, the intracellular metabolite fluxes can be calculated from metabolic flux analysis [68-70].

$$r_p = \frac{dC}{dt} + D(C - C_{\text{in}})$$

Equation 1-1: Flux calculation from approximated derivative, dilution rate, influent concentration and metabolite concentration (Mass balance around extracellular species [70]).

In this study, steady-state and transient state metabolic flux analyses in addition to metabolic control analysis were employed to model the metabolic adaptations and responses of *C. thermocellum* catabolism to environmental perturbation.

1.4.2 Metabolic Control Analysis

Metabolic control analysis (MCA) begun with Kacser and Burns, and Heinrich and Rapoport in the 1970's [71]. Metabolic control analysis is another powerful metabolic modeling tool that has been extensively exploited for mathematical modeling of microbial systems [9, 72-74]. Understanding the kinetic properties of the phenotype and genotype in the metabolic network forms the basis of MCA [72, 74, 75]. Metabolic control analysis is used to quantify both steady-state and transient state behaviors of a metabolic pathway in the form of control coefficients. Log-linear stoichiometric models that include enzyme kinetics data for each reaction step in the metabolic network have been adapted for MCA [9, 74, 76]. The system is characterized by enzyme kinetics (known as parameters) and, concentration and fluxes (known as variables) used to describe changes in fluxes and metabolite concentration due kinetic parameters [77, 78]. The influence of parameter variations on the system's state is derived by computing the flux and concentration control coefficients from measured data. Computations are based on local variables known as elasticity coefficients. An elasticity coefficient represents the relative change in an isolated reaction step due to infinitesimal changes in the concentration of a metabolite given that all others are constant [71, 78]. The control coefficients are fractional changes in fluxes and concentrations respectively due to changes in enzyme activities. These sensitivity coefficients may be denoted as

$\frac{d\vec{v}}{d\alpha}, \frac{d\vec{v}}{dS}, \frac{d\vec{v}}{dE}$, where v is the vector of intracellular metabolite fluxes, α represents the

vector of enzyme kinetic parameters, S is the vector of extracellular substrate concentrations, and E is the vector of active enzyme concentrations.

Computations of control coefficients are based on summation theorems which state that the sum of all flux control coefficients must equal unity and the sum of all concentration control coefficients must equal zero at steady state [9, 71, 79-81]. By letting the symbols C_F and C_C denote flux and concentration control coefficients and ϵ denote elasticity coefficient; we use an illustration by Fell et al., [71] to describe the metabolic control of a simple linear pathway as shown in Figure 1-2, where X is the metabolite and E is the enzyme.

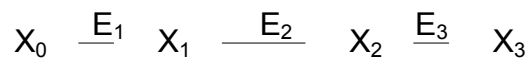


Figure 1-2: Schematic metabolic pathway (Fell and Sauro 1985)

Based on the summation theorems, $C_{F1} + C_{F2} + C_{F3} = 1$ and $C_{C1} + C_{C2} = 0$ where

$C_{C1} = C_{F1}\epsilon_1^1$, $C_{C2} = C_{F2}\epsilon_1^2$ for X_1 as product and substrate with enzymes E_1 and E_2 respectively. For X_2 , we have $C_{C1} = C_{F2}\epsilon_2^2$, $C_{C2} = C_{F2}\epsilon_2^3$ which leads to 3 equations:

$$C_{F1} + C_{F2} + C_{F3} = 1 \dots\dots\dots (A)$$

$$C_{F1}\epsilon_1^1 + C_{F2}\epsilon_1^2 = 0 \dots\dots\dots (B)$$

$$C_{F2}\epsilon_2^2 + C_{F2}\epsilon_2^3 = 0 \dots\dots\dots (C)$$

Equation 1-2: Connectivity Theorem Illustration

Equations A, B and C together may be expressed in matrix form to solve for C_F , C_C and ϵ . Metabolic control analysis has been treated extensively in the literature [71, 80, 81].

1.4.3 Whole Cell Modeling

Several attempts have been made at developing a complete model of the cell geared towards predicting the dynamic behavior of living cells [82, 83]. The concept of whole cell modeling is typically based on cell growth ability and variable volume [82-84]. A few of the proposed whole cell modeling methods are mentioned here and discussed later. Tomita [82] reports that the first whole cell model is the E-Cell software developed in 1996 at Keio University in Japan [82]. In 2004, Morgan et al., proposed a general framework for whole cell modeling applicable to all cell types [84]. A time dependent multi-algorithm simulation system has also been developed for whole cell modeling [85]. One other model for simulating whole cell is the DBsolve model developed by Goryanin et al., 1999 [86]. A minimal cell model built on an original *E. coli* model was proposed by Browning and Shuler [87].

The E-cell model is a graphical user interface computer simulation system written in C++ for molecular processes in a cell. The model has been designed into components denoted by “substance”, “reactor” and “system”. Inputs such as concentrations of metabolites (extracellular and intracellular), proteins, and enzymes, cell volume, pH and temperature are accepted in the “substance” section of the program to describe the state of the cell at a particular time [83]. Changes are made in the concentrations in an increment order over time by a simulator engine. The set of reactions in the metabolic pathway (mass action, equilibrium, and kinetic reactions) of the cell are defined in the reactor component while information on the genes (transcription and translation) goes into the system component of the model. Numerical integration methods of Euler and Runge Kutta have been integrated into the model to solve the set of equations discretely

[83]. The E-cell model allows user-defined inputs and assumes constant volume. The model interface is shown in Figure 1-3 below.

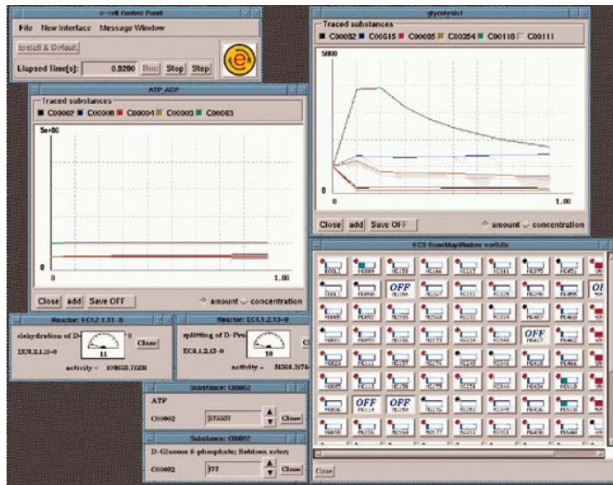


Figure 1-3: E-cell model user-interface (Tomita et al. 1999)

As an example of the E-CELL, the ‘virtual self-surviving cell’ was developed based on the metabolism of *Mycoplasma genitalium* known for having the smallest genome size among all living organisms and thus represents the best standard for whole cell modeling [82, 83]. The modeling method involved inputs from the cell’s cytoplasm (glycolysis) and membrane (lipid biosynthesis pathway). Components of the set of reactions included stochastic processes, complexes formed from substrates, transportation reactions and enzymatic roles, which yielded decreases in substrates and increases in products. The model was designed to observe cell behavior such as protein functions, “protein-protein interactions”, “protein-DNA interactions” and gene expressions in a graphical user interface. A set of 127 genes, 22 RNA-coding genes, 105 protein-coding genes and 495 metabolic reactions were incorporated into the simulation. Glucose is converted to lactate and ATP while the ATP enhances protein synthesis which transcribes the 127 genes into mRNAs [82, 83]. Observations from cell behavior showed changes in the concentrations of proteomic interactions [82, 83]. Other

examples of E-CELL models reported in the literature include ‘human erythrocyte model’, ‘mitochondria model’ and ‘signal transduction’ [82].

The framework of whole cell mathematical model proposed by Morgan et al., 2004 consists of a derived system of ordinary differential equations based on the assumptions that: (1) the total volume of the cell is the sum of the volumes of its cytoplasm and membrane when the cell is at rest; (2) the cell has constant osmotic pressure regulation; (3) reactions occur within the same regions or between adjacent regions in the cell; (4) the volume rate of change of the cytoplasm and membrane are not constant. So, given a system of reactions in a cell, the number of moles and concentrations of components in the cytoplasm and membrane are related through a set of ordinary differential equations governed by the rate of conversion of nutrients in the cell's environment into metabolites in the cytoplasm, the rate of conversion of metabolites into proteins and genes within the cytoplasm, and the reversible rate of protein conversion between the cytoplasm and membrane. By letting M , N , G , P , and P_{mem} denote concentrations of metabolites, nutrients, genes, proteins in the cytoplasm, and proteins in the membrane, the ordinary differential equations were defined as follows:

$$\begin{aligned}\frac{dM}{dt} &= F_1(C, k, \chi) - \alpha(C, k, \chi)M, \\ \frac{dG}{dt} &= F_2(C, k, \chi) - \alpha(C, k, \chi)G, \\ \frac{dP}{dt} &= F_3(C, k, \chi) - \alpha(C, k, \chi)P, \\ \frac{dP_{mem}}{dt} &= F_4(C, k, \chi) - H(V_{cyt})\alpha(C, k, \chi)P_{mem}, \\ \frac{dV_{cyt}}{dt} &= \alpha(C, k, \chi)V_{cyt},\end{aligned}$$

Equation 1-3: Set of differential equations (Morgan et al. 2004)

C , k , κ , and V_{cyt} denote a vector containing the various concentrations, vector of rate constants, the ratio of membrane volume to cytoplasm volume and volume of cytoplasm respectively. F_1 , F_2 , F_3 , F_4 and α all denote functions of C , k and κ while H is a function of V_{cyt} . The fifth equation suggests that variable volume is assumed in this method. The system of equations were further reduced by steady state assumptions and solved numerically in Maple using the seventh and eighth order Runge-Kutta method. The modeling method accounts for periodic changes in the cell while predicting a more realistic cellular behavior (because of inclusion of activities in both the cytoplasm and membrane) compared to other steady state modeling methods [84].

The DBsolve model is an object-oriented multi-functional program written in C++ for analyzing cellular metabolism and regulation. It takes input from a text file into a derived mathematical model, solves non-linear algebraic and ordinary differential equations, and performs constrained optimization to fit parameters to experimental data. The mathematical model accepts data in text file format containing experimental values, cell reactions and processes, cell components and database records. Cell reactions are converted to differential equations that are solved by built-in ODE and Implicit/Explicit solvers or a bifurcation analyzer depending on the type of problem. The resulting parameters may be optimized or fitted to experimental data. Figure 1-4 shows the DBsolve interface.

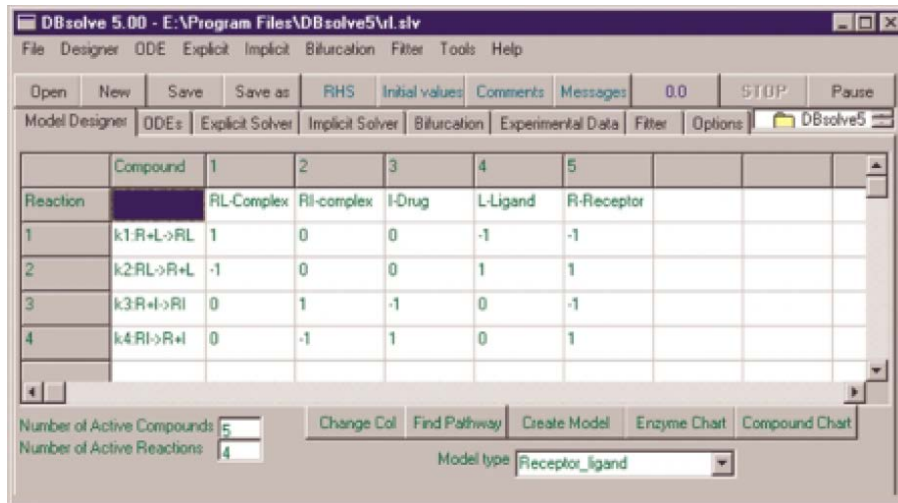


Figure 1-4: DBsolve (Goryanin et al. 1999)

The ODE solver is used to generate a set of initial values at steady state after performing a series of numerical method integrations. Any other forms of equation may be defined in the “RHS” environment and solved using the explicit solver. When it is desired to observe the effect of changes such as substrate and enzyme concentrations on product concentrations, control coefficients and overall steady flux, the implicit solver may be used. The bifurcation analyzer is used to determine whether a certain type of model method is feasible for non-linear systems [86].

The time dependent multi-algorithm simulation system for whole cell modeling consists of “data structure”, “driver algorithm” and “integration algorithm” modules. Within the data structure are defined classes for grouping data into a vector containing “steppers” and state variables (the model class). The steppers are further defined as a sub-vector component known as the “stepper class” to contain cell reactions or processes, time of reaction, time interval, step interval, step method and interruption method. Each “stepper” has an assigned state variable both of which change over time. This information is used to calculate a stepper dependency which is defined as a function of cellular processes and time. The driver algorithm outlines the steps to be

carried out in the simulations. Initial values of time and step intervals are defined for computing an initial stepper dependency which is updated at step size intervals over time. The original steppers are notified of the changes by an interruption procedure that replaces previous steppers with current ones. Corresponding state variables are recorded at the same time. The process continues for as long as the iteration runs until final time. The integration then uses the Euler method with a second order error term to compute the discretized form stepper equation as shown below:

$$x_j(\tau_i) = x_j + \Delta t_j \sum_{k \in \mathcal{S}} x'_{j,k} + O(\Delta t_j^2), \quad \Delta t_j = \tau_i - t_j$$

$$x'_{j,k} = \sum_{l \in P_k} \delta \rho_{k,l}$$

Equation 1-4: Euler method equation (Takahashi et al. 2004)

x_j is the last state variable, τ_i is the local time, t_j is the last updated global time, $\rho_{k,l}$ is the change in velocity of x_j by the l^{th} process of the k^{th} stepper and Δt_j is the corresponding change in time. The program was implemented by using an object-oriented programming languages like C++ and Python [85].

Browning and Shuler sought to develop a whole cell model for general cases based on an original *E. coli* model. They described this model as a “dynamic model of a free-living cell”. The concept of identifying the relationship between a cell’s genome and phenotype is adhered to here. Components of the *E. coli* model involved a set of time-dependent cell reactions (ODE-based kinetic equations) that requires initial conditions for solution. The model derives from the assumptions that cell characteristics such as shape, size and composition vary with environmental changes and thus respond to changes in the concentrations of carbon and nitrogen sources in a minimal medium to predict macromolecular composition, cell size, shape, cell replication and cell division

periods, point of initiation, and growth rate. All of DNA and RNA processes were “lumped” into single DNA and RNA equations respectively without losing a detailed representation of the cell.

Whereas the lumped equations in the *E. coli* are not constrained, the generalized cell model requires that the summation of mass balances for individual cell units must be equal to their respective lumped equations. The main objective of the generalized model was to be able to account for cell composition, growth rate, environmental changes, etc. based on scaling kinetic ratios. The kinetic ratio was defined as the ratio of the rate of all enzyme catalyzed reactions in a given model (for another organism) to the rate of all enzyme catalyzed reactions in the *E. coli* model. The “scaling” (for the generalized model) involved multiplying the kinetic ratios by each of the enzyme catalyzed equations in the cell under study to effect changes in the rate of occurrence of biosynthetic reactions. This is expected to cause dynamic changes in the cell from which schemes are developed for predicting cellular functions. To illustrate how “scaling” is done, an example of enzyme catalyzed reaction for amino acid biosynthesis is given below:

$$\left(\frac{dP_1}{dt}\right)_s = k_1 \left(\frac{K_{P_1}}{K_{P_1} + \frac{P_1}{V}} \right) \left(\frac{\frac{A_1}{V}}{K_{P_1 A_1} + \frac{A_1}{V}} \right) \left(\frac{\frac{A_2}{V}}{K_{P_1 A_2} + \frac{A_2}{V}} \right) V$$

Equation 1-5: An example of enzyme catalyzed equation (Browning and Shuler 2001)

Where P_1 is the mass of amino acids per cell, A_1 is the mass of intracellular ammonium ion, A_2 is the mass of intracellular glucose and associated compounds, V is the cell volume, k_1 is the maximum rate of amino acid synthesis per unit cell volume, and K_{P_1} , $K_{P_1 A_1}$, $K_{P_1 A_2}$ are saturated constants. So, multiplying the above equation by the kinetic

ratio in the generalized model will change k_1 and eventually change the mass of amino acid cells with respect to time. The same is applied to growth rate equations and other perturbation equations. Thus the effects of growth rate, cell composition, mutations or environmental changes are reflected in cell behavior. The generalized cell model is basically geared towards predicting reaction kinetics and mass transport process based on dimensionless parameters [88].

1.4.4 Errors/Sensitivity Analyses Applications

General areas of scientific and engineering require reliable and stable statistical computations. In mathematical modeling the major issues of concern are measurement and computational errors that can lead to inaccurate results especially when model performance is based on raw data. In reality, measurement data and computations are not entirely free of errors [89]. Errors may be random or systematic. Common sources of errors in these areas include pipettes, instrument readings, noise and biased data [90, 91]. Extensive studies on error and sensitivity analyses by Altman et al [89, 92] and highlight the need to avoid key sources of modeling errors such as “un-modeled measurement error”, “computer bugs”, “errors in data input”, “ill-conditioned input data”, “floating point underflow or overflow”, “rounding”, “non-random structure in random number generators”, “local optima or discontinuities in optimization landscapes”, “inappropriate or unlucky choices of starting values” and inadequate stopping criteria [89].

Metabolic flux analysis of biotechnological processes is somewhat complicated mostly due to scarcity of highly accurate and reliable measurement data [44, 93, 94] and possible inaccurate predictions from the model which may lead to loss of information on identifying key reactions [94, 95]. In MCA, errors are commonly associated with control

coefficients resulting from scaled first derivatives [96]. Errors due to noise have been identified as the source of most error effects on model. Filters in the presence of dynamic processes are primarily used to minimize noise error [94]. Errors from measurements and estimates may be eliminated by additional contributions from balancing techniques [94]. Consistency checks with respect to linear constraints in metabolic flux analysis have been applied to detect errors [97]. Indirect methods involving the use of elasticity and co-response coefficients for computing control coefficients have been proposed for better accuracy in MCA results [96]. Mass conservation balances may result in residual values used as estimated measurement errors. A common statistical test associated with modeling microbiological systems is the use of an 'h' function which determines the confidence level at which the resulting residual values are relatively close to zero (no gross errors are associated with measurements) [91, 98].

Statistical methods such as chi-square tests and Monte Carlo simulations have been established for error/sensitivity analysis in metabolic modeling [91, 99]. Chi-square tests determine the quality of data fit based on confidence interval estimates in a linear model [100]. In the Monte Carlo method, random numbers are generated from the mean and standard deviations of measured data. This is intended for simulating possible errors in measurements enough to reflect propagated errors in the model results. Monte Carlo simulations identify which experimental measurement need to be repeated for a considerable number of times and determined the shape of error distributions [99].

This study intends to develop predictive mathematical models (expected to reasonably reflect or capture and thus predict the behavior of "whole cell" model) based on steady-state and transient analysis (of *C. thermocellum* cell influenced by exogenous ethanol and dissolved hydrogen gas) in the presence of elevated pressures in continuous culture fermentations. Quality statistical evaluation of results considers chi-square tests and Monte Carlo simulations (MCS) of measurement data for

error/sensitivity analysis with MCS the most extensively used to determine the extent of uncertainty in measured data and model predictions [94, 96, 101-103].

1.5 OBJECTIVES

Clostridium thermocellum glycolytic metabolism will be investigated to develop a metabolic model for: i) its wild type and ethanol adapted cells toward end-product yields from cellobiose; ii) quantifying effects of dissolved hydrogen gas and pressure on end-product recovery/formation in wild type cells. The goal is to develop a predictive model for metabolic fluxes which corresponds to all metabolic phenotypes and genotypes for *C. thermocellum* glycolytic metabolism. This is expected to provide the platform for formulating optimal control theory to maximize ethanol yield.

1.6 THESIS ORGANIZATION

Chapter 1 (Introduction) provides general background and literature on microbial metabolism, metabolic modeling, organism selection and the need to develop a metabolic model for *C. thermocellum*.

Chapter 2 (Metabolic Flux and Control Analyses (MFCA) of Wild Type and Ethanol Adapted *C. thermocellum* Cells) presents a comparison between the technical details for constructing, calibrating, verifying, and evaluating flux distributions and control from measured amounts of some metabolites (both extracellular and intracellular) at steady state for both wild type (WT) and ethanol adapted (EA) cells.

Chapter 3 (Sensitivity Analysis of *Clostridium thermocellum* metabolic flux model) using the MFCA model to determine accuracy in modeling estimates from experimental data using inferential and descriptive statistical analyses (for example, chi-square distribution and Monte Carlo simulation).

Chapter 4 (Modeling Dissolved Hydrogen Gas (MDGG) and pressure effects in continuous culture fermentation of *C. thermocellum*) quantifies dissolved hydrogen gas flux on end-product recovery/formation of acetate and ethanol in the presence of 1) atmospheric ; 2) elevated pressure at steady state.

Chapter 5 (Transient Metabolic Flux Modeling of *C. thermocellum*) quantifies effects of dissolved hydrogen gas concentration on end-product recovery/formation of acetate and ethanol in the presence of 1) atmospheric ; 2) elevated pressure over time.

Chapter 6 (Future Development)

CHAPTER 2 METABOLIC FLUX AND CONTROL ANALYSES OF WILD TYPE AND ETHANOL ADAPTED CLOSTRIDIUM THERMOCELLUM CELLS

2.1 SYNOPSIS

A metabolic model based on metabolic flux and control analyses was developed to evaluate the glycolytic pathway of *Clostridium thermocellum*. The catabolism of *C. thermocellum* wild type (WT) and ethanol adapted (EA) cells grown on cellobiose in continuous culture were evaluated. Wild type cells averaged a 4% increase in carbohydrate uptake while only a 1% increase was observed in EA cells in the presence of exogenous ethanol. Less carbon was distributed towards lactate in WT (~4%) than in EA (~6%). Ethanol to acetate ratios increased in WT (4.8:1 to 6.1:1) at lower levels of exogenous ethanol while no significant changes in these ratios were observed for EA (5.1:1 to 5.5:1). However, WT cells appeared to be very sensitive to higher levels of exogenous ethanol (>1%v/v) and thus significantly decreased its ethanol to acetate ratio (i.e. from 4.8:1 to 2.1:1).

Keywords: Metabolic flux analysis; Control analysis; *Clostridium thermocellum*.

2.2 INTRODUCTION

2.2.1 Motivation for Lignocellulose Degradation

Increasing demands and prices of petroleum-based fuels have prompted the need to research and develop alternative fuels that can be produced from abundant renewable biomass. Ethanol has been identified as a potential alternative to fossil fuels [13-15]. Ethanol, as an oxygenated molecule, can reduce emissions of carbon dioxide, carbon monoxide, nitrogen oxide and hydrocarbons in compression-ignition engines [13]. Biomass production for alternative fuels affects the agricultural economy by increasing markets for farm owners and by increasing employment to process the biomass to fuels [13, 15, 16]. Tremendous efforts are being made to introduce renewable ethanol fuel production to reduce the world's dependence on non-renewable fuel resources. Since lignocellulosic biomass is a globally abundant source of stored energy, it seems appropriate to suggest lignocellulose for bioethanol production [16, 17]. Thus, renewable biomass resource conversion to ethanol continues to attract attention but economic assessment and research has shown limitations in developing and implementing effective techniques for utilizing biomass economically [18, 19]. "Highly effective cellulases and hemicellulases", "efficient and robust fermentative microorganisms", and "low-cost thermochemical pretreatment" are comprehensive measures that are being employed for biomass conversion into fuels and chemicals [18]. The importance many researchers placed on economically viable target products calls for more exploration of design and application of models. The National Biofuels Action Plan of 2008 states that increased knowledge of microbes and enzymes at the system level is needed to optimize the production of ethanol [104]. Metabolic flux and control analyses are process engineering (or metabolic modeling) methods that have been used to elucidate microbial and enzyme behavior at the system level. Process modeling and

simulation have been identified as promising tools for the dynamic analysis of ethanol fermentation process[23]. However, it has been discovered that fermentation conditions for producing high ethanol yield require the application of inhibitor-tolerant strains of microorganisms to metabolize all sugars (substrates) into ethanol as the major product [20]. Cells control their metabolism by regulating enzyme concentrations and activities, which affect material flows through different pathways. Thus, knowledge of the carbon flow through the microorganism will allow better understanding of metabolic processes such as catabolism, anabolism, and cell growth, enabling the controlled production of useful products in the chemical, engineering, fuel and pharmaceutical industries.

2.2.2 Organism Selection

Clostridium thermocellum is one of the most extensively studied anaerobic thermophiles. It is widely distributed in soil, has a very active cellulase system and has shown promise to achieve direct conversion of lignocellulosic biomass into ethanol at elevated temperatures [21, 29, 105] through consolidated bioprocessing (CBP). Consolidated bioprocessing is a term for a process where cellulase and hemicellulase production, hydrolysis and fermentation of pentose and hexose sugars occur simultaneously in the same reactor. Consolidated bioprocessing occurs in a single step and is considered to have outstanding potential because of its higher efficiency and low cost compared to other ethanol production methods [106]. The nature of CBP suggests the possibility of increasing ethanol production from higher hydrolysis rates when thermophiles, containing substrate-enzyme-microbe synergy, are involved [106]. *Clostridium thermocellum* is capable of converting cellulosic substrates in one reactor (known as consolidated bioprocessing) into products such as acetate, ethanol, lactate, H₂, CO₂ and recently formate [26, 45, 107, 108]. *Clostridium thermocellum* is one such

thermophile that has been used to demonstrate the usefulness of CBP in which the organism showed a cellulose conversion rate of 31% higher on than *Trichoderma reesei* and *Saccharomyces cerevisiae* [23]. The primary products of cellulose degradation by *C. thermocellum*'s cellulosome are cellobiose and cellodextrins [106]. However, research focus has been directed at improving ethanol production for commercial purposes by examining ethanol adaptation of *C. thermocellum* in relation to cell membrane fluidity [52, 56-58, 109-111]. Gram positive *Thermoanaerobacter ethanolicus* shares a common metabolic characteristic with *C. thermocellum* and the function of its alcohol dehydrogenase coupled with long chained fatty acids effects on ethanol production have been studied [38, 52, 57, 58, 110, 112, 113]. Alcohol dehydrogenase has been determined to prevent ethanol consumption in the presence of exogenous ethanol, resulting in increasing ethanol yield [113]. Upon detecting that nicotinamide adenine dinucleotide (NADH) inhibits pyruvate dehydrogenase (PDH) from channeling carbon from pyruvate to metabolic products in *Escherichia coli*; mutation of PDH minimized the inhibition effect. With the dominating effect of lactate dehydrogenase (LDH) on pyruvate, in relation to pyruvate formate-lyase (PFL) and PDH (all of which convert carbon from pyruvate to other products), a deletion of LDH in the *E. coli* cell was observed to increase metabolic product yields [114]. This concept may be exploited for *C. thermocellum*. Similarly, other studies claimed that a deletion of ferredoxin-hydrogenase (participating in the NADH and hydrogen production cyclic reaction between pyruvate and acetylCoA) in *C. thermocellum* has been detected to generate a maximum of 15-fold increase in ethanol production [115].

The use of exogenous ethanol revealed different sensitivity levels of WT and EA *C. thermocellum* cells in extensive studies of product selectivity and shift studies. In the presence of exogenous ethanol (solvent) the cells' metabolism and growth were influenced by protein function loss due to the interaction between cell membrane and

solvent. Changes in fluidity influence permeability through the membrane [56, 57, 109, 111, 112, 116]. Ethanol adapted cells accumulate a high percentage of longer fatty acid chains (>16:0) compared to wild type cells which accumulate shorter fatty acid chains (<16:0) in the presence of solvents. Wild type cells are sensitive to exogenous ethanol above the 1% level whereas ethanol adapted cells can tolerate as much as 8% exogenous ethanol. In the presence of exogenous ethanol, wild type cell membrane are less rigid (hence membrane fluidity increases) compared to ethanol adapted cell membrane. Ethanol adapted cell membrane seems not to tolerate any level of exogenous ethanol beyond 8% as was seen with increasing membrane rigidity (i.e. decreasing fluidity) [111]. Membrane fluidity thus affects growth rate [56] which in turn is inversely proportional to metabolic flux.

Optimum temperature is hindered by increasing amounts of exogenous ethanol in WT compared to EA [56]. Loss of protein function is affected by the presence of exogenous ethanol (or organic solvent) due to the interaction between cell membrane and solvent. Cell membrane lipid viscosity, which is a function of membrane thickness, increases with increasing amount of exogenous ethanol. Exogenous ethanol makes the membrane more rigid and thus, causes low fluid permeability through the membrane. Consequently, membrane fluidity changes coupled with loss of protein function influences cell growth and metabolism [56, 57, 109, 111, 112, 116]. Product selectivity and shifts in both exogenous ethanol containing WT and EA *C. thermocellum* are affected accordingly. Wild type tolerates exogenous ethanol amounts up to 1.5% (vol/vol), thereby producing short chained fatty acids in the WT cells [57, 58, 111-113]. Ethanol adapted cells favor beyond 5% vol/vol (as high as 8% vol/vol) exogenous ethanol to increase membrane fluidity [57, 58, 112, 113]. A higher percentage of long chained fatty acids were detected in EA cells due to high ethanol tolerance. In the presence of exogenous ethanol, ethanol adapted cells accumulate a high percentage of

longer fatty acid chains (>16:0) compared to wild type cells which accumulate shorter fatty acid chains (<16:0). This observation probably suggests why ethanologenic thermophiles have high tolerance to alcohols [113].

The progress of cellulose conversion by *C. thermocellum* may be hindered by a) relatively low ethanol tolerance and yield compared to yeast, and b) reduced cellulase synthesis under some typical growth and substrate conditions. An inverse relationship between membrane fluidity and order of fatty acid chains in the cell has been used to measure the cell's ethanol tolerance [111]. The mechanism known as anisotropy (A) is determined from the ratio of the orientation of light intensities from DPH labeled cells. Intensities are determined for horizontal and vertical excitations and emissions [111]. The ratio of horizontal excitation and vertical emissions (I_{hv}) to both horizontal excitation and emission (I_{hh}) defines a grating factor (g) for calculating A, where $A = \frac{I_{vv} - gI_{vh}}{I_{vv} + 2gI_{vh}}$. A high value of A corresponds to high order of fatty acids and hence, low membrane fluidity [111].

The limitations mentioned above have been recently addressed through genetic engineering (transcriptome and proteome analyses). Meanwhile, proteomic and transcriptome analyses do not sufficiently assess biological function [117], hence the need for intracellular metabolite analysis [118] to determine microorganisms' responses to important environmental stimuli (such as exogenous ethanol, substrate type, and substrate concentration). Measuring cellular response to a genetic or environmental perturbation provides a basis for rational "metabolic design" of these microorganisms [106]. However "metabolic design" is most effective to improve the performance of *C. thermocellum* when a metabolic model exists for the organism [119].

Mathematical models are simplifying abstractions that synthesize information and transform datasets into biological insight [40]. Existing essential tools for such modeling

include metabolic flux and control analyses. Metabolic flux analysis quantifies rate of material flow (distribution of fluxes) during metabolism in a microorganism.

Stoichiometric models, such as those used in metabolic flux analysis (MFA), have emerged as a powerful analysis tool to relate observable extracellular states with the intracellular carbon flux and energy distribution of an organism to form network models [120]. The stoichiometry for the central catabolic pathway of *C. thermocellum* is well-established. However, a metabolic model has not been developed for this organism.

Metabolic control analysis (MCA) characterizes the sensitivity of steady-state metabolic responses to changes in enzyme parameters using parameters such as elasticity coefficients, flux control coefficients and concentration control coefficients. The elasticity coefficients (ECs) are derived from the kinetics of the enzymes and can be defined as the fractional change in metabolite concentration with respect to rate of enzyme reaction. Elasticity coefficients are known as local parameters that describe the behavior of each pathway step in response to the respective enzyme activities and/or perturbation [121, 122]. The ECs are often used for estimating the flux and concentration control coefficients (FCCs and CCCs) that describe the extent to which enzyme activity or intracellular metabolite concentrations affect pathway components [71, 123]. The FCCs and CCCs are system parameters that illustrate the effects of changes in fluxes and metabolite concentrations on the metabolic pathway as a result of steady state perturbations. Metabolic control analysis (originally developed by [124]; and [125]) uses mathematical modeling to quantify the responses of metabolic pathways to control processes. The control process often involves perturbations in the microorganism's environment to generate possible effects on products of interest [126]. These effects are expressed in the form of FCCs and CCCs. This study focuses on investigating the capability of wild type and ethanol adapted *C. thermocellum* cells to adapt/adjust their metabolic responses to exogenous ethanol. Our capacity to collect quantitative

information on a microorganism has surpassed our ability to interpret these data [127]. The objective of the study was to develop a mathematical model to predict the responses of the wild type and ethanol adapted cells to w/v % ethanol treatment and to identify observable similarities and differences that may point to relevant information for enhancing/optimizing the cells' ethanol-producing pathway.

2.3 EXPERIMENTAL DATA AND STATISTICAL ANALYSIS

End-product concentrations produced by wild type (WT) and ethanol adapted (EA) *C. thermocellum* cultures grown on cellobiose substrate in steady state perturbations were taken from [118] for varying exogenous ethanol levels of 0%, 0.5%, 1% (for WT) and 0%, 1%, 5% (for EA). Wild type and EA strains were grown at 60°C and 55°C respectively at atmospheric pressure and fed with 4g/l cellobiose. Ethanol adapted strains are WT strains gradually adapted to increasing exogenous ethanol over time [118]. Replicates of metabolite concentrations within the experimental treatments (exogenous ethanol level) of WT and EA cells were analyzed using SAS PROC TTEST procedure to test the hypothesis of equal variances between observed metabolite concentrations. In the absence of replicate differences, we may then proceed to use the experimental data to perform metabolic flux and control analyses to determine elasticity coefficients, flux control coefficients (FCC) and concentration control coefficients (CCC). The observed levels of pyruvate in WT were reported [118] to be below detection limit so random values of pyruvate concentrations between 0.01mM and 0.09mM for all wild type cells were assumed.

2.4 MODELING METHODS

MFA and MCA were used to investigate the response of *C. thermocellum* metabolism to perturbations of exogenous ethanol concentrations in WT and EA strains.

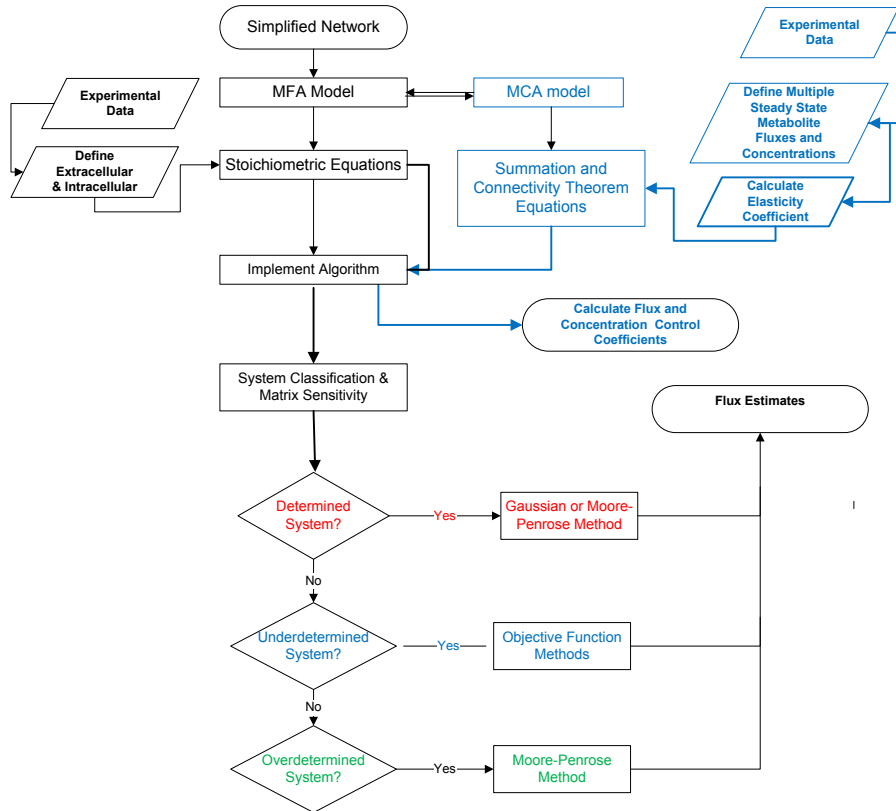


Figure 2-1: Overview of MFA and MCA methods

2.4.1 Metabolic Flux Analysis

Intracellular fluxes of metabolites in microbial cells are good indicators of cell phenotype. A metabolic flux analysis (MFA) is helpful to estimate the intracellular flux distributions given measured extracellular fluxes [121, 128]. MFA builds on the assumption that intracellular fluxes are in equilibrium with extracellular fluxes when the cells are at steady state. This assumption is satisfied when cells are grown in continuous cultures with nutrient limited growth [121].

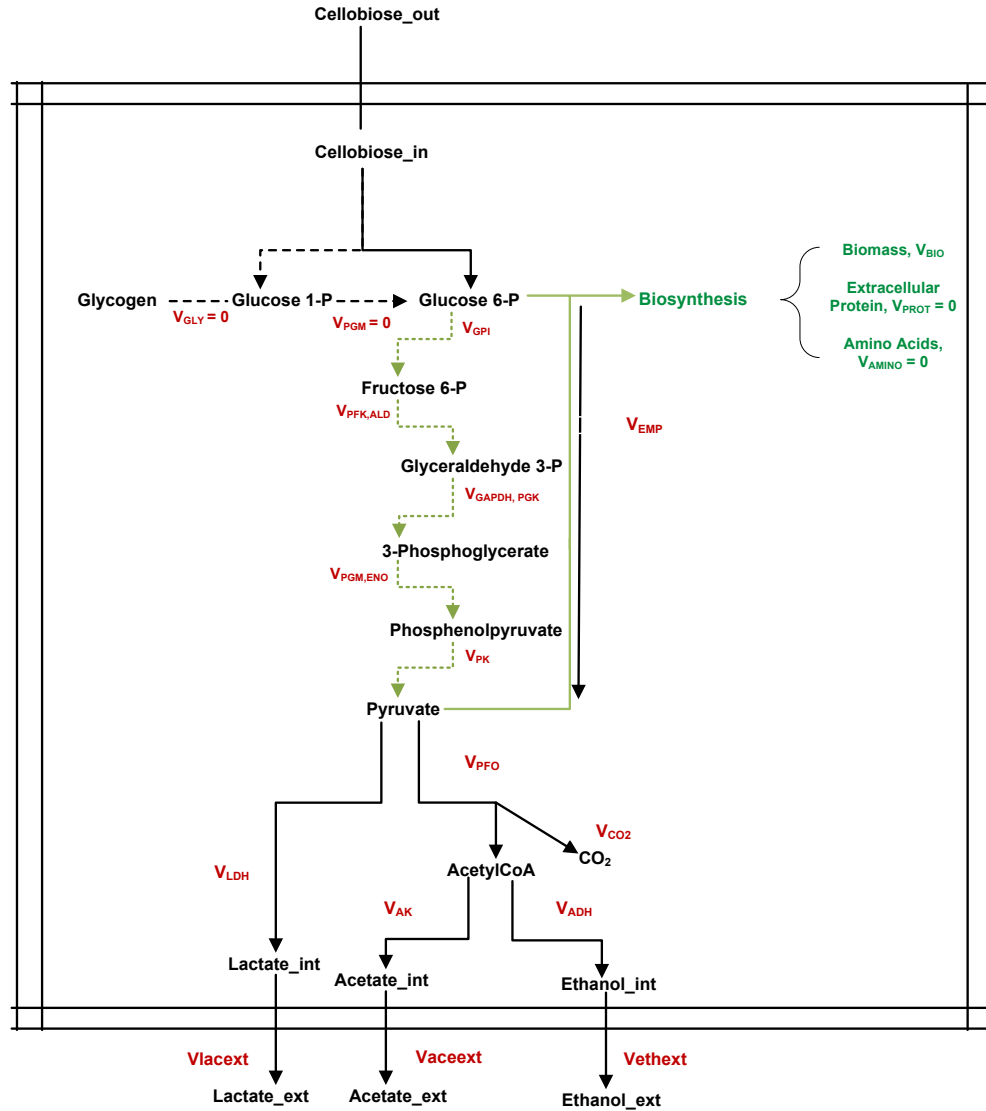


Figure 2-2: Simplified *C. thermocellum* Central Metabolic Pathway

Evaluation of the metabolic flux model suggested the system was consistent and determined. From Figure 2-2, mass balance principles were applied around each intracellular metabolite which resulted in a determined system of equations, consisting of an 8×14 stoichiometric matrix. The stoichiometric matrix N was used to develop a metabolic flux model in MATLAB. Let v denote the vector containing all fluxes then

$$N \cdot v = 0 \tag{A}$$

N was determined as:

-1.0	0.0	0.0	0.0	0.0	0.0	0.0	0.0	0.0	0.0	0.0	0.4	0.0	0.0
1.0	-1.0	0.0	0.0	0.0	0.0	0.0	0.0	-23.8	-24.2	-21.6	0.0	0.0	0.0
0.0	1.0	-1.0	-1.0	0.0	0.0	0.0	0.0	0.0	0.0	0.0	0.0	0.0	0.0
0.0	0.0	0.7	0.0	-1.0	-1.0	0.0	0.0	0.0	0.0	0.0	0.0	0.0	0.0
0.0	0.0	0.3	0.0	0.0	0.0	-0.3	0.0	0.0	0.0	0.0	0.0	0.0	0.0
0.0	0.0	0.0	1.0	0.0	0.0	0.0	0.0	0.0	0.0	0.0	0.0	-0.4	0.0
0.0	0.0	0.0	0.0	0.0	1.0	0.0	0.0	0.0	0.0	0.0	0.0	0.0	-0.4
0.0	0.0	0.0	0.0	1.0	0.0	0.0	-0.5	0.0	0.0	0.0	0.0	0.0	0.0

Equation (A) was partitioned into measured and non-measured fluxes that were rearranged with the unknown fluxes preceded by the known fluxes [12] as :

$$\begin{aligned}
 N_n \bullet v_n + N_b \bullet v_b &= 0 \\
 N_n \bullet v_n &= -N_b \bullet v_b
 \end{aligned}
 \tag{B}$$

Equation 2-1: Partition between measured and non-measured fluxes

N_b and v_b denote the stoichiometric matrix and flux vector corresponding to measured fluxes respectively. N_n and v_n denote corresponding matrix and vector for non-measured fluxes respectively. N_n and N_b were determined to be:

$N_n =$

-1.0	0.0	0.0	0.0	0.0	0.0	0.0	0.0
1.0	-1.0	0.0	0.0	0.0	0.0	0.0	0.0
0.0	1.0	-1.0	-1.0	0.0	0.0	0.0	0.0
0.0	0.0	0.7	0.0	-1.0	-1.0	0.0	0.0
0.0	0.0	0.3	0.0	0.0	0.0	-0.3	0.0
0.0	0.0	0.0	1.0	0.0	0.0	0.0	0.0
0.0	0.0	0.0	0.0	0.0	1.0	0.0	0.0
0.0	0.0	0.0	0.0	1.0	0.0	0.0	-0.5

$N_b =$

0.0	0.0	0.0	0.4	0.0	0.0
-23.8	-24.2	-21.6	0.0	0.0	0.0
0.0	0.0	0.0	0.0	0.0	0.0
0.0	0.0	0.0	0.0	0.0	0.0
0.0	0.0	0.0	0.0	0.0	0.0
0.0	0.0	0.0	0.0	-0.4	0.0
0.0	0.0	0.0	0.0	0.0	-0.4
0.0	0.0	0.0	0.0	0.0	0.0

An algorithm was developed for which the user is allowed to input known fluxes of extracellular metabolites for the prediction of fluxes of intracellular metabolites. Measured fluxes (mg metabolites /gram dry cell weight /hr) were obtained from experimental data by multiplying measured concentrations (in mM) by dilution rate (hr^{-1}) and metabolite molar mass (g/mol) and dividing by cell density (gcdw/l) for acetate, cellobiose, and lactate. Measured fluxes of cellobiose, lactate, and acetate were used as inputs in the model to predict intracellular fluxes and other extracellular fluxes. Glucose-6-phosphate, pyruvate and acetylCoa were identified as the key branch points. The principle of MFA has been previously described [64].

2.4.2 Flux Control Coefficient (FCC) and Concentration Control Coefficient (CCC)

With varying steady state perturbations of exogenous ethanol in WT and EA strains, the double modulation method was used to determine elasticity coefficients (an indirect way of determining control coefficients) and control coefficients to describe the metabolic system's behavior in response to perturbation. The method is based on the assumption that the steady state system is clearly defined with constant substrates and product concentrations.

The MCA procedure is illustrated by considering a simple linear pathway (Figure 2-3) to determine flux control coefficients, concentration control coefficients and elasticity coefficients.

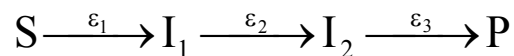


Figure 2-3: Schematic of simple linear pathway

S = substrate, ε = elasticity coefficient, I = intracellular metabolite, and P = product

Step 1: Write control matrix from pathway:

$$\begin{pmatrix} FCC_1 & FCC_2 & FCC_3 \\ CCC_1^1 & CCC_2^1 & CCC_3^1 \\ CCC_1^2 & CCC_2^2 & CCC_3^2 \end{pmatrix}$$

FCC = flux control coefficient, CCC = concentration control coefficient

FCC_1 = FCC due to 1st reaction

FCC_2 = FCC due to 2nd reaction

FCC_3 = FCC due to 3rd reaction

CCC_1^1 = CCC due to 1st reaction with respect to 1st intracellular metabolite

CCC_1^2 = CCC due to 1st reaction with respect to 2nd intracellular metabolite

CCC_2^1 = CCC due to 2nd reaction with respect to 1st intracellular metabolite

CCC_2^2 = CCC due to 2nd reaction with respect to 2nd intracellular metabolite

CCC_3^1 = CCC due to 3rd reaction with respect to 1st intracellular metabolite

CCC_3^2 = CCC due to 2nd reaction with respect to 2nd intracellular metabolite

Step 2: Write elasticity matrix from pathway:

$$\begin{pmatrix} 1 & \varepsilon_1^1 & \varepsilon_1^2 \\ 1 & \varepsilon_2^1 & \varepsilon_2^2 \\ 1 & \varepsilon_3^1 & \varepsilon_3^2 \end{pmatrix}$$

$\varepsilon_1, \varepsilon_2,$ and ε_3 = elasticity coefficients due to 1st, 2nd and 3rd reactions respectively.

ε_1^1 = elasticity due to 1st reaction with respect to 1st intracellular metabolite

ε_2^1 = elasticity due to 2nd reaction with respect to 1st intracellular metabolite

ε_3^1 = elasticity due to 3rd reaction with respect to 1st intracellular metabolite

ε_1^2 = elasticity due to 1st reaction with respect to 2nd intracellular metabolite

ε_2^2 = elasticity due to 2nd reaction with respect to 2nd intracellular metabolite

ε_3^2 = elasticity due to 3rd reaction with respect to 2nd intracellular metabolite

Step 3: Apply the summation and connectivity theorem: sum of flux control coefficients equal one, sum of concentration control coefficients equal zero, the sum of product of elasticity coefficients and their respective flux control coefficients for each reaction equal zero and the sum of product of elasticity coefficients and their respective concentration control coefficients for each reaction equal negative one. Given known elasticity (the approach to determining elasticity is detailed in the methods) coefficients, the FCCs and CCCs can be solved algebraically from the following expression:

$$\begin{pmatrix} FCC_1 & FCC_2 & FCC_3 \\ CCC_1^1 & CCC_2^1 & CCC_3^1 \\ CCC_1^2 & CCC_2^2 & CCC_3^2 \end{pmatrix} \begin{pmatrix} 1 & \varepsilon_1^1 & \varepsilon_1^2 \\ 1 & \varepsilon_2^1 & \varepsilon_2^2 \\ 1 & \varepsilon_3^1 & \varepsilon_3^2 \end{pmatrix} = \begin{pmatrix} 1 & 0 & 0 \\ 0 & -1 & -1 \\ 0 & -1 & -1 \end{pmatrix} \quad (C)$$

Six (6) key pathway steps and three (3) intracellular metabolites were used in the MCA model (Figure 2-4). Therefore the elasticity coefficients (denoted by ε) with respect to steps 1 through 6 were computed by incorporating small changes in fluxes and concentrations of glucose-6-phosphate, pyruvate and acetylCoA at different steady states.

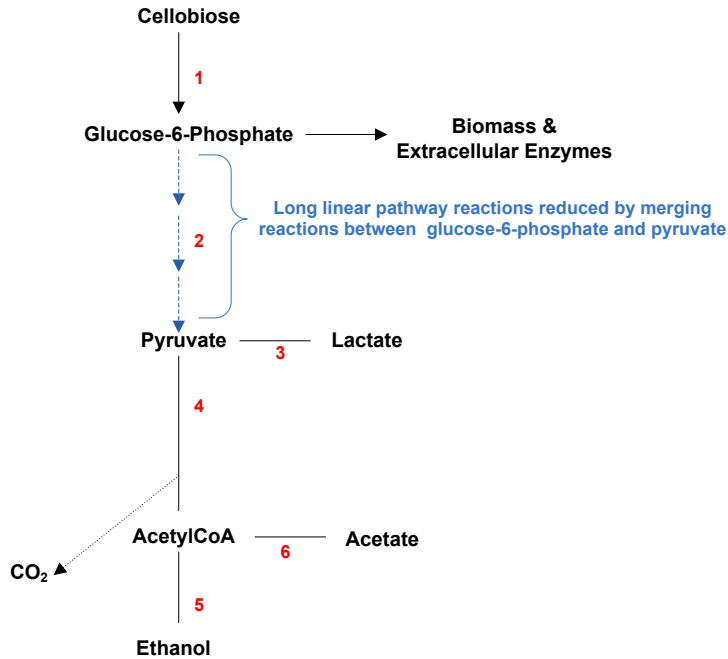


Figure 2-4: Six key pathway steps and intracellular metabolites identified for MCA model development

Eight elasticity coefficients denoted by $\varepsilon_1^{G6P}, \varepsilon_2^{G6P}, \varepsilon_2^{Pyr}, \varepsilon_3^{Pyr}, \varepsilon_4^{Pyr}, \varepsilon_4^{AcCoA}, \varepsilon_5^{AcCoA}, \varepsilon_6^{AcCoA}$ due to glucose-6-phosphate, pyruvate and acetylCoA (intracellular metabolites) were computed. Subscripts and superscripts represent each pathway step and intracellular metabolites (G6P, Pyr and AcCoA as nodes) respectively. For example to determine the elasticity coefficients of pyruvate and glucose-6-phosphate due to step 2 (the EMP pathway) in WT, small changes in the respective fluxes and concentrations between WT0% and WT0.5%, and between WT0% and WT1% (all assumed to be perturbed at steady state) may be used in simultaneous equations to solve for the unknown elasticity coefficients as in Equations (1) and (2) below.

$$\Delta J_{AB} = \varepsilon_2^{G6P} \Delta C_{G6P}^{AB} + \varepsilon_2^{Pyr} \Delta C_{Pyr}^{AB} \dots \dots \dots (1)$$

$$\Delta J_{AC} = \varepsilon_2^{G6P} \Delta C_{G6P}^{AC} + \varepsilon_2^{Pyr} \Delta C_{Pyr}^{AC} \dots \dots \dots (2)$$

$\Delta J_{jk} = \ln J_k - \ln J_j$; $\Delta C_{jk} = \ln C_k - \ln C_j$. ΔJ_{AB} is the small (differential) change in metabolite fluxes between treatments WT0% and WT0.5% and ΔJ_{AC} is the changes between WT0% and WT1%. Similarly, $\Delta C_{metabolite}^{jk}$ represents small changes in concentrations of the same metabolite between the j and k treatments. The unknown parameters ε_2^{G6P} and ε_2^{Pyr} , are the elasticity coefficients of G6P and pyruvate as described earlier. The same procedure is used to determine the other elasticity coefficients of intracellular metabolites in the other steps for WT and EA. Using Equation C, the FCCs and CCCs can be estimated accordingly [121, 124, 128-132]. These papers further demonstrate other alternatives to performing metabolic control analyses.

2.4.3 Statistical Analyses

The effects of exogenous ethanol treatment on carbon flux distribution, flux control and concentration control were considered for WT and EA types of the *C. thermocellum* pathway. An assessment of how much control of flux or concentration may be needed and the rate at which carbon is distributed within the pathway is of significant importance to relate phenotypic to genomic information.

T-tests were performed by pairing each of the exogenous ethanol treated strains (WT0%, WT0.5%, WT1%, EA0%, EA1% and EA5%) to determine how sensitive the level of exogenous ethanol in a cell type is to the rate of material flow (flux) through the pathway. The paired t-test was based on the null hypothesis (as shown below with the alternate hypothesis) that there is no significant difference (at both the 5% and 10% significance levels) between averages of paired fluxes (say between WT0 and EA0).

$$\begin{aligned}
 &H_0: \mu_{WT0} = \mu_{EA0} = \mu_{EA1} = \mu_{EA5}; \quad H_0: \mu_{WT0.5} = \mu_{EA0} = \mu_{EA1} = \mu_{EA5}; \quad H_0: \mu_{WT1} = \mu_{EA0} = \mu_{EA1} = \mu_{EA5}; \\
 &H_1: \mu_{WT0} \neq \mu_{EA0} \neq \mu_{EA1} \neq \mu_{EA5}; \quad H_1: \mu_{WT0.5} \neq \mu_{EA0} \neq \mu_{EA1} \neq \mu_{EA5}; \quad H_1: \mu_{WT1} \neq \mu_{EA0} \neq \mu_{EA1} \neq \mu_{EA5}.
 \end{aligned}$$

As an example, the paired t-test between WT0 and EA0 were defined using SAS

as:

```
Data CthermGrowth;
```

```
Input Wtflux0 EAflux0;
```

```
Datalines;
```

7.20	10.92
5.22	8.94
0.27	0.94
4.95	8.01
2.74	4.50
0.56	0.83

```
Proc ttest;
```

```
Paired Wtflux0*EAflux0;
```

```
Run;
```

Independent t-tests involving FCCs and CCCs grouped under WT and EA cells to determine whether flux and/or concentration controls are affected by the level of exogenous ethanol in both type of cells were also performed in SAS. Two types of null hypotheses (and alternate hypotheses) were set for this case (within strains and between strains) as:

$H_0: \mu_{WT0} = \mu_{WT0.5} = \mu_{WT1}; H_0: \mu_{EA0} = \mu_{EA1} = \mu_{EA5}; H_0: \mu_{WT} = \mu_{EA}$

$H_1: \mu_{WT0} \neq \mu_{WT0.5} \neq \mu_{WT1}; H_1: \mu_{EA0} \neq \mu_{EA1} \neq \mu_{EA5}; H_1: \mu_{WT} \neq \mu_{EA}$

For example, the PROC TTEST between WT0 and WT0.5 CCCs were defined as:

```
Data CthermGrowth;
```

```
Input treatment $ G6P Pyr AcCoA;
```

```
Datalines;
```

WT0	-2.295	-0.117	-0.330
WT0	4.291	0.982	2.765
WT0	-0.126	-0.055	-0.081

WT0	-2.307	-1.000	-1.487
WT0	0.363	0.157	-0.720
WT0	0.074	0.032	-0.147
WT05	-2.280	-0.111	-0.325
WT05	4.161	0.926	2.721
WT05	-0.085	-0.037	-0.055
WT05	-2.225	-0.964	-1.455
WT05	0.371	0.161	-0.768
WT05	0.057	0.025	-0.118

Proc ttest;

Class treatment;

Var G6P Pyr AcCoA

Run;

Proc boxplot;

Plot G6P* treatment;

Plot Pyr* treatment;

Plot AcCoA* treatment;

Run;

2.5 RESULTS AND DISCUSSION

The metabolic responses of WT and EA *C. thermocellum* to exogenous ethanol perturbations were compared by examining their carbon flux distributions, FCCs and CCCs with the intention of identifying any differences in their respective metabolisms.

In a two-way analysis of variance, predicted exogenous ethanol treatment effects and differences in flux distribution (rate of flow of material through pathway) were evaluated (Table 2-1 and Table 2-2). Exogenous ethanol treatment effects were blocked on node or flux location (glucose-6-phosphate, pyruvate and acetylCoA) for statistical analysis. There is a statistically significant probability that at least one flux varied with treatment in both WT and EA. Further analysis was required to determine which treatment means were significantly different from the others.

Paired t-tests were performed and evaluated at critical levels (α) of 10% within WT and EA cells to determine if these samples come from the same distribution with equal means or not (Table 2-3 and Table 2-4). The paired t-tests compared treatments at each pathway flux. A 'p' value less than α indicates that statistically, the means were significantly different from each other. At the 10% level, the p-values indicate significant differences between all WT pairs. In this case, the metabolic activities all WT cells vary with each increase in exogenous ethanol. The p-values at the 10% level show that at least one of the means of EA0 and EA1 are the same (Table 4). There is an indication that EA0 is significantly different from EA5 and EA1 is significantly different from EA5. The reaction of acetylCoA branch point towards acetate reaction involves acetate production from AMP and pyrophosphate (PPi) or from ADP and Pi. The former pair requires $3H^+$, which causes a less thermodynamically feasible acetate production than the latter pair [45]. The ATP/ADP ratio determines cellular energy, thus the higher this ratio the less likely it is for the reaction to go towards acetate. ATP/ADP ratios decreased across EA0, EA1 and EA5 (i.e. EA5 had the lowest ATP/ADP ratio, hence directs the reaction towards forming acetate where more ATP is produced for energy. Thus, the difference in EA1 and EA5 could be attributed to possible activation of the latter pair by the 5% exogenous ethanol concentration towards acetate production as shown in Figure 2-7 and Figure 2-8

Table 2-1: Two-way ANOVA for WT flux distribution

Source	SS	df	MS	F	Prob>F
Flux node	161.046	5	32.2092	106.7	0
Treatment	6.282	2	3.1404	10.4	0.0036
Error	3.019	10	0.3019		
Total	170.345	17			

Table 2-2: Two-way ANOVA for EA flux distribution

Source	SS	df	MS	F	Prob>F
Flux node	309.595	5	61.919	695.65	0
Treatment	0.893	2	0.4467	5.02	0.031
Error	0.89	10	0.089		
Total	311.378	17			

Table 2-3: Paired T-tests evaluated within WT

Paired T-tests	WT0% –WT0.5%	WT0% –WT1%	WT0.5% –WT1%
p	0.03	0.0168	0.0515

Table 2-4: Paired T-test evaluated within EA

Paired T-tests	EA0% –EA1%	EA0% –EA5%	EA1% –EA5%
p	*NSE(0.0903)	0.0689	0.0234

*NSE: no significant effect @ 0.1: this value is relatively very close to 0.1

2.5.1 Carbon Flux Distribution

Carbon flux distribution for the wild-type *C. thermocellum* cultured in differing concentrations of exogenous ethanol is presented in Figure 2-5, expressed in milliequivalent carbon per gram of dry cell weight per hour ($\text{meC}(\text{gdcwh})^{-1}$), and in Figure 2-6 in percent of the total carbon flow.

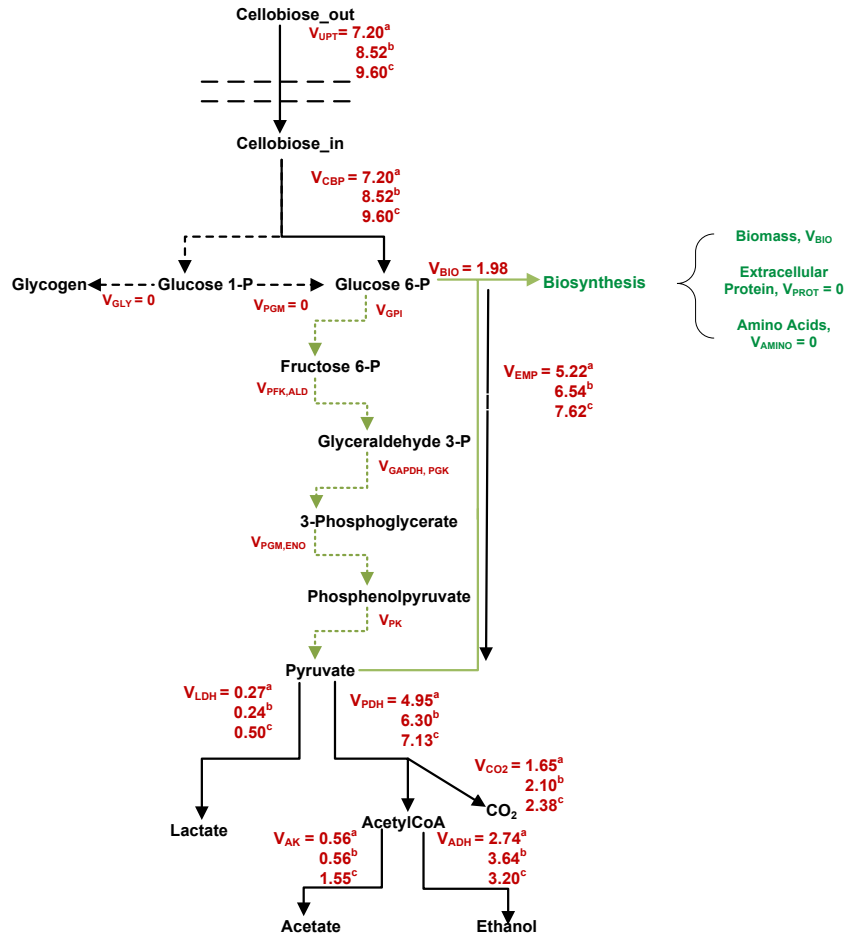


Figure 2-5: Predicted carbon flux distribution in a simplified model of *C. thermocellum*'s central pathway (units in meC/g cell h) – Wild type (a- WT0%, b-WT0.5% and c-WT1%)

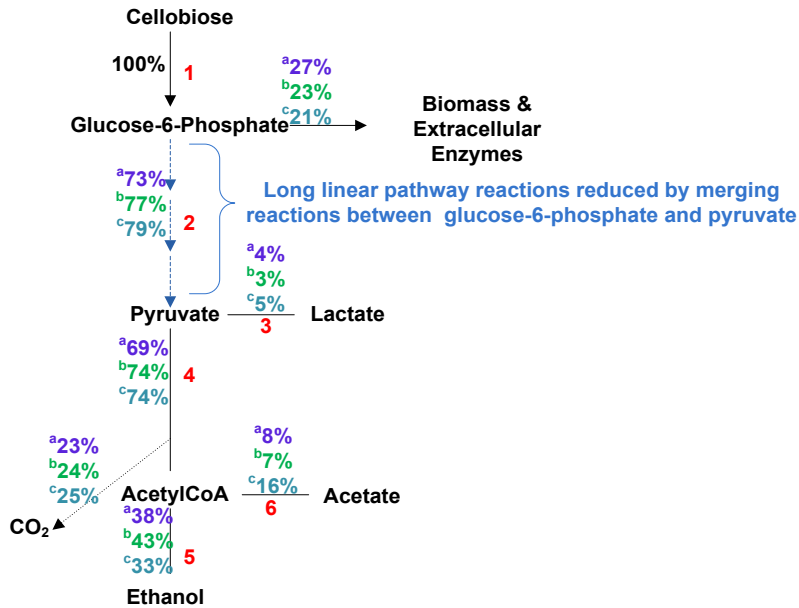


Figure 2-6: Flux Distribution in WT cells (a - WT0%, b - WT0.5%, c - WT1%) shown for key pathway steps. The first number in each triad represents the carbon flow in the WT0% treatment, the second and third number represents the WT0.5% and WT1% respectively.

The carbon distributed towards pyruvate, acetylCoA, and ethanol increased by 4%, 5%, and 5% respectively for the WT perturbed with 0.5% exogenous ethanol versus the WT with no exogenous ethanol. However the carbon diverted towards biosynthesis decreased by 4% when there was 0.5 exogenous ethanol compared to no exogenous ethanol. In the presence of 1% exogenous ethanol, carbon distribution in WT increased (6% over 0% and 2% over 0.5%) towards pyruvate but decreased carbon flow towards ethanol (5% decrease compared to the 0% exogenous ethanol treatment and 10% decrease compared to 0.5% exogenous ethanol treatment). Carbon flow towards acetylCoA was unchanged from the % carbon flow towards acetylCoA for WT with 0.5% exogenous ethanol, and slightly decreased towards biosynthesis (2%) compared to WT0.5%. Carbon distribution towards acetate in WT1% was approximately twice that of both WT0% and WT0.5%.

Timmons et al. (2009) quantified membrane fluidity (measured using anisotropy) for WT *C. thermocellum* and found that membrane fluidity is higher in the absence of exogenous ethanol [111]. It can be seen in Figure 2-5 and Figure 2-6 that the carbon flux distribution through the central pathway increased in WT cells as the amount of exogenous ethanol added increased from 0% and 1%. This may be attributed to more energy being required for maintenance leaving less for anabolism when the cells are ethanol stressed. Increasing the amount of exogenous ethanol causes the cell membrane to become more fluid and leakier, thereby decreasing membrane potential and proton efflux (proton towards outer membrane) while increasing proton influx (proton towards inner membrane). Electrochemical gradient is then decreased, which leads to subsequent decrease in proton motive force which requires cells to use more energy for metabolism [133, 134]. This hypothesis is consistent with the carbon flux distribution pattern in WT0%, WT0.5% and WT1%. As more energy is required for maintenance, more carbon is directed towards acetate formation due to the ATP generation involved with its formation [45], which is consistent with the pattern of carbon flux distribution in WT0%, WT0.5% and WT1% towards ethanol and acetate (less carbon flux towards ethanol and more towards acetate in WT1%). Figure 2-7 presents carbon flux distribution in ethanol adapted *C. thermocellum*. The changes in carbon distribution going from EA0% to EA1% and from EA0% to EA5% were identical except for acetate which showed a slight increase at the 5% exogenous ethanol level. Ethanol adapted cells generally had a lower percentage of their carbon branching off the pathway (Figure 2-8) towards biosynthesis compared to WT (9% less in the absence of exogenous ethanol and 4% for the 1% exogenous ethanol treatment).

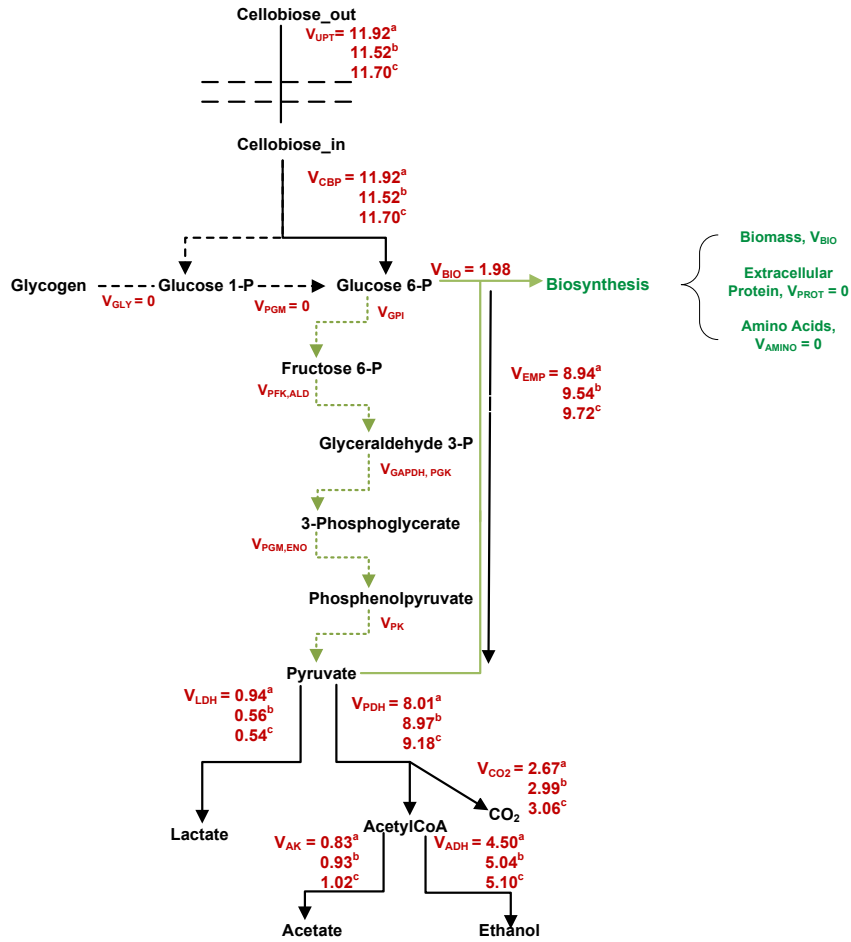


Figure 2-7: Carbon Flux Distribution in the simplified *C. thermocellum* central pathway (units in meC/g cell h) – Ethanol Adapted (a-EA0%, b-EA1% and c – EA5%)

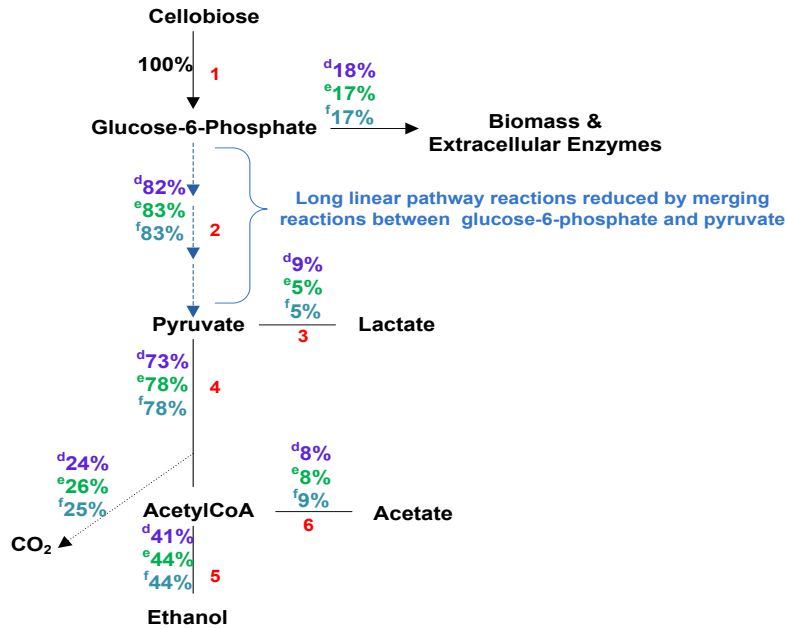


Figure 2-8: Flux Distribution in EA cells (d - EA0%, e -EA1%, f - EA5%) shown for key pathway steps. The first number in each triad represents the carbon flow in the EA0% treatment, the second and third number represent the EA1% and EA5% respectively.

Ethanol adapted cells' response to carbon distribution through the central pathway in the absence and presence of exogenous ethanol may be attributable to its ethanol tolerance mechanism. Cells' adaptation to ethanol cause changes in the composition of membrane fatty acids that influences membrane fluidity [111]. The more adapted cells are to ethanol, the longer the fatty acid chain and the less rigid the membrane becomes [58, 111], consequently directing more energy towards catabolism (as shown by the increases in carbon fluxes of the EMP pathway) and less towards anabolism in EA cells. However, in the presence of exogenous ethanol the membrane becomes too rigid [58, 111] to continuously allow further increases in catabolism, which explains why carbon flux distributions through the central pathway in EA1% and EA5% were not significantly different from EA0%.

Ethanol adapted exhibited the same pattern as WT except for acetate. However, the carbon flux distributions indicated some differences in WT and EA metabolic

activities. The predicted difference in carbon flux directed towards biomass and extracellular enzymes (biosynthesis) in EA0% and WT0% (Figure 2-5 and Figure 2-7) is consistent with the findings of Williams et al., (2007) that lower growth rates and cell yields occur in EA cells compared to WT in the absence of exogenous ethanol [58] It may be noted that EA cells in the presence of high exogenous ethanol levels (EA5%) did not decrease the carbon flux towards ethanol (contrary to WT in high exogenous ethanol concentrations). This suggests that EA cells do not need more energy in the presence of exogenous ethanol because energy is preserved by the cells' adaptation to ethanol as a result of increased membrane integrity [111, 135]. Similarly the predicted fluxes towards carbon dioxide in all strains suggest that exogenous ethanol may have no inhibitory effect on gaseous products.

Membrane fluidity, which affects growth rate, is inversely proportional to metabolic flux. The effect of membrane fluidity on flux may be accounted for by flux behavior within the Embden-Meyerhof-Parnas (EMP) pathway of the simplified metabolic networks shown in Figure 2-5 (for WT) and Figure 2-7 (for EA). This previous observation is supported by Williams et al., 2007 who found that proteins were down-regulated by 73% in the carbohydrate metabolism of ethanol adapted cells [58]. Knowledge of metabolic pathway flux distribution patterns will help interpret and understand the metabolic activity towards target product formation [112, 136].

2.5.2 Flux and Concentration Control Coefficients

A two-way analysis of variance to determine the effects of exogenous ethanol treatments on both FCCs and CCCs within WT and EA is shown in Table 2-5 and Table 2-6. The p-value results for CCCs are similar, and so are not shown. Rows represent exogenous ethanol treatment effect whereas columns indicate control coefficients for

each pathway. There were no significant differences in the control coefficients within the same type of strain regardless of exogenous ethanol treatment (WT ($p=1$) and EA ($p=0.9999$)). Meanwhile, flux control coefficient for each pathway was strongly affected by exogenous ethanol (WT ($p=0$) and EA ($p=0$)).

Table 2-5: Two-way ANOVA for WT flux control coefficients

Source	SS	df	MS	F	Prob>F
Flux node	22.4698	5	4.49396	1788.96	0
Treatment	0	2	0	0	1
Error	0.0251	10	0.00251		
Total		17			

Table 2-6: Two-way ANOVA for EA flux control coefficients

Source	SS	df	MS	F	Prob>F
Flux node	15.4546	5	3.09092	7448.03	0
Treatment	0	2	0	0	0.9999
Error	0.0041	10	0.00041		
Total	15.4588	17			

We may therefore deduce that the FCCs and CCCs in the catabolic pathway of *C. thermocellum* are independent of exogenous ethanol treatments. Thus values for control coefficients were averaged over same strain type (Table 2-7 and Table 2-8) at each flux location.

Table 2-7: Flux control coefficients (FCCs) for wild type and ethanol adapted strains at each reaction stage

Pathway Step	Wild Type	Ethanol Adapted
1	-0.72	3.47
2	0.89	-1.66
3	0.03	-0.04
4	0.45	-0.41
5	0.30	-0.31
6	0.06	-0.05

Table 2-8: Concentration control coefficients (CCCs) for wild type and ethanol type strains at each reaction stage

Pathway Step	CCCs of metabolite due to each pathway step					
	Glucose-6-phosphate		Pyruvate		AcetylCoA	
	WT	EA	WT	EA	WT	EA
1	-5.26	-41.79	1.17	20.68	-2.42	-18.80
2	2.71	28.18	-1.44	-9.92	2.97	9.02
3	0.09	0.68	0.01	-0.54	0.10	0.22
4	1.38	6.90	0.14	-5.46	1.51	2.21
5	0.92	5.18	0.10	-4.10	-1.82	6.32
6	0.17	0.85	0.02	-0.67	-0.34	1.03

2.5.2.1 Model - Wild Type

Flux control is shared among the cellobiose phosphorylase (CBP) activity step, enzymes within the EMP pathway, pyruvate ferredoxin oxidoreductase (PFO) and combined step of acetyl dehydrogenase and alcohol dehydrogenase activities (denoted as ADH). Activities of the enzymes within the EMP pathway (step 2) were determined to be the major controlling step for the wild-type strain adjusting to exogenous ethanol. This step is considered the major controlling step because it had the highest FCC as shown in Table 2-7 (0.89). Negative FCCs observed in metabolic networks normally occur in the of the presence of branched pathways that generate precursors for forming other products leading to increases in the outflow from that node and decreases glycolytic fluxes [137]. The negative FCC observed in the first step (-0.72) suggests that an increase in the enzyme activity of this step causes a decrease in flux [129, 138]. A corresponding negative CCC (-5.26) was observed in the same step. This can be interpreted as a 1% increase in enzyme activity between cellobiose and glucose-6-phosphate decreases the concentration of the latter by 5.26% [138]. G6P is formed from G1P and glucose which are branched products of cellobiose catalyzed by the enzyme, CBP (Figure 2-9). Additionally, G6P reversibly forms G1P. Thus, if an increase in CBP

activity causes a decrease in the flux towards G6P, then it is possible that the amount G6P reaches a limit beyond that required for central metabolism hence redirecting G6P towards G1P. This redirection could account for the decrease predicted in both flux and concentration of G6P when CBP activity is increased. Figure 2-7 and Figure 2-8 also show that an increase in the EMP pathway enzymes activity (denoted by step 2) will increase the concentrations of glucose-6-phosphate and acetylCoA (i.e. CCCs of 2.71 and 2.97 respectively) but decrease pyruvate concentration.

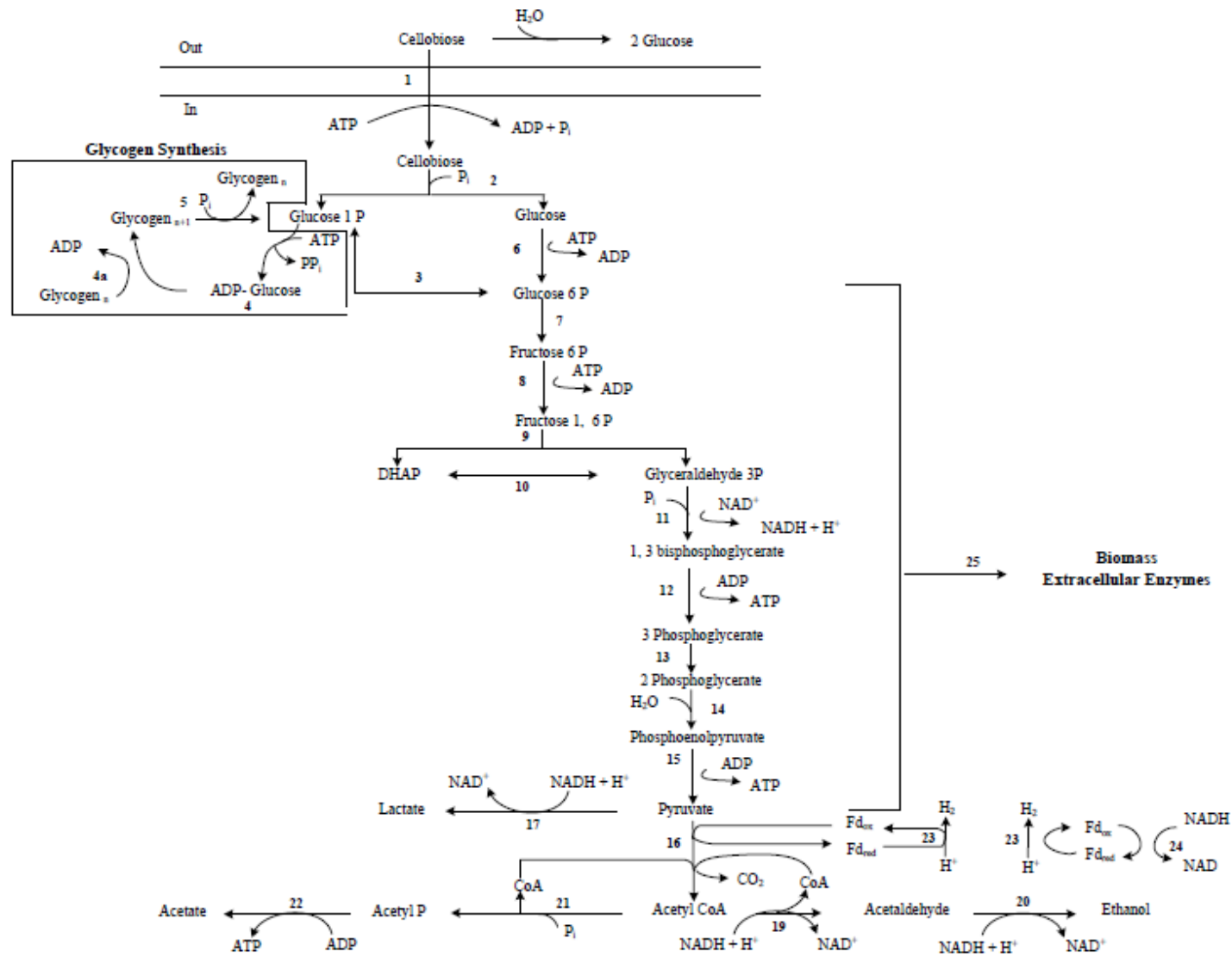


Figure 2-9: Central Metabolic Pathway of *Clostridium thermocellum*

2.5.2.2 Model - Ethanol Adapted

Typical values of FCCs fall between 0 and 1. However, it is possible to have FCCs of larger magnitudes in some cases, particularly when there are branched pathways involved [139] due to the summation theorem [139, 140]. Small FCCs (positive or negative) compared to the largest FCC represent negligible control effects from that pathway step [139]. Similar to WT, flux control is shared among the cellobiose phosphorylase (CBP) activity step, EMP pathway, and PDH and ADH activity steps except that the CBP pathway is the major controlling step in this case. The largest flux control coefficient (3.47) occurs between cellobiose and glucose-6-phosphate (Table 2-7). From Table 2-7 and Table 2-8, it can be seen that an increase in CBP activity will increase the flux in this pathway step and all fluxes downstream of G6P decrease in response to increases in the downstream enzyme activities. This means EA will not increase the rate of catabolism when enzyme activities increase downstream. Glucose-6-phosphate and acetylCoA concentrations increased in response to increases in enzyme activities downstream of G6P while pyruvate concentration decreased. The major controlling step (step 1) is reflected in the increasing concentration of G6P. Decreases in the pyruvate concentration may be attributed to an increasing shift in the metabolite reaction towards lactate as a result of allosteric activation of lactate dehydrogenase (LDH) by fructose-1,6-phosphate. This shift is then likely to cause the activation of the ferredoxin-dependent hydrogenase that catalyzes pyruvate, CoA, and $Fd_{(ox)}$ towards acetylCoA, hence an increase in acetylCoA concentration (Figure 2-7 and Figure 2-8).

The main difference between carbon flux distribution in EA and WT happened to lie in the effect of enzyme activities upstream and downstream of glucose-6-phosphate, indicating that flux control mainly occurs upstream of EMP in EA. The control of flux

exerted at the beginning of the pathway in EA (compared to WT) indicates that cells adapt to exogenous ethanol by changing protein expression relative to cellobiose metabolism. This shift in control parameters in EA cells may be due to changes in the response of ethanol adapted cells to CBP activity which catalyzes cellobiose metabolism. A study by [58] on *C. thermocellum* adapted to exogenous ethanol investigated protein expression. One third of the protein that were down-regulated were involved in cellobiose metabolism [58]. Cellobiose metabolism here refers to cellobiose uptake up to G6P and thus slow the building of biosynthetic precursors for growth of EA cells (as reported in Thakur's work [118]). Thakur 2008 studied intracellular metabolite responses of *Clostridium thermocellum* WT and EA cells to ethanol stress. G6P concentrations were observed to be 1.25mM and 0.6mM in EA and WT cells in the absence of exogenous ethanol respectively. As exogenous ethanol increased in the cells' environment, the concentrations of G6P decreased for EA (1.25mM EA0, 0.75mM EA1 and 0.3mM EA5%) and increased for WT (0.6mM WT0, 0.9mM and 1.5mM) [118]. These observations are consistent with our findings of higher magnitude CCC values of G6P in EA than WT in the EMP pathway where G6P is the substrate towards biosynthesis and catabolism. Non-detected pyruvate and close to zero acetylCoA concentrations were found in WT while the corresponding pyruvate values observed for EA, showed 1mM EA0, 1.25mM EA1 and 2.75mM EA5. From our findings, the magnitude of CCCs for pyruvate, the substrate for steps 3 and 4 (i.e. towards lactate and acetylCoA formation) were lower in WT than in EA. It may however be emphasized that the flux control coefficients at step 3 in both EA and WT are basically zero and thus indicate that changes in the microorganism's metabolism due to exogenous ethanol have negligible effect on the rate of lactate production.

The general results from control coefficients represent the property of the system as a whole according to the summation theorem where all FCCs sum up to unity and CCCs sum up to zero [141].

2.6 CONCLUSION

The observations made in this study lead to the deduction: 1) that the effects due to environmental perturbations such as exogenous ethanol treatment on the system are minimally influenced by the presence of lactate ; 2) that the organism likely does not have the ability to shut down by-product pathways to achieve high production of ethanol; 3) that the pathway is not controlled by one particular step or enzyme activity but a combination of several [139] ; 4) that metabolic control analysis identified differences in *C. thermocellum*.

An error and sensitivity analysis of the flux models are addressed in the Chapter 3.

CHAPTER 3 SENSITIVITY ANALYSIS OF *CLOSTRIDIUM THERMOCELLUM* METABOLIC FLUX MODEL

3.1 SYNOPSIS

Metabolic flux and control analyses were implemented to model the catabolic pathways of wild type (WT) and ethanol adapted (EA) *Clostridium thermocellum* to predict fluxes and control coefficients of intracellular and other relevant metabolites from measured extracellular fluxes. These fluxes and control coefficients may be influenced by error in the measured fluxes. It is therefore important to determine the level of uncertainty (by standard statistical techniques and sensitivity analyses) of measured data. Uncertainty is used as an indicator of the level of experimental and consequent model accuracy. Experimental data perturbation (small changes in measurements), chi-square distribution and Monte Carlo simulation methods were applied to evaluate the model predictions and experimental data quality. Relatively small percentage errors were detected between model predictions and experimental data. Random error estimations of experimental input data within plus or minus 5% consistently produced minimal errors in model predictions. Standard errors of means of the predicted flux control coefficients from Monte Carlo simulations were compared to the corresponding model predictions from experimental data. Model predictions of fluxes and control coefficients were smaller in EA strains (within 0.001 – 0.083) than in the WT (within 0.001 – 0.122). The chi-square distribution and Monte Carlo simulations methods for error and sensitivity analysis demonstrated the ability to detect, evaluate and possibly minimize variability between experimental data and metabolic model predictions.

Keywords: Error propagation; Model sensitivity analysis; Uncertainty.

3.2 INTRODUCTION

A metabolic flux model is a mathematical tool for describing the metabolism of microbial organisms into understandable variables that quantify the organisms' response to metabolic changes [142-144]. Metabolic flux and control analyses models were developed to evaluate carbon flux distribution patterns in *C. thermocellum* catabolism and to identify key pathway(s) that maximize ethanol production or yield. Metabolic fluxes are functions of measured cell growth rate, substrate, product concentrations (extracellular) and intracellular components (which are predicted from the extracellular fluxes). Experimental flux data and omitted relevant reactions in the model may be common sources of fundamental errors that are likely to affect the outcome of model results. Consequently, predicted fluxes (which may be sensitive to errors from measurements) from the model may misrepresent quantified parameters that describe cell physiology [101, 145]. Applying sensitivity analysis will verify model accuracy. Sensitivity analyses can identify potential problems in an algorithm or model in the absence of benchmark tests and experimental data [89]. Improved experimental procedures may be required to overcome these identified error sources.

Confidence interval analysis and Monte Carlo simulations have been identified as suitable methods to perform sensitivity analysis checks on predictive models. Confidence interval estimates determine the extent to which error in experimental data may affect the model's robustness [146, 147]. Confidence interval and chi-square distribution combined with error-weighted fitting or gaussian error propagation have also been used recently to evaluate the effects of error in some metabolic modeling methods [100, 101, 146]. Linear metabolic flux models are better suited to prokaryotes and fungi because there exists a linear relationship between metabolic and thermodynamic properties such as closed balances (element, energy or stoichiometric), achievable

equilibrium (steady reaction rates) and kinetics (cell growth rate and mass transfer). Eukaryotic cells (for example the mammalian cell) lack the necessary data to meet thermodynamic property requirements [148, 149]. Metabolic flux models derived from stoichiometric or mass balances are often linear with parameters estimated using general least square techniques [148, 150]. The least squares solutions method simplifies propagation of errors for model accuracy [148]. Kurata and co [151] discovered that models that include branched pathway reactions improve model accuracy. The model requires establishing enzyme-reaction rates and fluxes-genomics relationships relevant to the specific problem. Enzyme activities related to flux control in mutant and wild type *Escherichia coli* have shown relatively large errors in flux prediction for the mutant compared to wild [151]. Thus, augmenting a model, to include genetic modeling, requires the ability to identify the particular gene crucial for altering pathway reactions that lead to the desired product.

Predictive metabolic models require input variables (usually metabolic fluxes may be converted from experimental measurements) that are quite expensive, tedious and scarce to obtain especially for large systems [152]. Robust methods, including standard Monte-Carlo simulations (involving perturbing data) and chi-square tests have been suggested for sensitivity analyses on large scientific and engineering systems [89, 92, 103, 145, 153, 154] to minimize such problems. The methods identify key experimental data requirements, i.e., the replications required to achieve better precision [99, 155]. Continuous progress in science and technology provides mathematical modeling tools such as MATLAB, MAPLE, C++, R etc., available for simulating real-world systems including error or sensitivity analysis [102, 156, 157]. Most of these systems often have built in functions performing the sensitivity analyses.

This paper focuses on combining experimental data perturbation, chi-square distribution and Monte Carlo analyses for checking the extent to which random and

systematic errors in experimental data and model predictions influence the metabolic flux and control coefficients estimates for WT and EA *C. thermocellum* cells grown on cellobiose in continuous culture.

3.3 METHODS

Applications of inferential (chi-square distribution test) and descriptive statistical methods (experimental data perturbation and Monte Carlo simulations), were implemented to minimize variability between experimental data and model, establish model stability, and evaluate prediction accuracy and robustness in model.

3.3.1 Sensitivity Analysis by Introducing Error into the Measured Data

The model inputs of measured fluxes of cellobiose, lactate and acetate were changed by plus or minus 5%, 10% and 20% to determine the effect of potential measurement errors on the predicted ethanol fluxes. The inputs were changed one at a time while keeping the others constant at the measured value and rerunning the model. Ethanol flux predictions from these adjustments were examined and compared to the originally predicted ethanol fluxes. Figure 3-1 through Figure 3-12 present results for predicted ethanol fluxes and ethanol to acetate ratios due the changes in cellobiose, lactate and acetate.

3.3.2 Sensitivity Analysis by Chi-Square Tests

Further analysis was performed by implementing an inferential statistical test based on chi-square distribution. The chi-square statistical test is useful for determining gross errors and consistency in measurements. For a given metabolic pathway, material balances formulated at steady state is generally of the form:

$$\mathbf{N} \cdot \mathbf{v} = 0 \dots \dots \dots (1)$$

Equation (1) is reformulated into measured (m) and unknown /non-measured(n) components as:

$$\mathbf{N}_m \cdot \mathbf{v}_m = -\mathbf{N}_n \mathbf{v}_n \dots \dots \dots (2)$$

Equation (2) holds for ideal situations (i.e. there are no measurement errors). However, this may not be possible under practical conditions. Thus error terms ϵ_m and ϵ_n can be introduced to account for any measurement and predicted errors such that Equation 2 becomes:

$$\mathbf{N}_m \cdot \mathbf{v}_m + \epsilon_m = -\mathbf{N}_n \mathbf{v}_n + \epsilon_n \dots \dots \dots (3)$$

Given Equation (3), a statistical hypothesis test may be performed to establish a level of confidence that errors in model prediction are less than or equal to measurement errors using the chi-square distribution because all measured values are from the same distribution. The test was carried out by considering four (4) different cases; namely base case, scenario 1, scenario 2 and s cenario 3 defined as: Base case: input original values of acetate, cellobiose and lactate -> get predictions

Scenario 1: keep acetate and lactate constant, change cellobiose-> get predictions.

Scenario 2: keep acetate and cellobiose constant, change lactate-> get predictions

Scenario 3: keep lactate and cellobiose constant, change acetate-> get predictions

The base case hypotheses (Equation 4) and scenarios hypotheses (Equation 5, 6 and 7) are stated as follows:

$$\left. \begin{array}{l} H_0 : \epsilon_n \leq \epsilon_m \\ H_1 : \epsilon_n > \epsilon_m \end{array} \right\} \dots \dots \dots (4)$$

$$\left. \begin{array}{l} H_0 : \epsilon_n \leq \epsilon_m \mp 5\% \\ H_1 : \epsilon_n > \epsilon_m \mp 5\% \end{array} \right\} \dots \dots \dots (5)$$

$$\left. \begin{array}{l} H_0 : \epsilon_n \leq \epsilon_m \mp 10\% \\ H_1 : \epsilon_n > \epsilon_m \mp 10\% \end{array} \right\} \dots \dots \dots (6)$$

$$\left. \begin{array}{l} H_0 : \epsilon_n \leq \epsilon_m \mp 20\% \\ H_1 : \epsilon_n > \epsilon_m \mp 20\% \end{array} \right\} \dots \dots \dots (7)$$

The errors of measured values may be assumed to be normally distributed with a certain mean and variance. Uniformly distributed errors or small variations in model predictions would establish model stability (representing how reliable the model is in this case). The test statistic of the chi-square distribution in this case, estimates the probability of finding significant or non significant differences between measurement and predicted errors at a certain level of confidence. To estimate the chi-square test statistic, χ^2 , standard deviations and means of metabolite fluxes were calculated from their measured replicates and compared with values in the chi-square distribution table at both 5% and 10% probabilities (or 95% confidence and 90% confidence), where

$$\chi^2 = \sum \left[\left(\frac{[\text{metabolite}] - \mu([\text{metabolite}])}{\sigma([\text{metabolite}])} \right)^2 \right] \dots \dots \dots (8)$$

A calculated chi-square value less than the chi-square statistic from tables at a certain degree of freedom would suggest no evidence to reject the null hypothesis. The calculation of the chi-square statistic was addressed in two ways. In the first case, the replicate fluxes of acetate, cellobiose and lactate were averaged separately and their respective variances determined. The same calculations were repeated for fluxes of pyruvate, acetylCoA, and ethanol. In the second case, the replicate fluxes of acetate, cellobiose and lactate were averaged between measurement groups along with the determination of the respective variances. Again, the same calculations were repeated for fluxes of pyruvate, acetylCoA, and ethanol.

3.3.3 Sensitivity by Monte Carlo Simulation

Monte Carlo simulations were run in MATLAB 7.7.0 by assuming independently normally distributed experimental data, with means and standard deviations equal to the mean and standard error of mean for experimental data replicates. It was also assumed that errors associated with experiments were normally distributed. There were

three replicates for each experimental measurement. Standardized normal distributions of 2000 values were generated for each of acetate (A), lactate (L) and cellobiose (CB) using the following formula in MATLAB:

$$r_i = \sum_{i=1}^3 \begin{bmatrix} randn(i, 1) & 1 \\ randn(i, 2) & 1 \\ randn(i, 3) & 1 \end{bmatrix} \cdot \begin{bmatrix} SD_A & SD_L & SD_{CB} \\ \mu_A & \mu_L & \mu_{CB} \end{bmatrix}$$

(r is the simulated data point, sd is the observed standard error of mean, μ is the mean of experimental data replicates and n is the number of observations [2000 values in this case] from the standard distribution and $randn$ is the MATLAB command used for generating normally distributed values). The means and standard deviations of experimental data were compared to the means and standard deviations generated from Monte Carlo to check for similar estimates of these statistics. The acetate, cellobiose and lactate fluxes were used as inputs for predicting 2000 fluxes for each of the non-measured metabolites. The corresponding control coefficients were generated from the respective measured and predicted fluxes of metabolites and elasticity coefficients. The procedure for calculating control coefficients has been described elsewhere [73, 80, 81, 138]. Normal distribution and probability plots (from normality tests) were obtained for all Monte Carlo results (using MATLAB) to show and compare the normality of error distributions in each of the fluxes and control coefficients (Figure 3-13, Figure 3-14, Figure 3-15 and Figure 3-16). Further Monte Carlo applications may be found elsewhere [99, 158].

3.4 RESULTS AND DISCUSSION

Ethanol was used as the primary model output for evaluating the effect of errors in measured values on the model predictions.

Figure 3-1 presents the ethanol flux predicted by the MFA when the measured lactate flux was decreased 5%, 10% and 20%. Model predictions were unaffected by possible lactate flux measurement errors up to 20% change for both wild-type and ethanol adapted treatments (Figure 3-1 and Figure 3-4). This can be seen in Figure 3-1 by comparing the circle markers (representing WT in 0% ethanol). When the measured lactate value was changed by 5%, 10%, and 20%, the predicted ethanol value did not change (approx. 3.5 meC/g dcwh). Changes in acetate measurements resulted in little change in the predicted fluxes for all wild type and ethanol adapted treatments (Figure 3-2 and Figure 3-5). However, the 20% change in acetate showed relatively large effects on flux predictions compared to the corresponding 5% and 10% changes for both types of treatments. The 5% changes in measured cellobiose fluxes showed very small error effects on the predicted fluxes while noticeable error effects were observed for 10% and 20% changes in cellobiose fluxes for both wild type and ethanol adapted treatments (Figure 3-3 and Figure 3-6). Standard deviations were larger in the ethanol predictions for both 10% and 20% changes in cellobiose fluxes for ethanol adapted treatments, but this was an artifact of the method (standard deviation of input data varied with the mean, and hence standard deviation of the output data varied with the mean because the model is a linear transformation of the input data). The responses of model predictions to error were mostly affected by the 20% change in cellobiose fluxes (Figure 3-3) compared to the corresponding acetate and lactate. The predicted fluxes for all treatments may be unaffected by measurement errors due to lactate as a result of the low lactate values. Measurement errors of more than plus or minus 5% of the measured acetate and cellobiose fluxes significantly affect model predictions. Model predictions obtained within 5% of measured lactate, acetate, and cellobiose showed the least error effect thus representing the maximum level of data quality needed for model predictions.

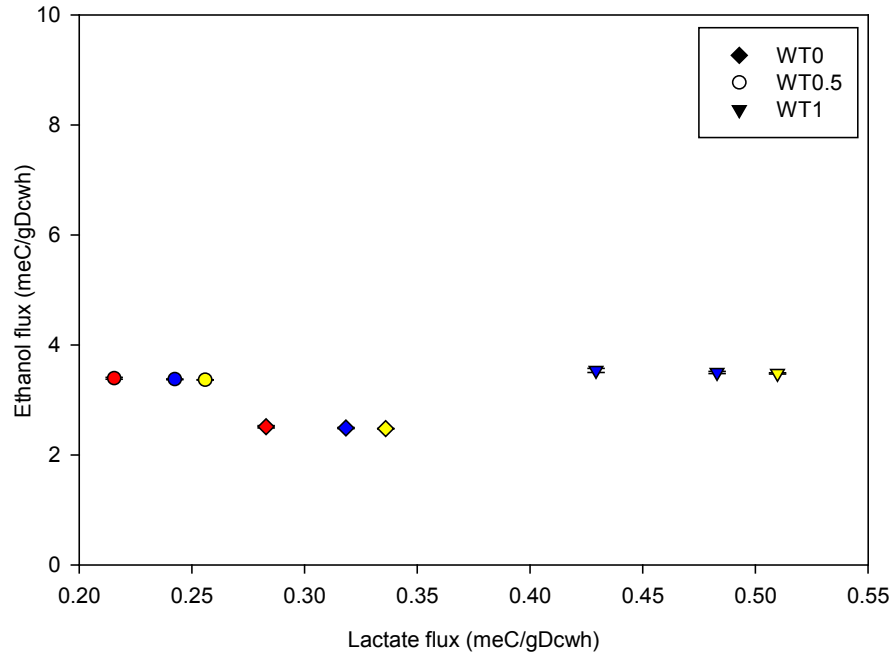


Figure 3-1: Predicted ethanol flux response to 5% (yellow), 10% (blue) and 20% (red) decreases in only lactate for exogenous ethanol treatments of 0%, 0.5% and 1% on wild –type (WT). Error bars showing sensitivity of predicted ethanol fluxes to possible errors

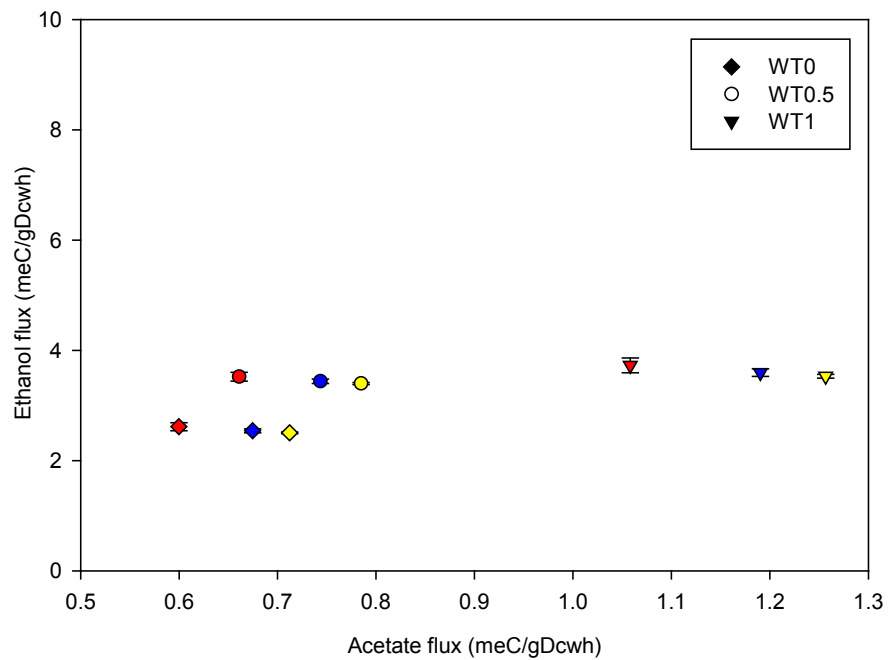


Figure 3-2: Predicted ethanol flux response to 5% (yellow), 10% (blue) and 20% (red) decreases in only acetate for exogenous ethanol treatments of 0%, 0.5% and 1% on wild –type (WT). Error bars showing sensitivity of predicted ethanol fluxes to possible errors in acetate.

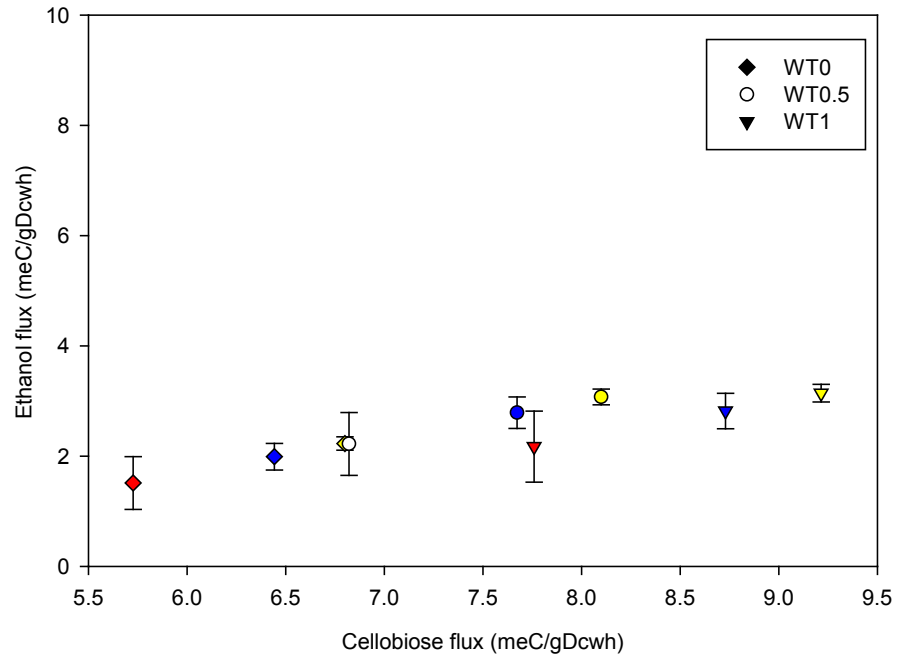


Figure 3-3: Predicted ethanol flux response to 5% (yellow), 10% (blue) and 20% (red) decreases in only cellobiose for exogenous ethanol treatments of 0%, 0.5% and 1% on wild -type (WT). Error bars showing sensitivity of predicted ethanol fluxes to possible errors in cellobiose.

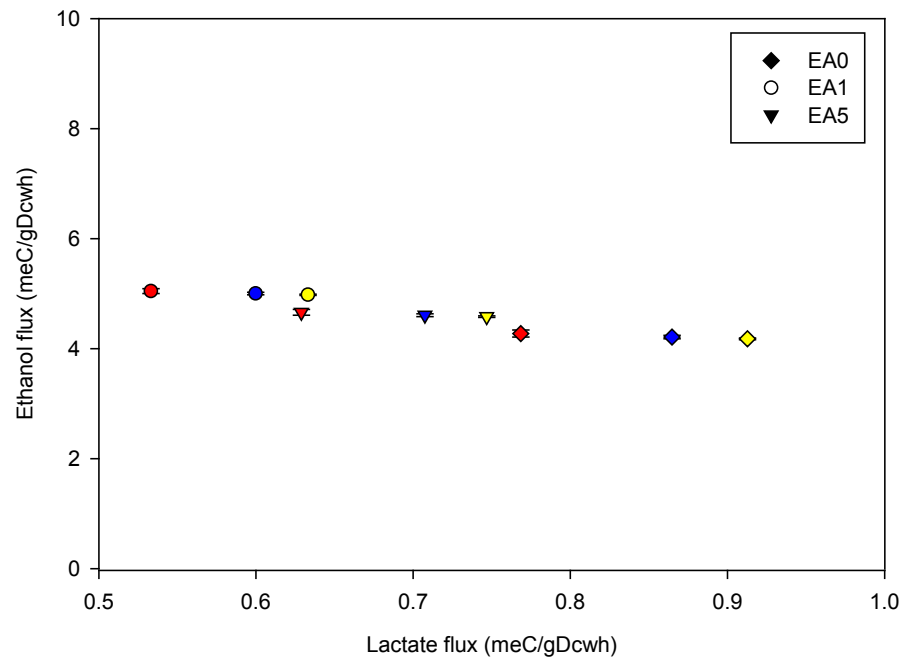


Figure 3-4: Predicted ethanol flux response to 5% (yellow), 10% (blue) and 20% (red) decreases in only lactate for exogenous ethanol treatments of 0%, 0.5% and 1% on ethanol adapted (EA). Error bars showing sensitivity of predicted ethanol fluxes to possible errors in lactate.

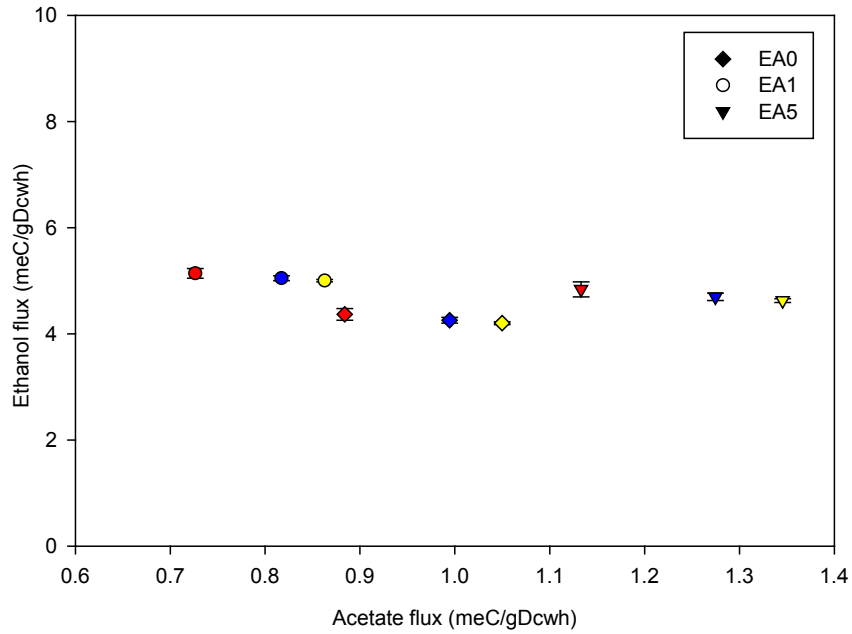


Figure 3-5: Predicted ethanol flux response to 5% (yellow), 10% (blue) and 20% (red) decreases in only acetate for exogenous ethanol treatments of 0%, 0.5% and 1% on ethanol adapted (EA). Error bars showing sensitivity of predicted ethanol fluxes to possible errors in acetate.

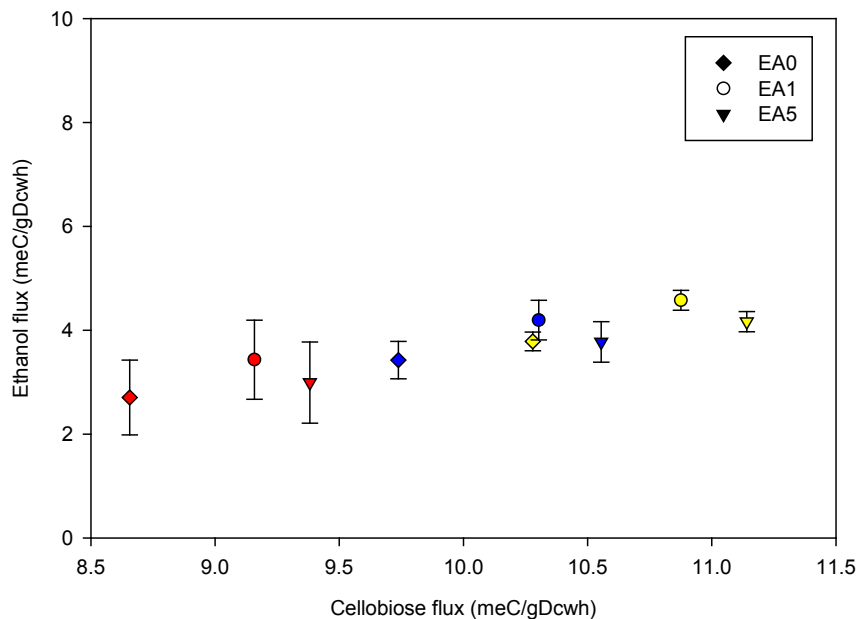


Figure 3-6: Predicted ethanol flux response to 5% (yellow), 10% (blue) and 20% (red) decreases in only cellobiose for exogenous ethanol treatments of 0%, 0.5% and 1% on wild-type (WT). Error bars showing sensitivity of predicted ethanol fluxes to possible errors in cellobiose.

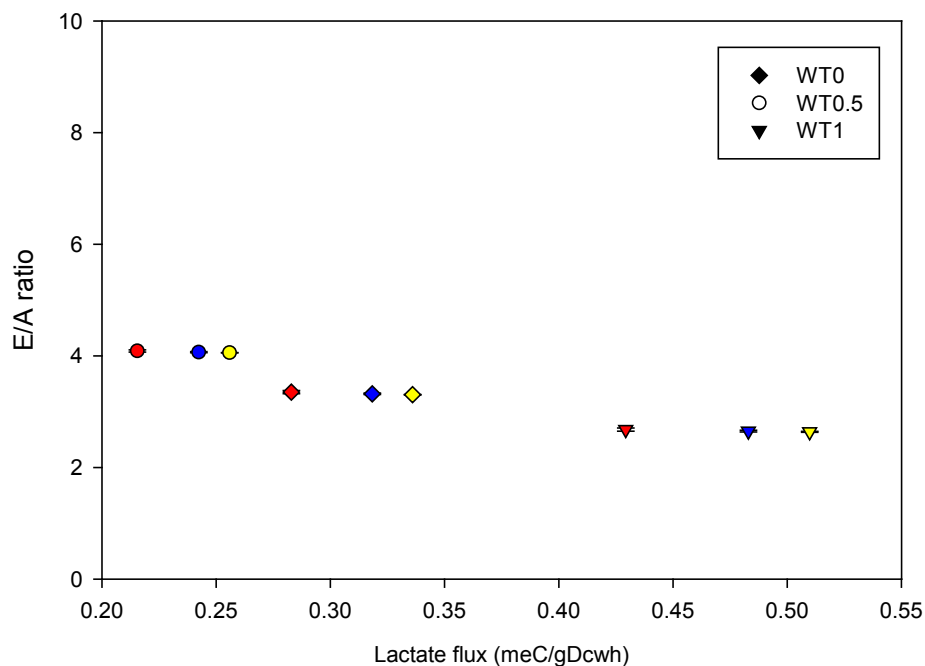


Figure 3-7: Ethanol to acetate ratio (E/A) response to 5% (yellow), 10% (blue) and 20% (red) decreases in only lactate for exogenous ethanol treatments of 0%, 0.5% and 1% on wild-type (WT). Error bars showing sensitivity of predicted ethanol fluxes to possible errors in lactate.

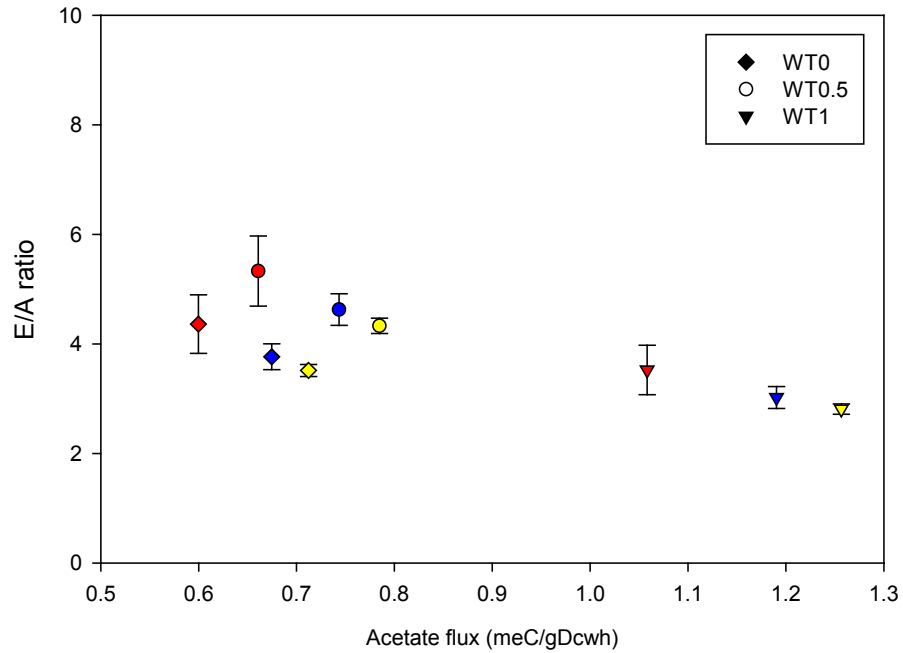


Figure 3-8: Ethanol to acetate ratio (E/A) response to 5% (yellow), 10% (blue) and 20% (red) decreases in only acetate for exogenous ethanol treatments of 0%, 0.5% and 1% on wild -type (WT). Error bars showing sensitivity of predicted ethanol fluxes to possible errors in acetate.

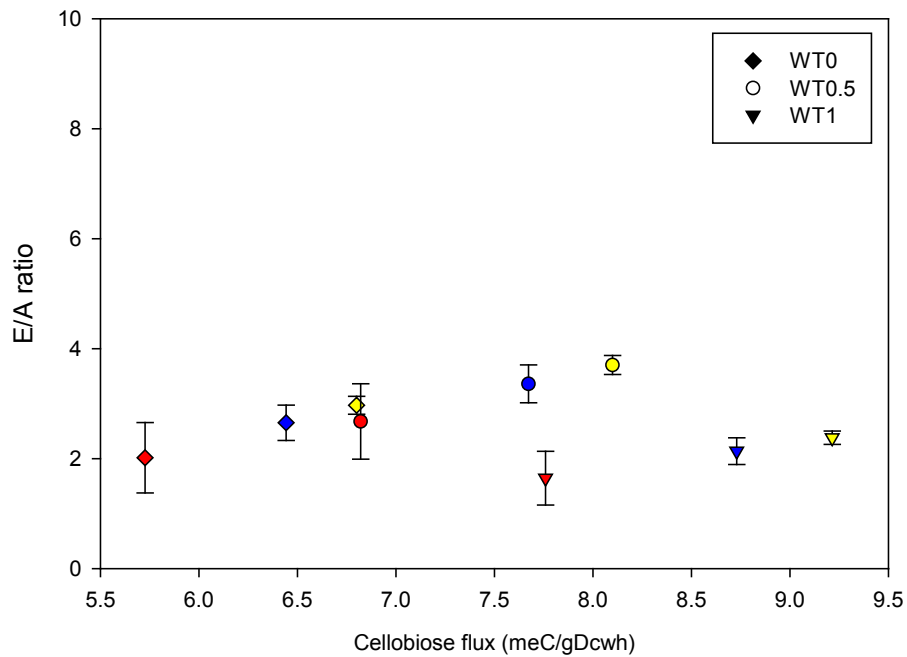


Figure 3-9: Ethanol to acetate ratio (E/A) response to 5% (yellow), 10% (blue) and 20% (red) decreases in only cellobiose for exogenous ethanol treatments of 0%, 0.5% and 1% on wild -type (WT). Error bars showing sensitivity of predicted ethanol fluxes to possible errors in cellobiose.

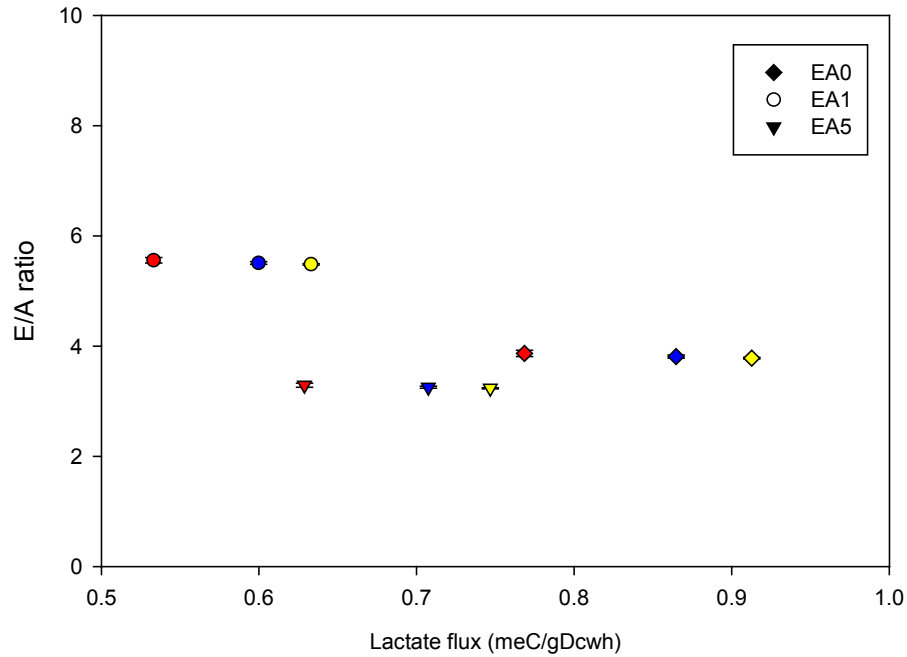


Figure 3-10: Ethanol to acetate ratio (E/A) response to 5% (yellow), 10% (blue) and 20% (red) decreases in only lactate for exogenous ethanol treatments of 0%, 0.5% and 1% on ethanol adapted (EA). Error bars showing sensitivity of predicted ethanol fluxes to possible errors in lactate.

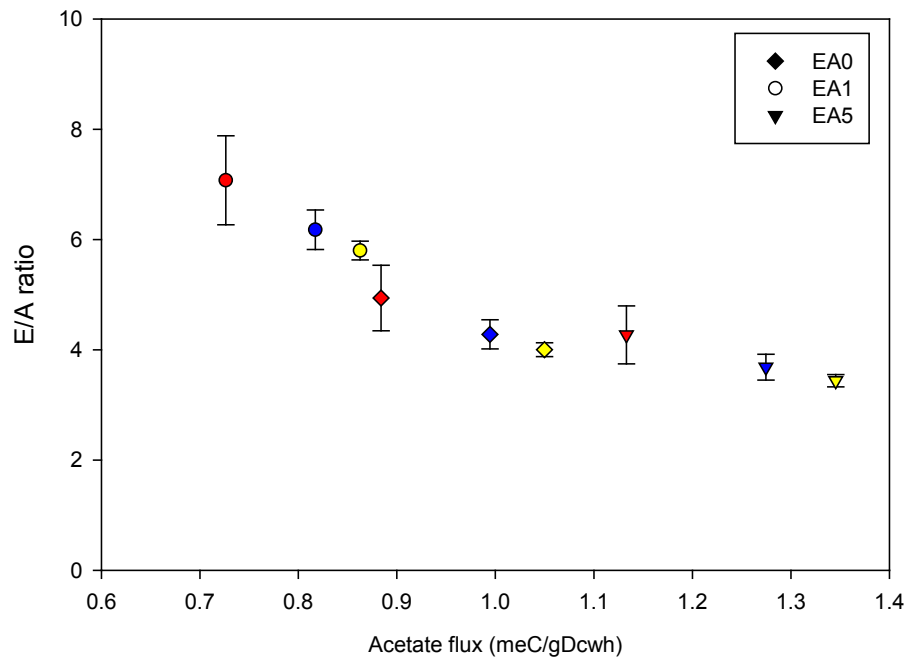


Figure 3-11: Ethanol to acetate ratio (E/A) response to 5% (yellow), 10% (blue) and 20% (red) decreases in only acetate for exogenous ethanol treatments of 0%, 0.5% and 1% on ethanol adapted (EA). Error bars showing sensitivity of predicted ethanol fluxes to possible errors in acetate.

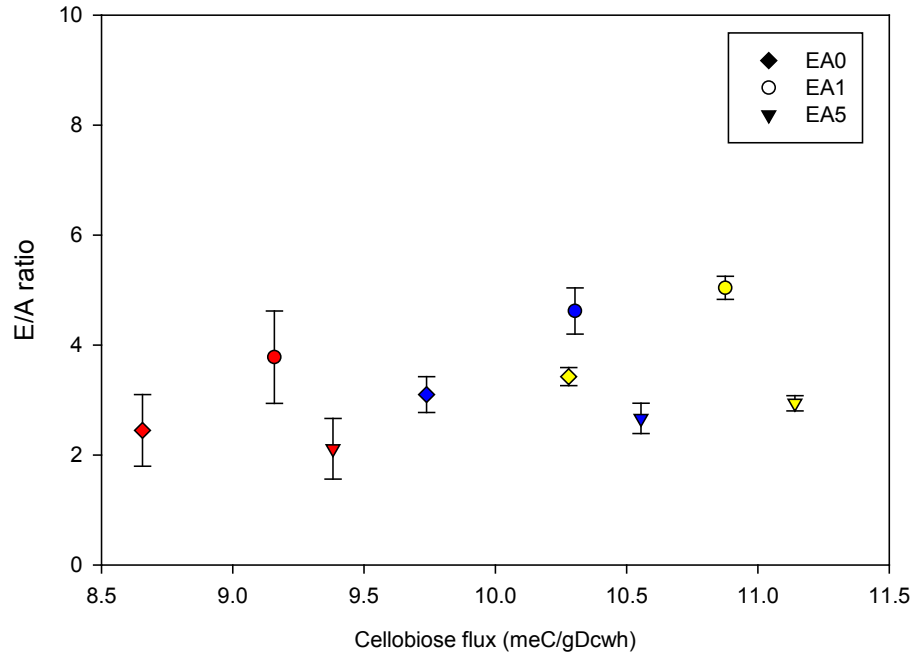


Figure 3-12: Ethanol to acetate ratio (E/A) response to 5% (yellow), 10% (blue) and 20% (red) decreases in only cellobiose for exogenous ethanol treatments of 0%, 0.5% and 1% on ethanol adapted (EA). Error bars showing sensitivity of predicted ethanol fluxes to possible errors in cellobiose

As stated earlier, chi-square test statistics were calculated for two cases. For example for the first case, in WT cells, the three replicates of cellobiose flux (in meC/gdcwh) are 7.13, 7.18 and 7.18 with mean and standard deviation, 7.163 and 0.029 respectively. Therefore,

$$X_{CB}^2 = \left(\frac{7.13 - 7.163}{0.029}\right)^2 + \left(\frac{7.18 - 7.163}{0.029}\right)^2 + \left(\frac{7.18 - 7.163}{0.029}\right)^2 = 2$$

For acetate, the replicate fluxes are 1.02, 0.61, and 0.61 with mean, 0.747 and standard deviation, 0.237. The corresponding

$$X_{ace}^2 = \left(\frac{1.02 - 0.747}{0.237}\right)^2 + \left(\frac{0.61 - 0.747}{0.237}\right)^2 + \left(\frac{0.61 - 0.747}{0.237}\right)^2 = 2$$

For lactate flux, we have replicates of 0.37, 0.37, and 0.32 with mean, 0.353 and standard deviation, 0.029. The test statistics

$$X_{lac}^2 = \left(\frac{0.37 - 0.353}{0.029}\right)^2 + \left(\frac{0.37 - 0.353}{0.029}\right)^2 + \left(\frac{0.32 - 0.353}{0.029}\right)^2 = 2$$

In the second case, for the first group of measurements the fluxes (in meC/gdcwh) were cellobiose (7.13), acetate (1.02) and lactate (0.37). The mean and standard deviation are 3.729 and 2.84 respectively. Therefore,

$$X_1^2 = \left(\frac{7.13 - 3.729}{2.84}\right)^2 + \left(\frac{1.02 - 3.729}{2.84}\right)^2 + \left(\frac{0.37 - 3.729}{2.84}\right)^2 = 2$$

For second group of measurements, the fluxes are cellobiose (7.18), acetate (0.61) and lactate (0.37) with mean, 3.864 and standard deviation, 2.72. The corresponding chi-square statistic is calculated as

$$X_2^2 = \left(\frac{7.18 - 3.864}{2.72}\right)^2 + \left(\frac{0.61 - 3.864}{2.72}\right)^2 + \left(\frac{0.37 - 3.864}{2.72}\right)^2 = 2$$

The third data set gives cellobiose flux (7.18), acetate flux (0.61) and lactate flux (0.32) with mean, 3.880 and standard deviation 2.72. Therefore,

$$X_3^2 = \left(\frac{7.18 - 3.880}{2.72}\right)^2 + \left(\frac{0.61 - 3.880}{2.72}\right)^2 + \left(\frac{0.32 - 3.880}{2.72}\right)^2 = 2$$

Since both cases gave similar χ^2 results, the second case was used to determine the χ^2 for the predicted fluxes (pyruvate, acetylCoA and ethanol), calculated as follows:

$$X_1^2 = \left(\frac{5.14 - 1.624}{4.023}\right)^2 + \left(\frac{4.77 - 1.624}{4.023}\right)^2 + \left(\frac{2.16 - 1.624}{4.023}\right)^2 = 2$$

$$X_2^2 = \left(\frac{5.2 - 1.401}{4.213}\right)^2 + \left(\frac{4.83 - 1.401}{4.213}\right)^2 + \left(\frac{2.61 - 1.401}{4.213}\right)^2 = 2$$

$$X_3^2 = \left(\frac{5.2 - 1.395}{4.24}\right)^2 + \left(\frac{4.88 - 1.395}{4.24}\right)^2 + \left(\frac{2.64 - 1.395}{4.24}\right)^2 = 2$$

Table 3-1 and Table 3-2 show the calculated test statistic together with the corresponding values from chi-square distribution tables. The chi-square distribution test showed similar variance between the measured and predicted fluxes as indicated by the same calculated chi-square (χ^2) value of 2 which was less than the test statistic at both 5% and 10% significant levels (see Table 3-1 and Table 3-2) thus, satisfying the null hypothesis. It is important to note that these analyses were performed on previously

taken off-line measurements which are typically obtained at low sampling rate which is more likely to provide better accuracy than on-line measurements.

Table 3-1: Fluxes of measured extracellular and predicted key metabolites (WT 0% ETOH)

Metabolites	Replicates			Mean	Standard Deviation	Calculated Chi-Square, X ²	X ² @ 90% From tables	X ² @ 95% From tables
	1	2	3					
Cellobiose	7.13	7.18	7.18	7.163	0.029	2	4.61	5.99
Lactate	0.37	0.37	0.32	0.353	0.029			
Acetate	1.02	0.61	0.61	0.747	0.237			
Pyruvate	5.14	5.20	5.20	5.180	0.034			
AcetylCoA	4.77	4.83	4.88	4.827	0.055			
Ethanol	2.16	2.61	2.64	2.470	0.269			

Table 3-2: Fluxes of measured extracellular and predicted key metabolites (EA 0% ETOH)

Metabolites	Replicates			Mean	Standard Deviation	Calculated Chi-Square, X ²	X ² @ 90% From tables	X ² @ 95% From tables
	1	2	3					
Cellobiose	10.57	10.34	10.82	10.577	0.240	2	4.61	5.99
Lactate	0.81	0.98	1.10	0.963	0.382			
Acetate	1.54	0.82	0.96	1.107	0.963			
Pyruvate	8.59	8.36	8.84	8.597	0.240			
AcetylCoA	7.78	7.38	7.74	7.633	0.220			
Ethanol	3.65	4.10	4.20	3.983	0.293			

Monte Carlo simulations showed little variation in model predictions compared to the corresponding model predictions from experimental measurements for all types of treatments. The same observations were made in the corresponding predicted fluxes.

Estimates of control coefficients from the Monte Carlo analysis were also not significantly different from control coefficients obtained from the fluxes of experimental measurements (appendix B). The variability in results from both Monte Carlo simulations and experimental measurements showed normal distributions for all wild type (WT) and ethanol adapted (EA) treated strains. Figure 3-13 and Figure 3-14 show normal probability plots for assessing whether our predictions come from a normal distribution using ethanol flux predictions from WT and EA respectively. More importance is attached to the ethanol results here because it was the target product for our metabolic modeling analyses. In Figure 3-15 and Figure 3-16 Monte Carlo predictions for flux control coefficients were compared to the predictions from experiments for WT and EA, respectively. Model simulations were consistent with experimental data, implying that in the absence of sufficient data and certainty (this is a big challenge in bioprocess control [152, 159]), metabolic models can be used to determine the solution spaces that accurately represent the physicochemical system.

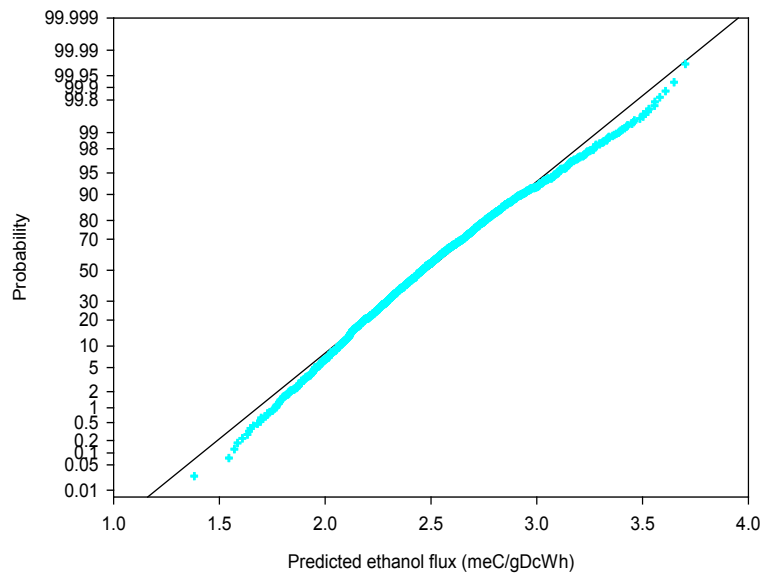


Figure 3-13: Normal probability plot for predicted ethanol fluxes - WT

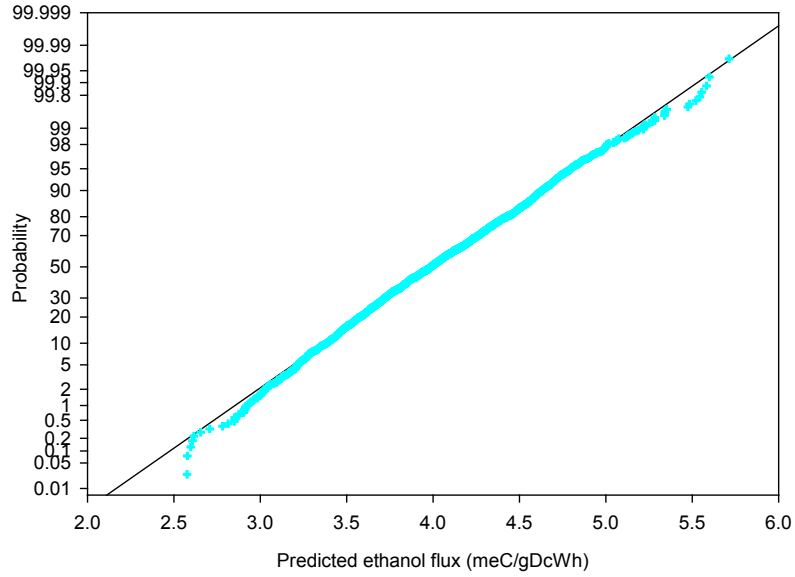


Figure 3-14: Normal probability plot for predicted ethanol fluxes - EA

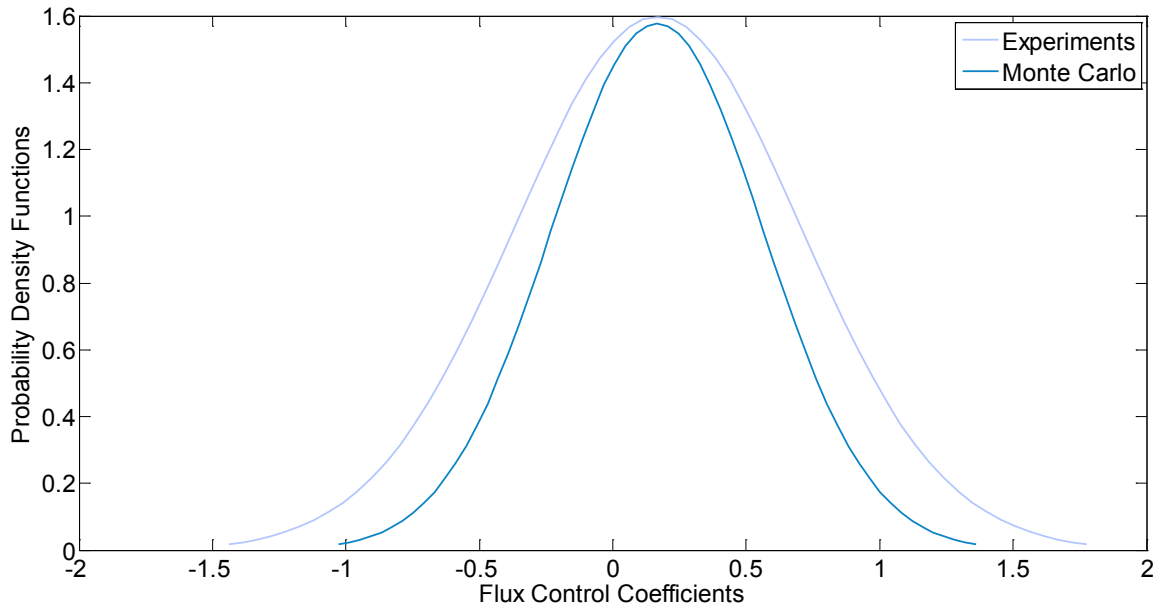


Figure 3-15: A comparison between experiments and Monte Carlo simulations by normal distribution curve in WT

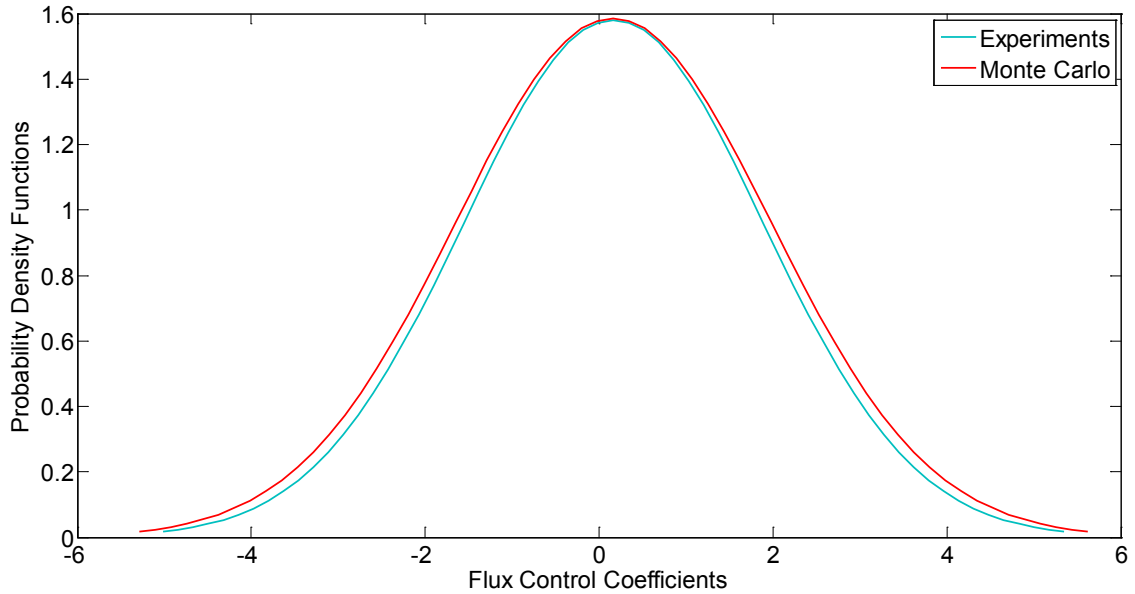


Figure 3-16: A comparison between experiments and Monte Carlo simulations by normal distribution curve in EA

3.5 CONCLUSION

Sensitivity analysis provides an evaluation of confidence in model predictions that error in measurement inputs do not lead to model instability (i.e model predictions with that have high error). Model robustness and how well it performs depends on the type of sensitivity or error analysis approach used. Experimental measurement uncertainty was found to contribute to minimal error in predicted and measured input variables subjected to perturbation changes. Statistical analytical methods for determining normal distribution of data provide reliable insight into measurement errors and model predictions. The chi-square distribution provides a good platform for normality testing. An observation that data is normally distributed indicates that experimental data and model predictions are free of systematic error, thus, enhancing model correctness. The Monte Carlo analysis is useful for approximating experimental data while ensuring minimal

errors. Monte Carlo analysis also accounts for an interdependent relationship between measured and predicted data. The overall sensitivity analyses satisfy the ultimate goal of achieving an accurate representation of the solution space for the central metabolic network of *C. thermocellum*.

CHAPTER 4 STEADY STATE MODELING OF DISSOLVED HYDROGEN GAS EFFECT ON THE METABOLISM OF WILD TYPE CLOSTRIDIUM THERMOCELLUM CELLS

4.1 SYNOPSIS

It has been experimentally demonstrated that during the conversion of cellobiose by *C. thermocellum*, increased pressure and increased dissolved hydrogen gas concentrations shift the acetate/ethanol ratio in favor of ethanol production. However the mechanism underlying this shift has not been elucidated. Flux Spectrum Analysis (FSA) is a tool for evaluating metabolic models and provides indicators of the confidence with which we can ascribe biological significance to model predictions because FSA incorporates interval bands (to avoid predicting point-wise values) in order to document uncertainties in the flux distribution. Additionally, FSA predicts reversibility constraints to partially determine the thermodynamic plausibility of the pathway flux. The catabolic pathway consisting of cellobiose conversion into acetate, biomass, ethanol, lactate, carbon dioxide, and hydrogen formed the basis of the metabolic network. Product formation as a function of dissolved hydrogen gas concentration was predicted by stoichiometric modeling of the cell based on FSA. Ethanol yields (mol ethanol/mol cellobiose) were predicted to increase from a range of 0 - 0.5 (@ 0.1MPa) to 1.5 - 2 (@ 7MPa) and 2 - 2.5 (@ 17.3MPa) under conditions of increasing pressure and hydrogen flux across all dilution rates. The model predicted an effect of even small amounts of dissolved hydrogen gas in the under elevated pressure on *C. thermocellum* product selectivity. Based on the model predictions, it was determined that as high as 3 - 3.5 mol ethanol/mol cellobiose can be obtained when hydrogen flux is maintained below 4.81 mM/hr (optimum hydrogen flux) with pressure increased to 17.3MPa. The predicted range of ethanol and acetate yields under conditions of dissolved hydrogen gas

concentration and hydrostatic pressures agreed with the corresponding experimental observations for ethanol and acetate yields. The model was used to quantify the influence of dissolved hydrogen on the cofactor - metabolite relationships which partially regulate *C. thermocellum* catabolism.

4.2 INTRODUCTION

Several studies have been conducted to determine the influence of dissolved hydrogen gas on the metabolism of fermentative anaerobes. Hydrogen gas is produced in the cell from reversible oxidation reactions involving NAD(P)H/NAD(P). Additionally, hydrogen coupled with high partial pressure greatly impacts the oxidation of cofactor Nicotinamide adenine dinucleotide (NADH) and limits acetate production [44, 160-164]. Therefore the concentration of hydrogen gas affects the direction of the oxidation reactions, which in turn affect the fermentation product distribution. The main fermentation products, including acetate, lactate, and ethanol, are derived from pyruvate which is formed as a result of NADH/NAD re-oxidation. Thus the re-oxidation of NADH/NAD forms the core of most fermentation processes. Gibbs free energy changes (ΔG) due to hydrogen partial pressure control the direction of this reaction. Therefore according to Equation 1 which describes this process (as defined in Rodriguez et al. ([44]), an increase in the hydrogen partial pressure will increase the NAD(P)H/NAD (P) ratio in the metabolic pathway. As a result of the increased partial pressure of hydrogen, acetate formation is inhibited [38, 44, 165-168].

$$\frac{\text{NADH}}{\text{NAD}} = P_{\text{H}_2} \cdot 10^{\text{pH}_{\text{int}}} \cdot \exp\left(\frac{\Delta G_{\text{H}}^{\circ} - \Delta G_{\text{min}}}{R \cdot T}\right) \text{----- (1)}$$

Where pH_{int} is intracellular pH, ΔG_{min} is minimum Gibbs energy change required by the reaction (kJ/mol), ΔG_H° is the Gibbs free energy change of the hydrogen production path from NADH/NAD (kJ/mol), R is the gas constant ($JK^{-1}mol^{-1}$), T is the temperature (K) and P_{H_2} is the partial pressure of hydrogen.

Metabolic parameters including growth rate, product yield and selectivity have been reported to be influenced by dissolved gas concentrations (hydrogen or carbon dioxide) under elevated pressures [38, 169]. Experimental observations of cellobiose fermentation by *C. thermocellum* under conditions of elevated hydrogen partial pressures have shown product shifts towards ethanol production [34, 38]. Significant research interests in large scale ethanol production by *C. thermocellum* from cellulosic biomass have led to studying cell metabolism at both the phenotypic and genomic level using metabolic models in addition to laboratory studies. Measurements of metabolites, especially intracellular metabolites in anaerobic fermentation (including gases) pose a challenge because of possible culture contamination issues and difficulties involved in measuring the controlled variable(s), thus leading to measurement uncertainties. To simplify the biotechnological process, metabolic models have been utilized to reduce measurement tasks, predict the microbial metabolic profile and optimize process control.

Traditional metabolic flux analysis (MFA) is useful for describing flux distributions in metabolic network systems. The method depends solely on stoichiometry and the amount of available measured data for flux analysis. MFA has consistency limitations due to uncertainty in measurement data, lack of sufficient data, and mathematical problems with the set of metabolic flux equations, namely redundancy, determinancy, calculability, and balanceability (causing redundancy) of fluxes [68, 150, 152]. Recent studies have shown the importance of applying other constraints to obtain more reliable flux estimates. Metabolic modeling methods that implement constraints include flux-sum

analysis, flux spectrum analysis (FSA) or a probability distribution approach called possibilistic metabolic flux analysis (PMFA) of the metabolic network [93, 152, 170]. Flux-sum analysis (using a metabolite-centric approach by implementing mixed integer programming) accounts for metabolite turnover rates and imposes nonlinear constraints which are otherwise absent in MFA. The method is capable of capturing key metabolite functions that relate target products to the phenotypic properties of the biotechnological process. The method is based on mixed integer programming [170] compared to the MFA, FSA and PMFA which use linear programming.

The flux spectrum analysis applies an interval approach to MFA. Thermodynamic principles pertaining to reversibility of reactions are also applied in this method. Linear programming is used to obtain the solutions. The flux-spectrum method provides time-interval estimates of fluxes even in the absence of sufficient data (for example during the transition period after the cultivation is perturbed). Flux predictions can be obtained for determined, underdetermined and overdetermined systems. Consistency and uncertainty in data are also accounted for by the flux spectrum approach. PMFA is a more flexible and efficient version of the flux spectrum approach as it is capable of handling large-scale metabolic networks [68, 152]. Further details on flux-sum analysis, FSA and PMFA are available in the literature [93, 152, 170].

FSA was used in this study to produce ranges/bands of feasible estimates of metabolite activities and flux distributions to reflect measurement and prediction uncertainties. The aim of this study was to develop a steady-state metabolic model using the flux spectrum approach of metabolic flux analysis to predict ethanol and acetate flux responses to changes in the presence of dissolved hydrogen concentrations under anaerobic continuous culture fermentation of cellobiose by *C. thermocellum*.

4.3 MATERIALS AND METHODS

4.3.1 Experimental Data

Experimental data for offline measured extracellular metabolites from continuous culture growth of *C. thermocellum* on cellobiose under conditions of pH 6.7, temperature 60°C and varying hydrostatic pressure conditions of 0.1MPa, 7MPa and 17.3MPa [38] was used to validate model. Measured concentrations of cellobiose (mM), acetate (mM), ethanol (mM), lactate (mM), and biomass (or cell density in OD (600 nm) converted to g/L) at 0.05/hr, 0.21/hr and 0.32/hr for all pressure conditions were available from the literature [38]. Maximum solubility values (mM) of dissolved hydrogen gas were determined by the temperature dependent Henry's law for 0.1MPa, 7MPa and 17.3MPa and assumed to be always the case in the model [38]. The concentrations of the metabolic products (acetate, lactate and acetate) and substrate (cellobiose) consumption (mM) were converted to fluxes as functions of cell density (g/l) and dilution rates for the modeling by dividing the concentration by the total fermentation time elapsed at the sampling time and the cell density when the sample was taken. Hydrogen fluxes were calculated as functions of cell physical properties (cell diameter and length) and Henry's law at 60°C. Maximum solubilities of hydrogen at each pressure are given in Table 4-1. Standard deviations associated with acetate, ethanol, and lactate measurements were given and thus incorporated into the measured fluxes [38]. For our modeling purposes, the accumulation of glycogen was assumed to be very small (hence a flux of 0.005mM/hr was assumed) because it is typically near zero values when constant limited cellobiose concentration is fed into the culture and thus very low contribution to carbon recovery in cellulolytic clostridia [163, 171, 172]. Detailed flux calculations may be found in appendix C.

Table 4-1: Selected experimental data (measured concentrations of metabolites) on pressurized continuous culture growth of *C. thermocellum* on cellobiose from literature (Bothun et al. 2004)

Parameter	0.1MPa	7MPa	17MPa
	<i>0.05/hr dilution rate^e</i>		
Biomass conc (g/l) ^b	0.450	0.2625	0.1500
Residual cellobiose (mM) ^c	0.142	0.192	0.042
Acetate produced (mM) ^a	20.2 ± 0.7	8.5 ± 1.6	7.4 ± 0.3
Ethanol produced (mM) ^a	1.0 ± 0.3	12.2 ± 2.0	17.6 ± 3.5
Lactate produced (mM) ^a	1.0 ± 0.2	2.0 ± 0.5	0.9 ± 0.3
Maximum solubility of hydrogen (mM) ^f	0.7	50.9	130.4
	<i>0.15/hr dilution rate^e</i>		
Biomass conc (g/l) ^b	0.500	0.3000	0.1875
Residual cellobiose (mM) ^c	0.19	0.100	0.150
Acetate produced (mM) ^a	14.5 ± 1.2	10.2 ± 0.4	8.8 ± 1.4
Ethanol produced (mM) ^a	2.9 ± 1.6	16.5 ± 0.2	17.4 ± 1.3
Lactate produced (mM) ^a	1.0 ± 0.2	0.4 ± 0.2	0.9 ± 0.5
Maximum solubility of hydrogen (mM) ^f	0.7	50.9	130.4
	<i>0.21/hr dilution rate^e</i>		
Biomass conc (g/l) ^b	0.525	0.350	0.2500
Residual cellobiose (mM) ^c	0.017	0.317	0.767
Acetate produced (mM) ^a	14.1 ± 0.3	9.5 ± 0.2	8.2 ± 1.4
Ethanol produced (mM) ^a	4.4 ± 1.3	15.0 ± 1.7	16.6 ± 2.1
Lactate produced (mM) ^a	1.2 ± 0.2	0.4 ± 0.2	0.4 ± 0.2
Maximum solubility of hydrogen (mM) ^f	0.7	50.9	130.4
	<i>0.32/hr dilution rate^e</i>		
Biomass conc (g/l) ^b	0.550	0.400	0.1500
Residual cellobiose (mM) ^c	0.017	0.042	1.942
Acetate produced (mM) ^a	12.6 ± 0.3	10.1 ± 0.8	7.4 ± 0.3
Ethanol produced (mM) ^a	4.6 ± 0.5	16.1 ± 0.7	10.4 ± 0.8
Lactate produced (mM) ^a	0.9 ± 0.2	0.4 ± 0.3	0.2 ± 0.1
Maximum solubility of hydrogen (mM) ^f	0.7	50.9	130.4
Cellobiose feed (mM) ^d			
	5.84	5.84	5.84

a ± standard deviations from mean experimental measurements

b, c values were read from graph

d Constant cellobiose feed (converted from the 2g/l cellobiose feed given) at all pressures

e For convenient comparison between pressures, dilution rates 0.16 and 0.15 were assumed equal. The assumption was made for dilution rates 0.20 and 0.21

f Maximum solubility of dissolved hydrogen gas for each pressure

4.3.2 Central Metabolic Network of *Clostridium thermocellum*

Estimates of flux distributions as a function of dissolved hydrogen gas and cell physical properties (diameter and length) were predicted from a metabolic model based on a simplified *C. thermocellum*'s catabolic pathway (Figure 4-1).

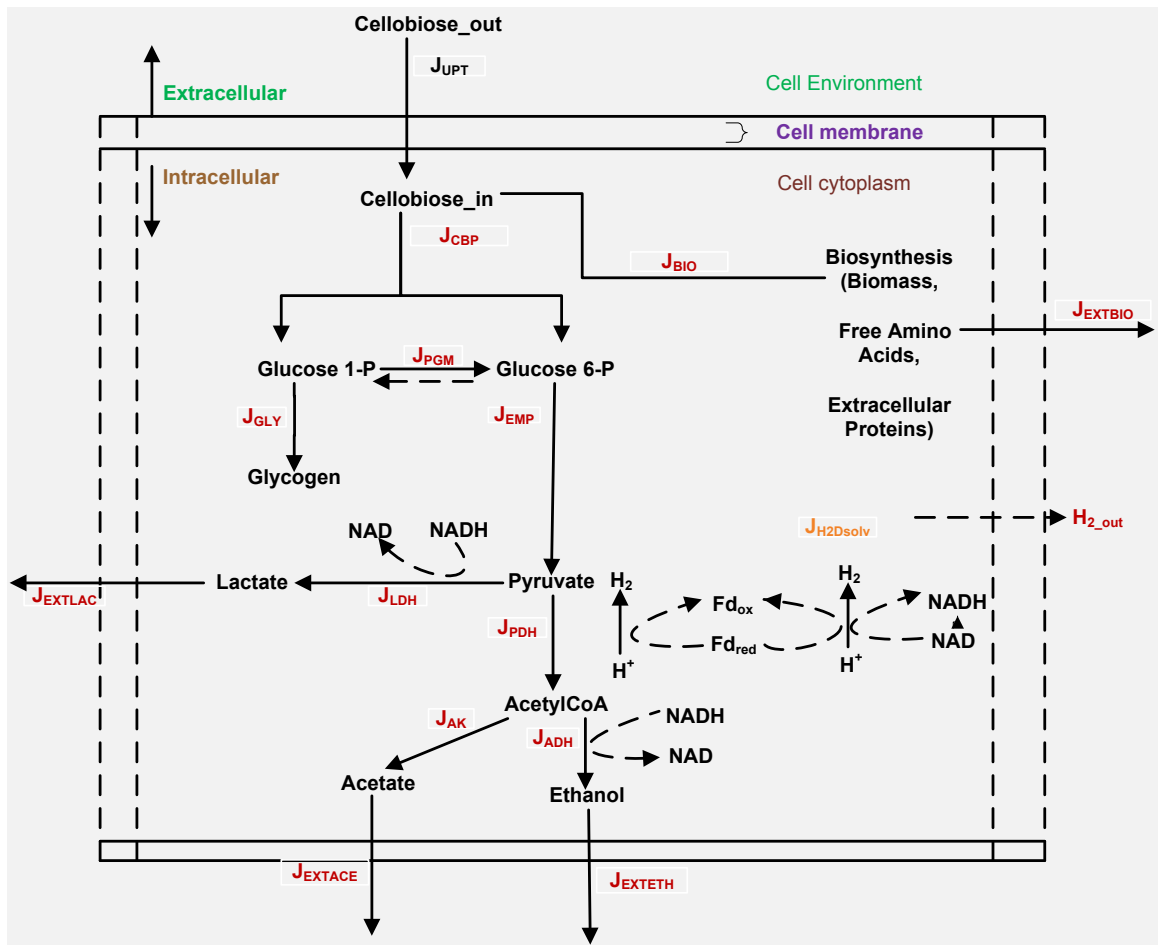


Figure 4-1: Simplified glycolytic pathway of *C. thermocellum*. J_{UPT} : Cellulose available for uptake (Cellulose_out), Intracellular cellulose (J_{CBP} : consumed; Cellulose_in), Hydrogen inside cell (environment; $J_{H2Dsolv}$), Extracellular production of acetate, ethanol and lactate denoted by J_{EXTACE} , J_{EXTETH} and J_{EXTLAC} respectively.

4.3.3 Metabolic Flux Analysis Using Flux Spectrum Approach

A stoichiometric matrix (15 x 21), N was generated from the simplified metabolic network shown in Figure 4-1, corresponding to 15 intracellular metabolites and 21 fluxes (i.e. 21 reactions). By letting u represent the vector containing all fluxes, a pseudo-steady state equation was formulated as:

$$N \cdot u = 0 \quad (1)$$

N represents the overall stoichiometric matrix of the network. Equation (1) was partitioned into measured and non-measured fluxes and rearranged such that the unknown fluxes preceded the known fluxes [12] as shown in equation (2).

$$\mathbf{N}_m \cdot \mathbf{u}_m + \mathbf{N}_n \cdot \mathbf{u}_n = \mathbf{0} \quad (2)$$

N_m and u_m denote the stoichiometric matrix and flux vector corresponding to measured fluxes respectively. N_n and u_n denote corresponding matrix and vector for non-measured fluxes respectively. However, the flux spectrum approach requires constrained solutions to maximum and minimum values based on Equation 2 as follows:

$$\begin{aligned} & \text{Min } u \geq 0 \\ & \text{s.t} \\ & \mathbf{N}_m \cdot \mathbf{u}_m = - \mathbf{N}_n \cdot \mathbf{u}_n \quad (3) \\ & \text{Max } u \geq 0 \\ & \text{s.t} \\ & \mathbf{N}_m \cdot \mathbf{u}_m = - \mathbf{N}_n \cdot \mathbf{u}_n \end{aligned}$$

The method is better understood by illustrating with a simple example. Figure 4-2 shows a hypothetical metabolic network which involves the uptake of metabolite A and production of metabolites C, D, and E. A, C, D and E are extracellular metabolites whereas B and C are intracellular metabolites. Mass balance at steady state (based on the MFA concept) is applied at nodes B and C.

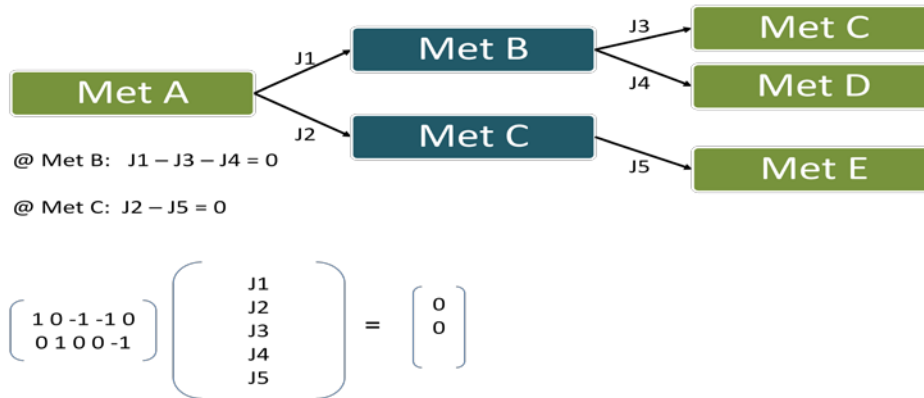


Figure 4-2: A hypothetical metabolic network for illustrating the FSA method

Assuming J_1 , J_2 and J_4 are measured, N_m , u_m , N_n and u_n , according to Equations 1 and 2 are determined from the network as:

$$N_m = \begin{bmatrix} 1 & 0 & -1 \\ 0 & 1 & 0 \end{bmatrix},$$

$$N_n = \begin{bmatrix} -1 & 0 \\ 0 & -1 \end{bmatrix}$$

$$u_n = \begin{pmatrix} J_3 \\ J_5 \end{pmatrix}$$

$$u_m = \begin{pmatrix} J_1 \\ J_2 \\ J_4 \end{pmatrix}$$

This partition is useful even in FSA for convenient arrangement of the stoichiometric matrix in order of unmeasured and then measured metabolites. This way, the input fluxes will be represented in the latter columns of the matrix N and indexing for programming becomes easier. In this case, the rearranged N becomes:

$$N = \begin{bmatrix} -1 & 0 & 1 & 0 & -1 \\ 0 & -1 & 0 & 1 & 0 \end{bmatrix}$$

A constraint is set assuming that all fluxes are irreversible. Once the stoichiometric matrix is generated, FSA is initiated by defining uncertainties within which reasonable

results are expected to provide high degree of confidence. Let us assume measurement uncertainty within 5% (relative error) of experimental data, (just an example to illustrate the FSA concept). However, the best case scenario is to define maximum and minimum flux vectors by mixing absolute and relative error tolerance to avoid boundary problems with near zero measurements. For example, if one of the input fluxes is 0.15mM/hr and is within $\pm 0.05\text{mM/hr}$ (absolute error, denoted by abserr), and the relative error (relerr) is defined as 5%, the product of the flux and relative error (i.e. $0.15 \times \text{relerr}$) gives 0.0075mM/hr which is less than the absolute error so the maximum and minimum of the flux are calculated as $0.15\text{mM/hr} \pm 0.05\text{mM/hr}$. Assume another flux is 2mM/hr and is also within $\pm 0.05\text{mM/hr}$, then the product of the flux and relative error ($2 \times \text{relerr}$) gives 0.1mM/hr which is greater than the absolute error. In this case, the maximum and minimum of the flux are defined as $2\text{mM/hr} \pm 0.1\text{mM/hr}$. At this stage, the problem may be solved using any programming language to perform the flux spectrum analysis. Using MATLAB, a function (named vspectrumCb_opt and given in appendix C) was written to automatically solve Equation 3 [68].

The estimated maximum and minimum flux vectors are passed to this function to solve the example problem.

```
clear all
clc

%% Stoichiometric Matrix
N=[-1  -1  0  1  0;
    0  0  -1  0  1];
%% All fluxes assumed to be irreversible
irrev=[ones(1,5)];
%% Indexed measured fluxes
ind= [3, 4, 5];

%% assumed vector of measured data for the known fluxes
J1 = 0.3 ; J2 =0.08 ; J4=0.7 ;

%% assuming +/- 5% uncertainty in measurements
%%mixed relative and absolute error tolerance
a_max=max(0.4, J1*1.05);
a_min=min(0.2, J1*0.95);
```



```

[a_min a_max];

b_max=J2*1.05;
b_min=J2*0.95;
[b_min b_max];

c_max=max(0.8,4*1.05);
c_min=min(0.3,J4*0.95);

Jm_max= [a_max b_max c_max ]';
Jm_min= [a_min b_min c_min]';

% Initializing resulting flux spectrum
Rmin=[];
Rmax=[];

for i=1:length(J1)
    options=optimset('LargeScale','off','Simplex','on');
    [J_mina,J_maxa,flag] =
vspectrumCb_opt(N,irrev,ind,Jm_min(:,i),Jm_max(:,i),options);
    if exist('Rmin','var')
        Rmin=[Rmin J_mina];
        Rmax=[Rmax J_maxa];
    else
        Rmin=[];
        Rmin=[J_mina];
        Rmax=[J_maxa];
    end

end

end

%% plot results
figure()
%% To calculate midpoint, lower and upper values of each flux.
J_midpoint=(Rmax+Rmin)/2;
J_lower=J_midpoint-Rmin;
J_upper=Rmax-J_midpoint;

%% Errorbar Plot.
h3= errorbar(1:5,J_midpoint,J_lower,J_upper,'>','LineWidth',2,
'Color', [ 1 0 1]);
hold on;
%% Measured data plot differentiated by color.

h2=errorbar([3;4;5],[J_midpoint(3);J_midpoint(4);J_midpoint(5)],[J_lower(3);J_lower(4);J_lower(5)],[J_upper(3);J_upper(4);J_upper(5)],'ob','LineWidth',2);
xlabel('Flux Index'),ylabel('Flux Value'),grid
set(gca,'XTick',[1 2 3 4 5])
set(gca,'XLim',[0.5 5.5])
set(gca,'YLim',[0 1])
set(gca,'FontSize',11);

```

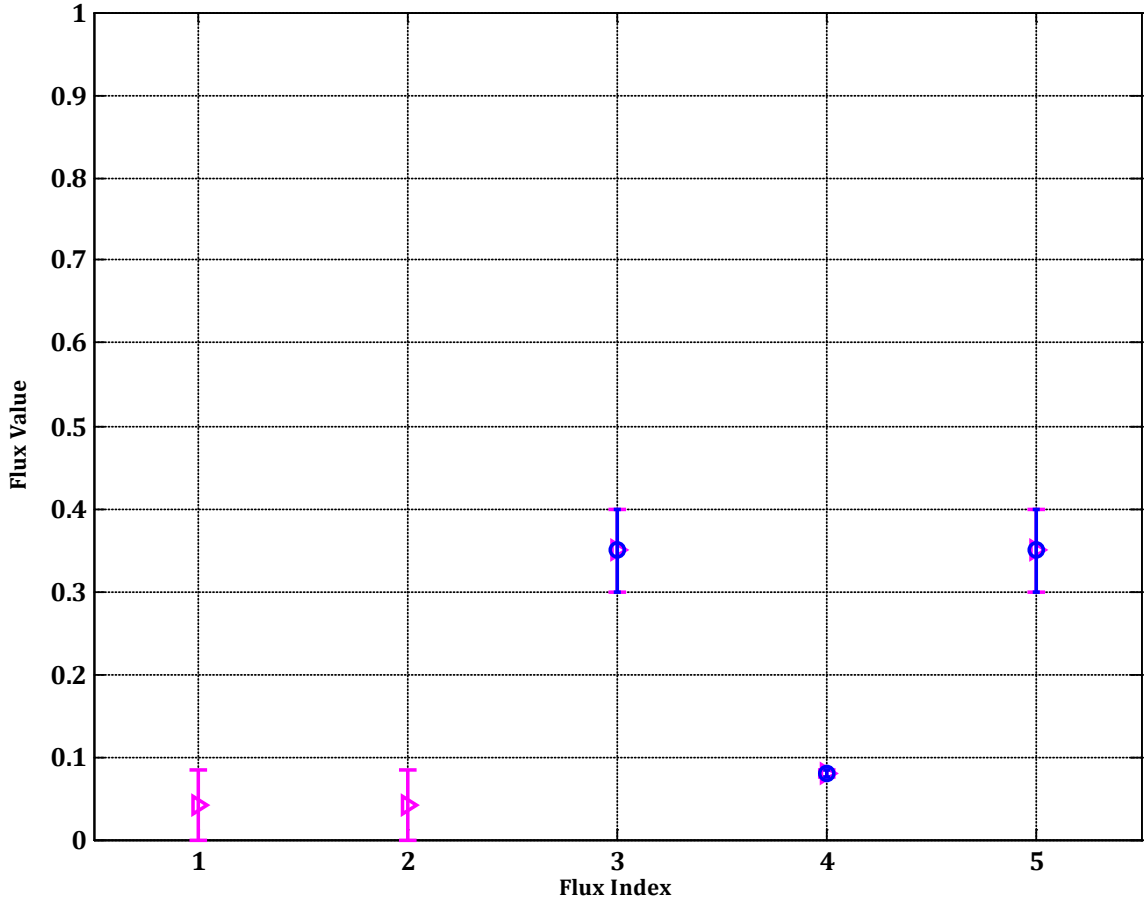


Figure 4-3: Plot of results for above example – the intervals denoted by blue represents measured inputs and the intervals denoted by magenta represent predicted fluxes of Met C and Met E.

Figure 4-3 shows the maximum, mean and minimum possible flux range/spectrum (within +/- 5%) for both measured (inputs) and predicted fluxes. The narrowly observed intervals of predicted fluxes indicate that any uncertainties in the measured inputs may have little or no impact on prediction uncertainties.

For this study, in order to model hydrogen at atmospheric pressure mass balances for both liquid and gas phases were required. At elevated pressures (7MPa and 17MPa), the system required only a liquid phase balance because the experimental conditions provided no headspace in which gaseous hydrogen could partition. The method for estimating liquid-to-gas mass transfer in anaerobic processes given in the

literature [173] was modified and applied to the hydrogen balance for only the liquid phase when there was no headspace (and therefore no gaseous hydrogen) when the system was hydrostatic. The rate of change of hydrogen was defined as:

$$\frac{dH}{dt} = \text{Biological rate} + KLa([H_2]^*) \quad (4)$$

Where KLa is the volumetric transfer coefficient (hr^{-1}) for hydrogen and $[H_2]^*$ is the solubility of hydrogen (mM). The biological rate was assumed to be represented by the pyruvate: ferredoxin oxidoreductase flux branching off the pyruvate node toward FdH_2 and subsequently toward H_2 with a stoichiometric ratio of 2:1 between Fd and H_2 respectively. The effect of hydrogen on catabolism in the model is represented by J_{pto} . The gas phase balance (mainly involving volumetric gas production rate and gas partial pressure) was added to only atmospheric pressure conditions and in this case is defined as:

$$\frac{dH}{dt} = - \left(\frac{V_l}{V_g} KLa([H_2]^*) \right) - D \frac{P}{RT} \quad (5)$$

Where D is the dilution rate (hr^{-1}), P is the partial pressure of hydrogen gas (Pa), R is the universal gas constant ($8,314 \text{ Lmol}^{-1}\text{K}^{-1}\text{Pa}$), V_l is the volume of reactor (ml) and V_g is the volume of gas (ml). In addition to the hydrogen and cofactor (NADH/NAD) balances, intracellular cellobiose, glucose-1-phosphate, glucose-6-phosphate, pyruvate, and AcCoA were considered to be the key branch points in the catabolic pathway at which the stoichiometric balances were obtained. Stoichiometric balances for intracellular fluxes of cellobiose, ethanol, lactate and acetate were linked to their corresponding extracellular components in order to reduce the system's degrees of freedom (i. e. to minimize under-determinancy).

In validating the model with Bothun et al. (2004) data, it was taken into account that hydrogen was produced in both liquid and gas phases at atmospheric pressure but remained in the liquid phase only at elevated pressures. Thus, only Equation 4 was used

when modeling data for higher pressures (7MPa and 17MPa) because there is no H₂ in the headspace in a hydrostatic system.

The stoichiometric matrix, N was generated in MATLAB using traditional MFA. This work combines MFA analysis that checks matrix sensitivity, determinancy, redundancy, balanceability and calculability with an adapted previously described FSA model for estimating the flux distributions. Further details to the FSA solution using the procedure described by [68] in MATLAB is available in appendix C. The solutions to flux vector were optimized through linear programming in MATLAB's optimization toolbox. Even though one can assume reversibility for any flux, for this case, fluxes of pyruvate ↔ lactate; glucose-1-phosphate ↔ glucose-6-phosphate; and NADH ↔ H₂ reactions were assumed to be exceptions to the irreversibility constraint of fluxes set in the model because these reactions are capable of proceeding in either direction [45, 164, 174]. Redox balances (O/R) were checked to ensure that the fermentation was balanced. "Available" hydrogen balance, O/R ratio and carbon balance constituted the redox balance checks using cellobiose, acetate, lactate, ethanol carbon dioxide, hydrogen and biomass. The number of carbons and hydrogen in each of these compounds were determined and recorded. For each corresponding flux of a compound, the O/R ratios were calculated from the oxidation states of the elements making up the compound. The fluxes were multiplied to their corresponding O/R values. The number of hydrogen atoms present in each compound was also determined and multiplied by their corresponding fluxes. Carbon equivalents of the fluxes were estimated as the product of the number of carbons and fluxes.

4.4 RESULTS

Cellobiose, hydrogen, lactate, biomass and glycogen fluxes were defined as independent variables (i. e. used as model inputs) while ethanol and acetate fluxes were predicted along with other intracellular metabolites including the NADH flux for the reversible NADH/NAD reaction. Glycogen flux was assumed to be 0.005mM/hr because it is almost negligible. Product yields from cellobiose consumed were also calculated to determine sensitivity of the products' distribution to changes in pressure. Using a $\pm 20\%$ uncertainty band, the predicted flux for ethanol and acetate fluxes generally provided estimates consistent with experimental data. Predicted ethanol yields were higher than the corresponding acetate yields at elevated pressures (> 0.1 MPa). As an example, Table 4-2, Table 4-3, and Table 4-4 show model predictions of ethanol and acetate compared to experimental data for all pressures (0.1MPa, 7MPa and 17.3MPa) 0.05/hr dilution rate.

Table 4-2: Predicted ethanol and acetate fluxes versus their measured fluxes for 0.05hr^{-1} at 0.1MPa

Model			Experiment	
(mM/hr)	Max	Min	Value	Std
Ethanol	0.067	0.0	0.05	± 0.015
Acetate	1.129	1.039	1.01	± 0.035

Table 4-3: Predicted ethanol and acetate fluxes versus their measured fluxes for 0.05hr^{-1} at 7MPa

Model			Experiment	
(mM/hr)	Max	Min	Value	Std
Ethanol	0.856	0.265	0.64	± 0.1
Acetate	0.748	0.00	0.43	± 0.08

Table 4-4: Predicted ethanol and acetate fluxes versus their measured fluxes for 0.05hr⁻¹ at 17MPa

Model			Experiment	
(mM/hr)	Max	Min	Value	Std
Ethanol	1.158	0.637	0.88	±0.175
Acetate	0.505	0.00	0.37	±0.08

4.4.1 Redox Balance

Table 4-5: Fermentation equation balance, hydrogen balance and carbon recovery estimates

Compound	Carbon	Hydrogen	Flux (mmol/Lhr)	Oxidation/Reduction (O/R)	O/R (mmol/Lhr)	Available H	Available H (mmol/hr)	meC/Lh
Cellobiose	12	22	0.34	0	0	44	14.960	4.080
Acetate	2	4	1.08	0	0	8	8.672	2.168
Lactate	3	6	0.05	0	0	12	0.600	0.150
Ethanol	2	6	0.03	-2	-0.0668	12	0.401	0.067
CO ₂	1	0	1.08	2	2.16	0	0.000	1.080
H ₂	0	2	1.51	-1	-1.51	2	3.020	0.000
Biomass (C ₅ H ₇ O ₂ N)	4	7	0.21	-1.5	-0.315	8	1.680	0.840
A					-1.892		14.373	4.305
B					0.876		1.041	1.055

A: 1) Sum of O/R ratio for all others except CO₂ = -1.892 , 2) Sum of available H in all products =14.373 and 3) The ratio of sum of milliequivalent of all other compounds except cellobiose = 4.305

B: 1) Ratio of absolute value of the sum of O/R for all others divided by CO₂ O/R , 2) Ratio of available hydrogen in cellobiose divided by sum of available H in all products = 1.041 and 3) The ratio of ratio of sum of milliequivalent carbon of all other compounds divided by milliequivalent carbon of cellobiose.

4.4.2 Effect of Pressure

At elevated pressures (7MPa and 17MPa), predicted ethanol fluxes were greater than the predicted acetate fluxes. The 17MPa pressure showed relatively higher

predicted ethanol fluxes than predicted acetate fluxes. These observations are consistent with experimental data as shown in Figure 4-4 below for 0.05hr^{-1} dilution rate.

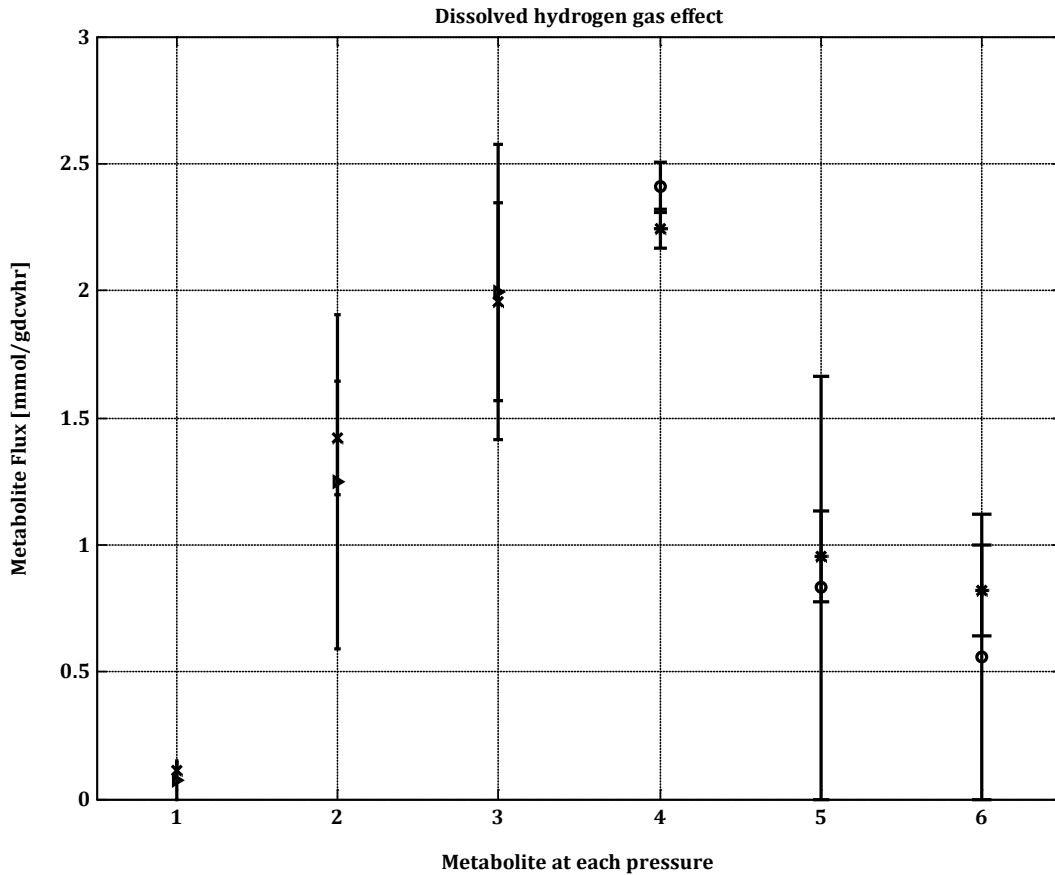


Figure 4-4: Flux spectrum analysis results for predicted ethanol and acetate fluxes at 0.05hr^{-1} dilution rate. The predicted flux interval estimates are shown in bands with triangles for ethanol and circles for acetate. The corresponding measured fluxes are denoted in bands with crossbars and stars respectively. The numbering on the x-axis corresponds to each metabolite at a certain pressure where, "1" denotes ethanol at 0.1MPa, "2" denotes ethanol at 7MPa, "3" denotes ethanol at 17MPa, "4" denotes acetate at 0.1MPa, "5" denotes acetate at 7MPa, "6" denotes acetate at 17.3MPa.

Predicted NADH flux consumed for hydrogen production by the hydrogenase in the reversible $\text{NADH} + \text{H} \leftrightarrow \text{NAD} + \text{H}_2$ increased with increasing pressure at all dilution rates (Table 4-6). Similarly the total NADH consumed by fluxes of lactate dehydrogenase and alcohol dehydrogenase increased with increasing pressure at all dilution rates (Table 4-6). However, NADH consumption fluxes by the hydrogenase

(J_{nadh}) were higher than NADH consumption fluxes by lactate and alcohol dehydrogenases at atmospheric pressure (0.1MPa) while NADH consumption fluxes by lactate and alcohol dehydrogenases were higher than NADH consumption fluxes by the hydrogenase at elevated pressures , 7MPa and 17.3MPa (Table 4-6).

Table 4-6: Predicted fluxes of NADH consumed for hydrogen production by hydrogenase compared with fluxes of NADH consumed by lactate and alcohol dehydrogenases at all pressures over dilution rates (hr^{-1}).

Dilution rate (hr^{-1})	0.1MPa		7MPa		17.3MPa	
	J_{nadh}	NADH consumed	J_{nadh}	NADH consumed	J_{nadh}	NADH consumed
0.05	0.38	0.12	0.8	1.23	1.35	1.85
0.16	1.21	0.34	1.77	2.96	2.32	3.72
0.21	1.52	0.32	2.22	3.73	2.81	4.58
0.32	2.44	0.35	3.12	5.31	3.86	6.80

4.4.3 Effect of Dissolved Hydrogen Gas

Considering the fact that many carbon sources including cellobiose, utilize NADH/NAD for cell growth, the effect of hydrogen on metabolic products due to NADH consumption was tracked by defining an NADH flux (J_{nadh}) for the reversible reaction $\text{NADH} + \text{H} \leftrightarrow \text{NAD}^+ + \text{H}_2$ in the model. Hydrogen flux is a function of this J_{nadh} . Predicted J_{nadh} flux increased with increasing hydrogen flux along with the predicted total NADH consumption by ethanol (J_{adh}) and lactate production (J_{ldh}). This defined a linear relationship between predicted dissolved hydrogen gas and NADH (Figure 4-5).

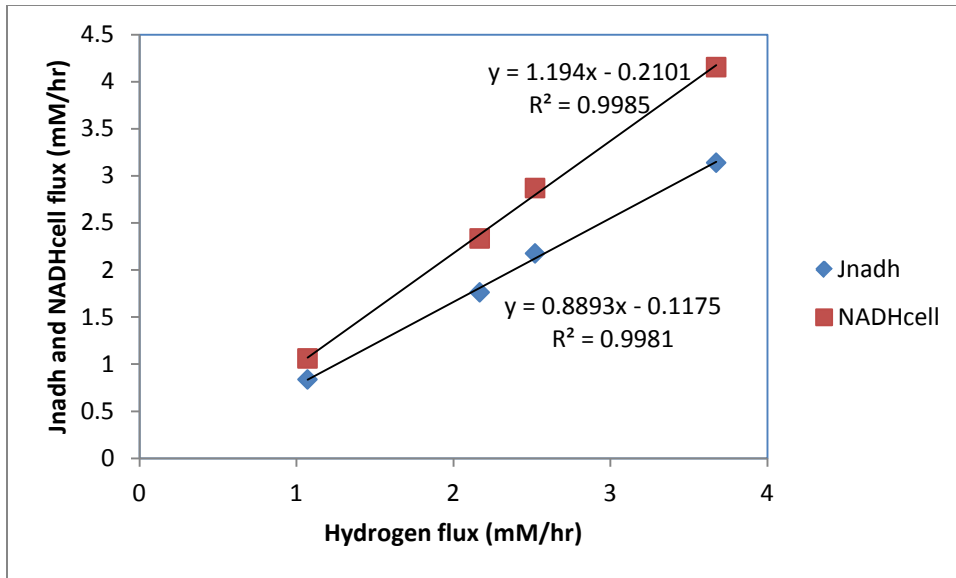


Figure 4-5: Relationship between Hydrogen flux and NADH consumption by lactate and alcohol dehydrogenases (NADHcell), and NADH consumption by hydrogenase

4.4.4 Predicted Combined Effect of Hydrogen and Pressure

Flux estimates of NADH consumed by the lactate and alcohol dehydrogenases, ethanol, and acetate are represented in 3-D (Figure 4-6, Figure 4-7 and Figure 4-8) to depict the solution space that encompasses possible flux distributions of both predicted and measured fluxes when varying hydrogen and pressure. The solution space corresponds to all metabolic phenotype and genotype.

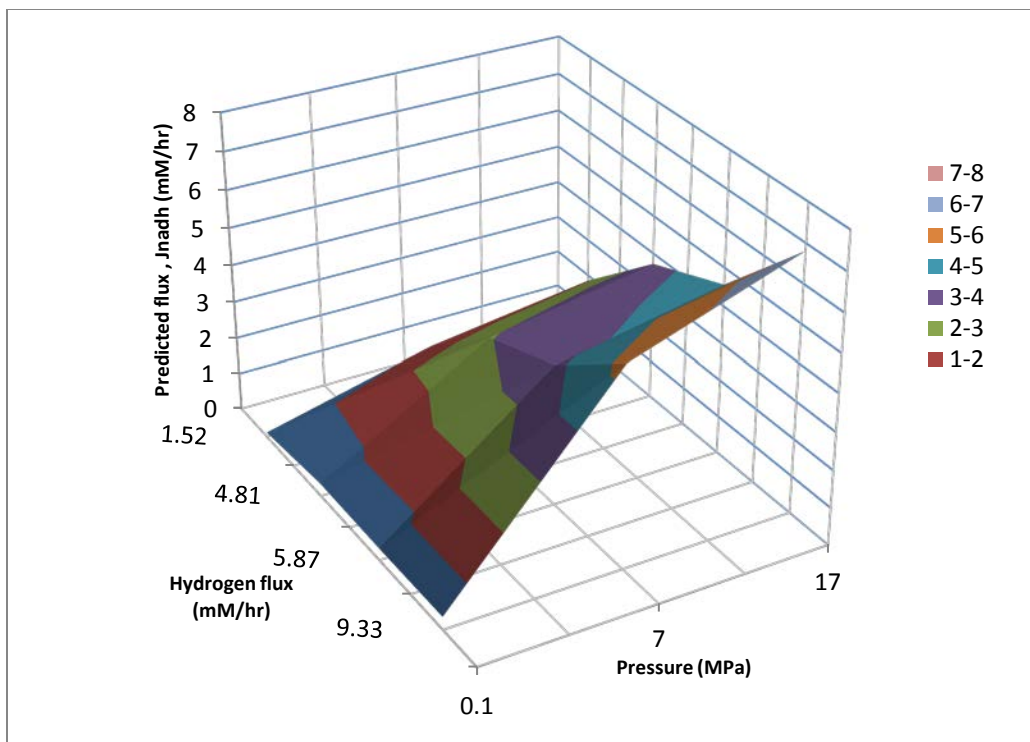


Figure 4-6: Effect of both pressure and hydrogen flux on mean predicted J_{nadh} flux

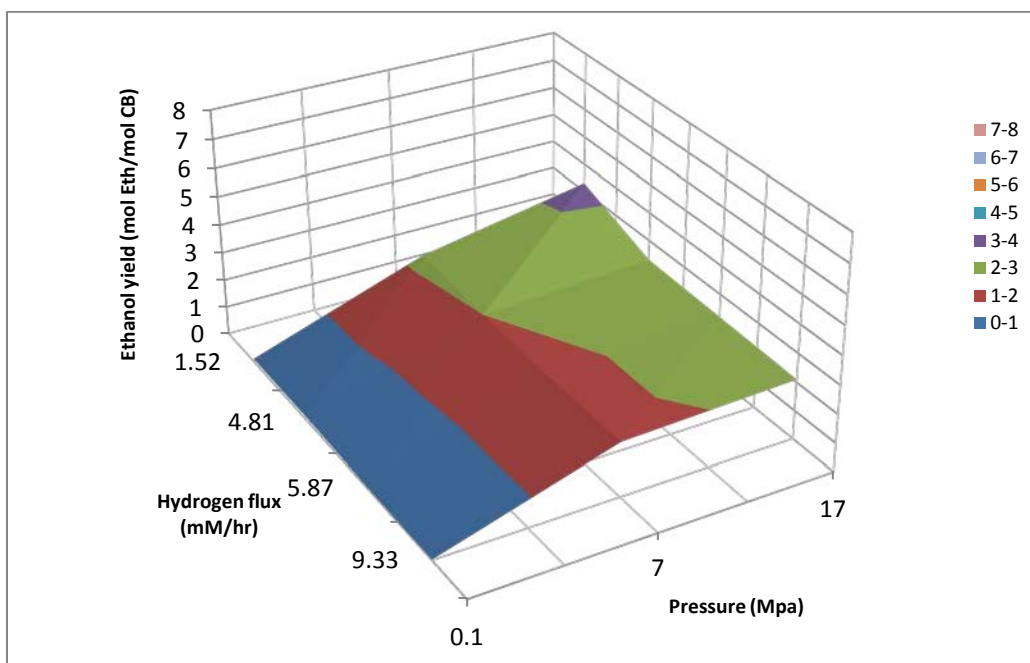


Figure 4-7: Effect of both pressure and hydrogen flux on mean predicted ethanol yields

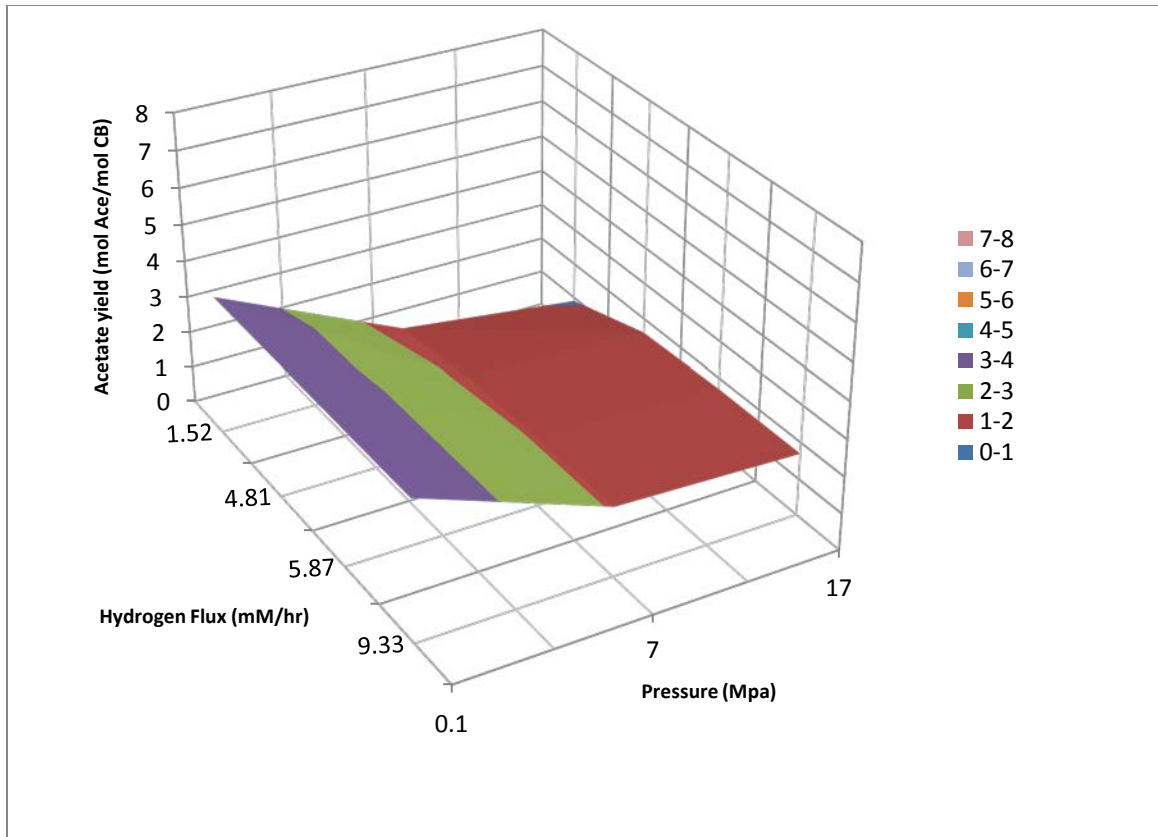


Figure 4-8: Effect of both pressure and hydrogen flux on mean predicted acetate yields

4.5 DISCUSSION

The difficulty associated with measuring key biotechnological process control parameters and the lack of adequate data from steady state experiments for metabolic flux analysis motivates the need to develop a model that incorporates some level of uncertainty in describing/interpreting microbial pathway metabolic flux distribution. Common errors associated with experimental measurements (whether offline or online) are expected to be minimized [44, 68, 159]. Metabolic flux distribution provides quantitative insight into how substrate is utilized towards end-product formation and other relevant metabolic steps. However, metabolic modeling based on stoichiometry requires as many measurements as possible to accurately predict the flux solution space [44, 68].

Experimental observations from literature have shown increased ethanol production (the target product) and decreased acetate production (the by-product) under conditions of elevated pressures and/or pH and the presence of increasing dissolved hydrogen gas [34, 38, 44]. These conditions continue to influence the control of NADH/NAD pairs towards target product formation [162, 175, 176]. The model predicted the flux spectrum of metabolic distribution to account for ethanol and acetate yields as functions of dissolved hydrogen gas and pressure alongside the NADH/NAD effect. Acetate and ethanol yields mostly agreed with the corresponding values reported as shown in Table 4-2, Table 4-3, and Table 4-4 [38]. Product selectivity mainly shifted from acetate to ethanol at elevated pressures. The pattern of acetate and ethanol production at different dilution rates were similar to this study [38]. The assumed zero flux of glycogen had little or no impact on the predicted flux spectrum and consequently the effect dissolved hydrogen gas and pressure. However, based on model predictions, varying hydrogen flux across dilution rates for each pressure versus keeping hydrogen flux constant for each pressure significantly influenced ethanol yields. These observations provide important information for conditions under which ethanol yields may be highest. It was determined that ethanol yields are at their highest when hydrogen flux is maintained at about 4.81 coupled with pressure at 7MPa and above (Figure 4-7).

All products formed in the cytoplasm must be transported across the cell membrane. However some of the products require facilitated or active transport across the cell membrane. Acetate, being the main competitor to ethanol in *C. thermocellum* catabolism requires this phenomenon while products are being formed. This suggests that ethanol yields may be improved at high dilution rates by introducing an active transport or facilitated diffusion medium for which more acetate is transported across the cell since the literature reports high intracellular concentrations of acetate due to simple diffusion [161, 177-180].

The role of NADH/NAD is significant for controlling product selectivity in fermentation processes [163, 164, 176]. It is expected that more NADH consumption will continuously produce hydrogen in the oxidation-reduction which will in turn inhibit acetate formation and cause acetylCoA to move towards ethanol and hence result in a higher ethanol yield [176]. This explains the linear relationship observed between NADH consumption flux and hydrogen flux (Figure 4-6) under conditions of elevated pressures which confirms NADH's effect on the metabolic flux distribution. It is also useful to note that the observed linear relationship between NADH consumption and hydrogen flux is analogous to the relationship between NADH/NAD ratio and hydrogen under pressure reported in the literature [165, 175, 180]. For this reason, it was useful to incorporate an NADH flux due to the reversible NADH reaction into the model in order to quantify and interpret the effect of relative changes in NADH/NAD ratio due to hydrogen and pressure on the metabolic flux distribution end-products especially ethanol. It was determined that ethanol is brought up to an approximate ratio of 1.4: 1 of NADH flux due to the reversible NADH reaction when pressure is elevated.

4.6 CONCLUSION

Flux spectrum approach provides a convenient way for describing microbial physiology in the absence of adequate data. The less measurement data available for model input, the more under-determined the system. The model presented another way of estimating the flux distribution in *C. thermocellum* catabolism by combining stoichiometry with partial thermodynamic principles incorporated in FSA. It has been postulated that the FSA approach eliminates the need to conduct statistical hypothesis test for measurement consistency (as is often the case when performing MFA) assessed by the chi-square (χ^2) method [68]. Hence the flux interval estimates provide statistically

significant results. Predicted fluxes with narrow interval bands indicate that they are the least sensitive to uncertainties in measured inputs. This determines reliability of the predicted fluxes. Carbon redirection towards acetate and ethanol due to glycolytic reactions involving NADH/NAD, Fdox/Fdred, and H^+/H_2 was incorporated into the model. This allows for the quantification of NADH fluxes to determine how much of an influence it has on ethanol production. Experimental measurements obtained under similar conditions are expected to meet model specifications. Meanwhile, the model may be improved by integrating dynamic flux estimates into the FSA approach.

A metabolic model solely based on stoichiometry does not reflect the transient profile of the microorganism. Transient state models are expected to give more realistic predictions of the biological process as they describe the dynamic behavior of the microorganism. This then gives better understanding of the interrelationship between the science and mathematics involved in the biological process. The development of a model to predict the transient profile of the microorganism based on experimental data measured over time is discussed in chapter 5.

CHAPTER 5 TRANSIENT STATE MODELING OF DISSOLVED HYDROGEN GAS EFFECT ON THE METABOLISM OF WILD TYPE CLOSTRIDIUM THERMOCELLUM CELLS

5.1 SYNOPSIS

Biotechnological process and control would be enhanced by the development of dynamic models for simulating microbial metabolic networks to estimate and predict whole cell metabolic responses to environmental stimuli. However, limited kinetic information continues to hinder complete dynamic whole cell metabolic modeling. Regardless, most studies have exploited available information to quantify and describe metabolic profile changes over time to establish the microorganism's genotypic and phenotypic relationship. A dynamic model based on the flux spectrum approach of metabolic flux analysis was developed to investigate the metabolic responses of anaerobic *C. thermocellum* production in the presence of dissolved hydrogen gas. The results showed that ethanol yield increased by approximately 300% while acetate decreased by ~400% at elevated pressures. Acetate was produced at 3 times the rate of ethanol production under atmospheric conditions. A significant shift in product selectivity resulted in an ethanol production about 6 times the rate of acetate production at elevated pressures. The model established significant relationship between hydrogen gas, cofactor (NADH) and metabolic products (acetate and ethanol) changes over time. These observations were consistent with what has been reported in the literature. The model is capable of predicting changes in the metabolic profile (solution space) over time from which genetic modifications to NADH consumption pathways may be deduced. It has been demonstrated that in the absence of sufficient data, reliable fluxes estimates may be predicted for key metabolites in *C. thermocellum*'s central metabolism from

which concentrations can be derived. Also the Gibbs free energy estimate provided more insight into the possibility of more ethanol being retained in the cell.

5.2 INTRODUCTION

Steady state flux analyses of microbial cell metabolism have limitations, such as the inability to exploit kinetic data [65, 180-182]. Difficulty associated with obtaining kinetic data on intracellular metabolites has led to the alternate approach of coupling stoichiometric or mass balances with Gibb's free energy for predicting thermodynamically feasible fluxes [44, 68, 180, 181] and their response to environmental perturbation. Predicting the transport of extracellular fluxes across the cell membrane in the model has been useful for thermodynamic analyses [44, 180]. Additionally, accounting for cell volume fractions has been used to provide more information regarding the concentration of metabolites in the cell, and the metabolic regulation of the cells [183].

Kinetic models typically consist of differential equations describing substrate uptake and production formation. The dynamics of the system with regard to all species present can be obtained by solving the entire set of differential equations and there are existing models that have implemented this approach for describing microbial dynamic performance [184, 185]. Metabolic models based on mass balances constrained by key thermodynamic parameters have been found to provide a better interpretation of cell biochemical behavior [180]. Thermodynamic data are readily available in the literature [180, 186, 187]. Thermodynamics provide scientific insight to help identify the regulatory components of cell metabolism [186] and consequently, the metabolic capabilities of whole cell [187, 188]. More reliable model predictions from thermodynamics-based

constraints than from model predictions based solely on stoichiometry have been demonstrated for *E. coli* [181, 186, 188].

Notwithstanding the benefits demonstrated by thermodynamic-based metabolic flux modeling, it is necessary to consider situations where measured data are limited or unavailable [93, 182]. Linear programming has been used to predict solution spaces of fluxes (flux spectrum) over time [68, 93]. This aspect of metabolic modeling considers a flux-spectrum and probability based analyses for predicting metabolic fluxes over time [68, 182]. The flux spectrum approach (FSA) incorporates basic thermodynamic properties by imposing thermodynamic constraints on the direction of metabolic reactions for the best possible flux solution. The probability-based approach, known as possibilistic metabolic flux analysis (PMFA) aims at predicting the closest possible solution of the flux states comparable to experimental data. Both FSA and PMFA methods can also be coupled with isotopic tracer experiments. PMFA have been demonstrated to provide relatively more reliable and richer flux estimates (stochastic solution) than FSA. PMFA is also suitable for large metabolic network systems

The objective of this study is to predict the time-variant metabolic flux spectrum of *C. thermocellum* ethanol and acetate production responses to changes in dissolved hydrogen concentrations and pressure under anaerobic conditions.

5.3 MATERIALS AND METHODS

5.3.1 Experimental Data

Data were taken from experimental measurements of extracellular metabolites from continuous culture growth of *C. thermocellum* on cellobiose at 60°C under varying hydrostatic pressure conditions of 0.1MPa, 7MPa and 17.3MPa [38]. Measured concentrations of cellobiose (mM), acetate (mM), ethanol (mM), lactate (mM), and

biomass (or cell density in g/l) at 0.05/hr, 0.21/hr and 0.32/hr dilution rates for all pressure conditions were obtained. Maximum solubility values (mM) of dissolved hydrogen gas were calculated for 0.1MPa, 7MPa and 17.3MPa to be 0.7mM, 50.9mM and 130.4mM respectively [38].

Table 5-1: Selected experimental data on pressurized continuous culture growth of *C. thermocellum* on cellobiose from literature [38]

Parameter	0.1MPa	7MPa	17MPa
<i>0.05/hr dilution rate^e</i>			
Biomass conc (g/l) ^b	0.450	0.2625	0.1500
Residual cellobiose (mM) ^c	0.142	0.192	0.042
Acetate produced (mM) ^a	20.2 ±0.7	8.5±1.6	7.4±0.3
Ethanol produced (mM) ^a	1.0 ±0.3	12.2±2.0	17.6±3.5
Lactate produced (mM) ^a	1.0 ±0.2	2.0±0.5	0.9±0.3
Dissolved hydrogen gas (mM) ^f	0.7	50.9	130.4
<i>0.32/hr dilution rate^e</i>			
Biomass conc (g/l) ^b	0.550	0.400	0.1500
Residual cellobiose (mM) ^c	0.017	0.042	1.942
Acetate produced (mM) ^a	12.6±0.3	10.1±0.8	7.4±0.3
Ethanol produced (mM) ^a	4.6±0.5	16.1±0.7	10.4±0.8
Lactate produced (mM) ^a	0.9±0.2	0.4±0.3	0.2±0.1
Dissolved hydrogen gas(mM) ^f	0.7	50.9	130.4
Cellobiose feed (mM) ^d	5.84	5.84	5.84

a ±standard deviations from mean experimental measurements

b,c values were read from graph

d Constant cellobiose feed (converted from the 2g/l cellobiose feed given) at all pressures

e For convenient comparison between pressures, dilution rates 0.30 and 0.32 were assumed equal.

f Maximum solubility of dissolved hydrogen gas for each pressure

For studies involving dynamic behavior, approximation methods (for example Euler or Runge Kutta) and non-linear observers are available for estimating fluxes from measured metabolite concentrations. The non-linear observers are typically preferred for online measurements whereas for offline measurements, approximation methods are preferred. Fluxes are directly obtained from the non-linear observer equation. For this study, we are interested in determining and interpreting the transient profile of organism's central metabolic pathway when moving from one steady state that has experienced perturbation to the next steady state. Therefore we used the non-linear

observer method because the method allows for direct conversion of measured concentrations to fluxes compared to approximation methods that require estimating the derivative before converting of the measured metabolite concentrations to fluxes.

The concentrations of cellobiose, lactate and biomass were converted to fluxes at time step intervals. Given measured concentrations of extracellular metabolites, the non-linear observer dynamic balance equation (Equation 1) was implemented using the algorithm presented in [68] and used to solve for the fluxes using the standard MATLAB solver, ode45. The ode45 combines both 4th and 5th order Runge-Kutta method to solve first order differential equations numerically.

$$\frac{dC_{obs}}{dt} = J_{obs} \cdot X - D \cdot C - 2 \cdot \theta \cdot (C_{obs} - C) \quad (1)$$

$$\frac{dJ_{obs}}{dt} = -\theta^2 \cdot \frac{(C_{obs} - C)}{X}$$

Where C_{obs} is the observed extracellular concentration (mM), J_{obs} is the corresponding flux of observed metabolite concentration (mM/hr), C is the metabolite's concentration determined at each time point, D is the dilution rate (hr^{-1}), X is biomass concentration (g/l) and θ is a constant variable referred to as unique adjustable parameter for regulating errors and filtering measurements. The choice of θ depends on whether data sensitivity to noise or fast convergence is more important to the modeler. For our modeling purposes, preference was given to the maximum allowable θ values for which error is minimized [68, 189]. As a function of dilution rate, θ was chosen to be 0.11 for $0.05hr^{-1}$ and 0.20 for $0.32hr^{-1}$. The accumulation of glycogen was assumed to be negligible. Due to the large number of iterations required to predict each dataset modeling predictions were limited to two dilution rates ($0.05/hr$ and $0.32/hr$). For illustrative purposes, the cellobiose flux at $0.05hr^{-1}$ dilution rate is calculated with each of the parameters defined as: $C_{obs} = 5.84mM$; $D = 0.05hr^{-1}$; $X = 0.45g/l$ and $\theta = 0.11$. The set of differential equations defined previously becomes,

$$\frac{dC_{\text{obs}}}{dt} = J_{\text{obs}} \cdot 0.45 - 0.05 \cdot C - 2 \cdot 0.11 \cdot (5.84 - C)$$

$$\frac{dJ_{\text{obs}}}{dt} = -0.11^2 \cdot \frac{(5.84 - C)}{0.45} \quad (2)$$

Initial conditions, $C_0=0.15\text{mM}$ (for residual cellobiose) and $J_{\text{obs}}^0 \cong 0.02\text{mmol/gdcwh}$ (corresponding flux for residual cellobiose) were used to solve Equation (2). Choosing initial time $t = 0\text{hr}$ and final time $t = 24\text{hr}$, a window size $n = 600$, to implement Runge Kutta, and the time step h equals 0.04 . Using MATLAB, an m-file is created to define a function dy as:

```
function dy= cellobiose(t,CB)
global C J_obs Co J_obs^0 %C and J_obs are components of CB
dy=zeros(2,1) % to ensure dy is a column vector
dy(1)=J_obs*0.45-0.05*C-2*0.11*(5.84-C)
dy(2)=-0.11^2*(5.84-C)/0.45
end
```

Another m-file is created to solve for CB as follows:

```
global C J_obs Co J_obs^0
t=[0:0.04:24];
Co=0.15;
J_obs^0=0.02;
[t,CB]= ode45('dy', t,[Co ;J_obs^0]);
```

The resulting flux estimates are given in the second column of CB. The respective flux estimates of lactate and hydrogen are calculated by repeating the same procedure.

5.3.2 Central Metabolic Network of *Clostridium thermocellum*

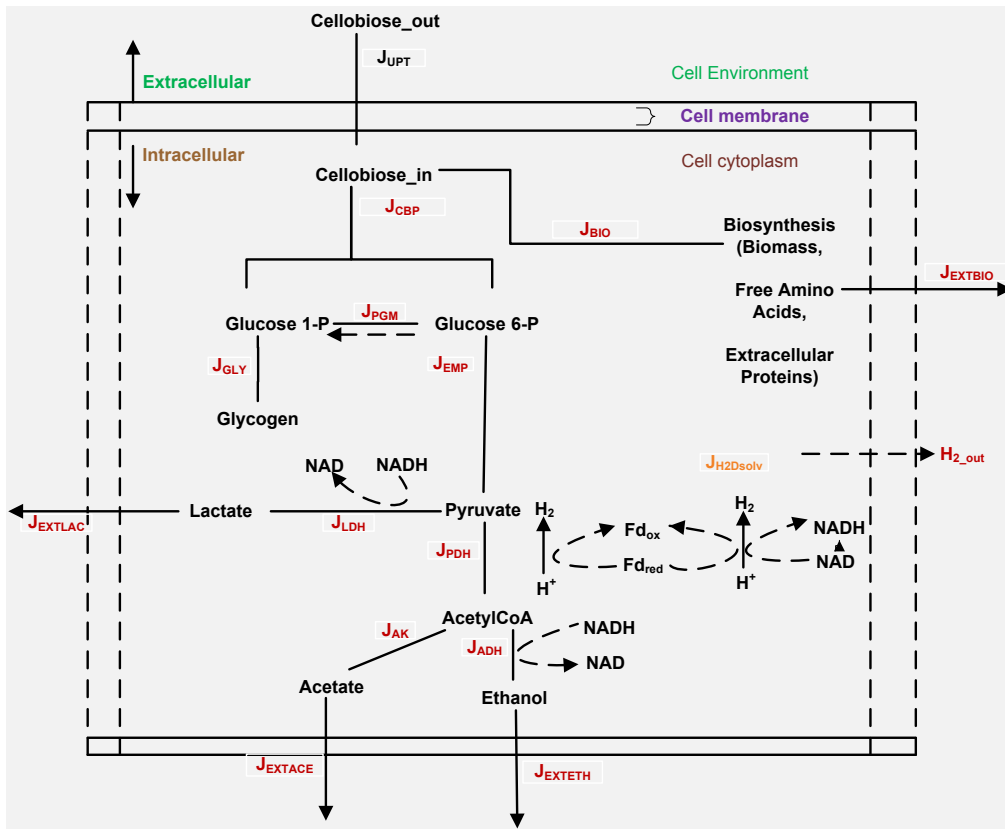


Figure 5-1: Modified glycolytic pathway of *C. thermocellum*. Cellobiose uptake (Cellulose_out), Intracellular cellobiose (consumed; Cellulose_in), Hydrogen transport across cell membrane as a function of hydrogen outside cell (environment; H_{2_out}) and Hydrogen inside cell (environment; $J_{H2Dsolv}$), Extracellular production of acetate, ethanol and lactate denoted by J_{EXTACE} , J_{EXTETH} and J_{EXTLAC} respectively.

Estimates of flux distributions as a function of dissolved hydrogen gas and cell physical properties were predicted from a metabolic model based on the simplified *C. thermocellum*'s catabolic pathway shown in Figure 5-1.

5.3.3 Metabolic Flux Estimation over Time Using Flux Spectrum Approach

A stoichiometric matrix (15 x 21), N was generated from the simplified metabolic network shown in Figure 5-1, corresponding to 15 intracellular metabolites and 21 fluxes (i.e. 21 reactions). By letting u represent the vector containing all fluxes, a pseudo-steady state equation was formulated as:

$$N \cdot u = 0 \quad (2)$$

N represents the overall stoichiometric matrix of the network. Equation (2) was partitioned into measured and non-measured fluxes and rearranged such that the unknown fluxes preceded the known fluxes [12] as shown in Equation (3).

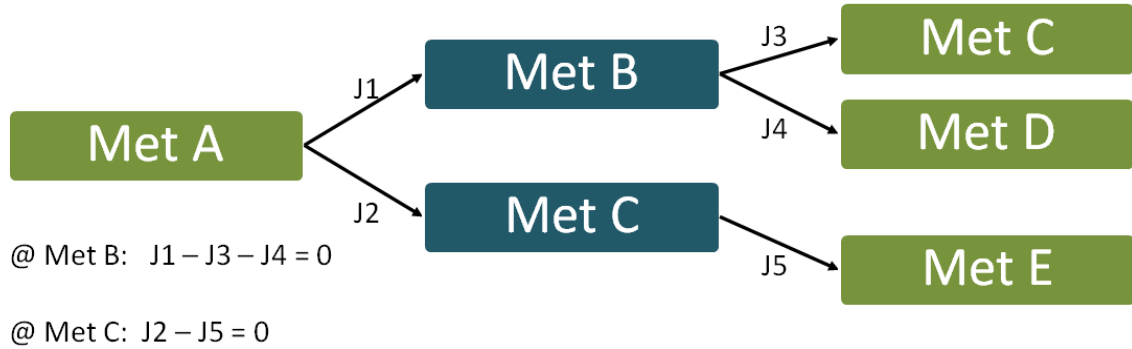
$$N_m \cdot u_m + N_n \cdot u_n = 0 \quad (3)$$

N_m and u_m denote the stoichiometric matrix and flux vector corresponding to measured fluxes respectively. N_n and u_n denote corresponding matrix and vector for non-measured fluxes respectively. However, the flux spectrum approach requires constrained solutions to maximum and minimum values based on Equation 3 as follows:

$$\begin{aligned} & \text{Min } u \geq 0 \\ & \text{s.t} \\ & N_m \cdot u_m = - N_n \cdot u_n \\ & \text{Max } u \geq 0 \\ & \text{s.t} \\ & N_m \cdot u_m = - N_n \cdot u_n \end{aligned} \quad (4)$$

The method is better understood by illustrating with a simple example. Figure 5-2 shows hypothetical metabolic network involving the uptake of metabolite A and production of metabolites C, D, and E. A, C, D and E are extracellular metabolites whereas B and C

are intracellular metabolites. Mass balance at steady state (based on MFA concept) is applied at nodes B and C.



$$\begin{pmatrix} 1 & 0 & -1 & -1 & 0 \\ 0 & 1 & 0 & 0 & -1 \end{pmatrix} \begin{pmatrix} J_1 \\ J_2 \\ J_3 \\ J_4 \\ J_5 \end{pmatrix} = \begin{pmatrix} 0 \\ 0 \end{pmatrix}$$

Figure 5-2: A hypothetical metabolic network for illustrating the FSA method

Assuming J_1 , and J_2 are measured over time, N_m , u_m , N_n and u_n , according to Equations 1 and 2 are determined from the network as:

$$N_m = \begin{bmatrix} 1 & 0 \\ 0 & 1 \end{bmatrix},$$

$$N_n = \begin{bmatrix} -1 & -1 & 0 \\ 0 & 0 & -1 \end{bmatrix}$$

$$u_m = \begin{pmatrix} J_1 \\ J_2 \end{pmatrix}$$

$$u_n = \begin{pmatrix} J_3 \\ J_4 \\ J_5 \end{pmatrix}$$

The partitioned stoichiometric matrices and vectors for measured and non-measured metabolites are useful even in FSA for convenient order of arrangement. The measured fluxes will be represented in the latter columns of the matrix N preceded by non-

measured fluxes so that indexing becomes easier for programming purposes. In this case, the rearranged N becomes:

$$N = \begin{bmatrix} -1 & 0 & 1 & 0 & -1 \\ 0 & -1 & 0 & 1 & 0 \end{bmatrix}$$

For this simple example, we assume all reactions occur in one direction and set a constraint assuming that all fluxes are irreversible. Once the stoichiometric matrix is generated, we may proceed with FSA by defining uncertainties around measured data (J1 and J2) say $\pm 5\%$. In chapter four, measured inputs were scalars (i.e. represented each flux distributions at one particular instant). In the current case J1 and J2 are now vectors because they represent multiple datasets measured over time. So they are defined slightly different in MATLAB from the example shown in chapter 4. Based on the $\pm 5\%$ uncertainty, the maximum and minimum flux vectors may be defined for the measurements by multiplying them with 1.05 and 0.95 respectively. At this stage, suitable programming language may be implemented to solve for the metabolic flux spectrum. Due to the multiple datasets for each measured flux as input data, a “for loop” is implemented in a simple FSA function named vspectrumCb_opt defined in an m-file, (see appendix D) to solve for the problem given in Figure 5-2. The “for loop” was needed to handle multiple datasets.

```
clear all
clc

%Stoichiometric Matrix
N=[-1  -1  0  1  0;
    0   0  -1  0  1];

irrev=[ones(1,5)];
ind= [4, 5];
% assumed vector of measured data for the two known fluxes (J1 and J2)
% this data fulfills the constraints
J1=[0 0.4 0.7 0.75 0.7 0.6 0.3 0.1]';
J2=[0 0.7 1.2 1.45 1.7 1.9 2 2]';
```



```

% assuming +/- 5% uncertainty in measurements
J1_max=max(0.001,J1*1.05);
J1_min=J1*0.95;
[J1_min J1_max]; % need an even minimal interval 0-0.001

J2_max=max(0.001,J2*1.05);
J2_min=J2*0.95;
[J2_min J2_max];
Jm_max= [J1_max J2_max]';
Jm_min= [J1_min J2_min]';

% Initializing resulting flux spectrum
Rmin=[];
Rmax=[];

for i=1:length(J1)
    options=optimset('LargeScale','off','Simplex','on');
    [J_min,J_max,flag] =
vspectrumCb_opt(N,irrev,ind,Jm_min(:,i),Jm_max(:,i),options);
    if exist('Rmin','var')
        Rmin=[Rmin J_min];
        Rmax=[Rmax J_max];
    else
        Rmin=[];
        Rmin=[J_min];
        Rmax=[J_max];
    end

end

end

%% plot results
figure
for i=1:1:size(N,2)
    subplot(2,3,i)
    hold on,xlabel('Time'),ylabel('flux'), grid, box,axis([0 10 0 2.5])
    set(gca,'FontSize',11);
    FScenter = (Rmin(i,:)+Rmax(i,:))/2;
    FSdown   = FScenter-Rmin(i,:);
    FSup     = Rmax(i,:)-FScenter;
    h3= errorbar(1:length(a),FScenter,FSdown,FSup,'.r');
    set(h3, 'LineStyle', 'none', 'LineWidth', 1, 'Color', [0 1 0]);
end
end

```

Figure 5-3 shows the results for flux estimates over time for the above example. It may be observed that uncertainty in measured fluxes, J1 and J2 practically did not affect predictions for fluxes J3, J4 and J5 as shown by their small interval sizes. Again, this demonstrates the benefits of the FSA method in the absence of sufficiently known data.

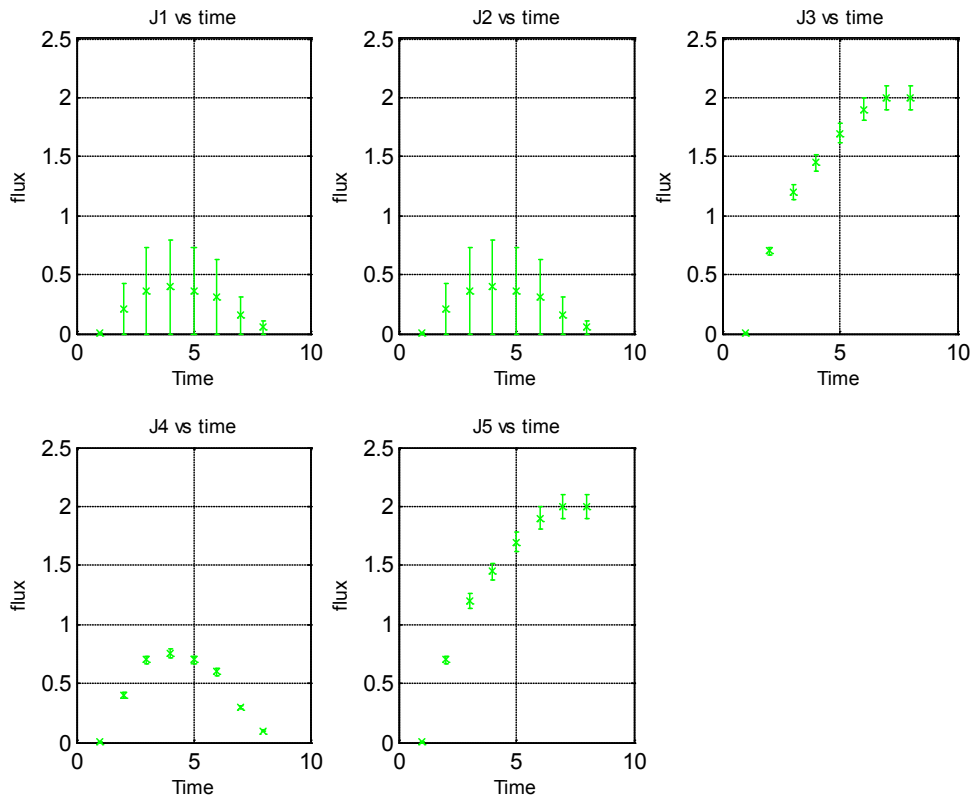


Figure 5-3: Resulting flux (mM/hr) (both predicted and inputs) over time using FSA

In contrast to the steady state assumptions made in chapter 4, the stoichiometry of hydrogen at both atmospheric and elevated pressures was derived from both Equations 5 and 6. Hydrogen fluxes were calculated as functions of cell physical properties and temperature dependent Henry's law given the maximum solubilities of hydrogen at each pressure. The gaseous metabolite balance method given in a previous study [173] was simplified by assuming zero physicochemical rate, zero influent and effluent rates and applied to hydrogen balance for liquid phase defined as:

$$\frac{dH}{dt} = \text{Biological rate} + \text{Kla}([\text{H}_2]^*) \quad (5)$$

Where Kla is the volumetric transfer coefficient (hr^{-1}) for hydrogen and $[\text{H}_2]^*$ is the solubility of hydrogen (mM). The biological rate was denoted by the pyruvate:ferredoxin oxidoreductase flux branching off pyruvate node toward FdH_2 and subsequently toward

H₂. The gas phase balance was applicable to only the atmospheric pressure condition in this case is defined as:

$$\frac{dH}{dt} = -\left(\frac{V_l}{V_g} K_{la}([H_2]^*)\right) - D \frac{P}{RT} \quad (6)$$

D is the dilution rate (hr⁻¹), P is the partial pressure of hydrogen gas (Pa), R is the universal gas constant (8,314 Lmol⁻¹K⁻¹Pa), V_l is the volume of reactor (ml) and V_g is the volume of gas (ml). Glucose-1-phosphate, glucose-6-phosphate, pyruvate, and AcCoA were the key nodes considered for intracellular metabolite mass balances. Mass balances based on metabolic flux analyses derived for cellobiose transport, ethanol, lactate and acetate transports were also included.

The overall equations for producing acetate, ethanol and lactate have been derived for *C. cellulolyticum*, an organism with similar metabolic network as *C. thermocellum* [172]. Based on the principle in previous studies [180], the equations were applied to estimate the transport and glycolytic components of Gibbs energy (ΔG) for acetate and ethanol production predicted fluxes. An estimate resulting in negative (ΔG) value is indicative of an energetically favorable reaction. The maximum predicted ethanol and acetate fluxes were used for the computations (data not shown). Standard Gibbs free energy values were estimated from the Handbook of Chemistry and Physics [190].

The stoichiometric matrix N was generated in MATLAB using traditional MFA. This work combines MFA analysis that checks matrix sensitivity, determinancy, redundancy, balanceability and calculability with an adapted previously described FSA model [68, 152] for estimating the flux distributions. N was consistent and determined. The solutions to metabolic flux spectrum were estimated from an improved version of vspectrumCb defined as vspectrumCb_opt. The latter applies the option to switch between large scale and simplex optimization methods. All MATLAB codes are made

available in appendix D. The optimized solutions to the metabolic flux distribution were obtained using MATLAB's optimization toolbox for linear programming. Fluxes of pyruvate \leftrightarrow lactate; glucose-1-phosphate \leftrightarrow glucose-6-phosphate; and NADH \leftrightarrow H₂ reactions were exceptions to the irreversibility constraints of fluxes as these were allowed to be reversible.

5.4 RESULTS AND DISCUSSION

Cellobiose consumption patterns were compared between 0.05hr⁻¹ to 0.32hr⁻¹ dilution rates over 24hr and 120hr. Time profile fluxes of cellobiose consumption, acetate, ethanol, lactate and hydrogen production were observed for increases in pressure from 0.1MPa to 7MPa and 17 MPa over 120hr. The resulting ethanol and acetate yields were also estimated over time. NADH consumption relative to increases in hydrogen flux and pressure were also predicted. The model predicted a high correlation between hydrogen flux and NADH consumption (Figure 5-13 and Figure 5-14) that was consistent with what is known from the literature [176]. The combined effect of pressure and dissolved hydrogen gas fluxes on acetate and ethanol demonstrates the extent to which the metabolic shifts in products occur.

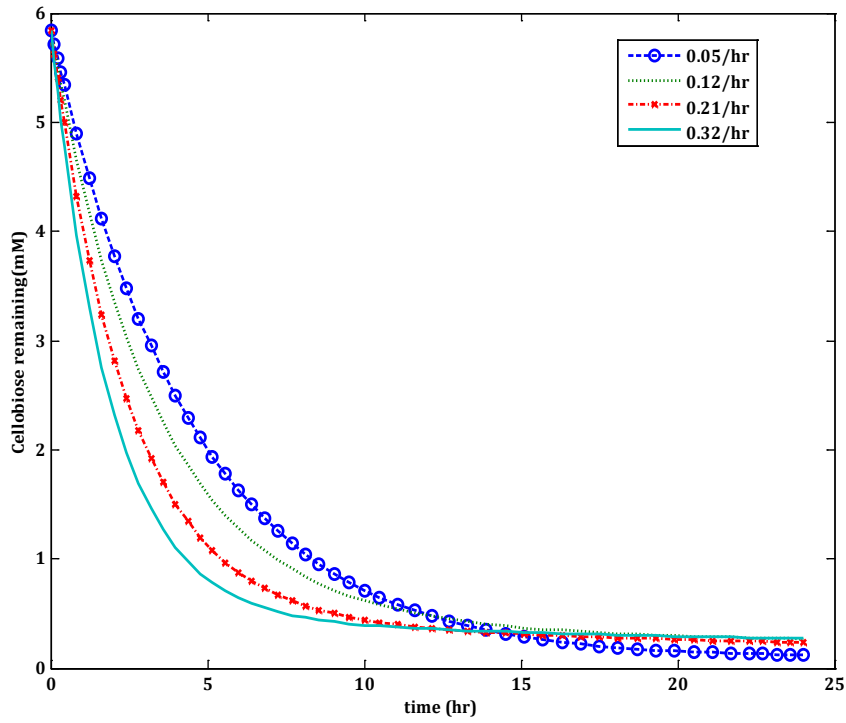


Figure 5-4: Amount of Cellobiose (mM) remaining over 24hr

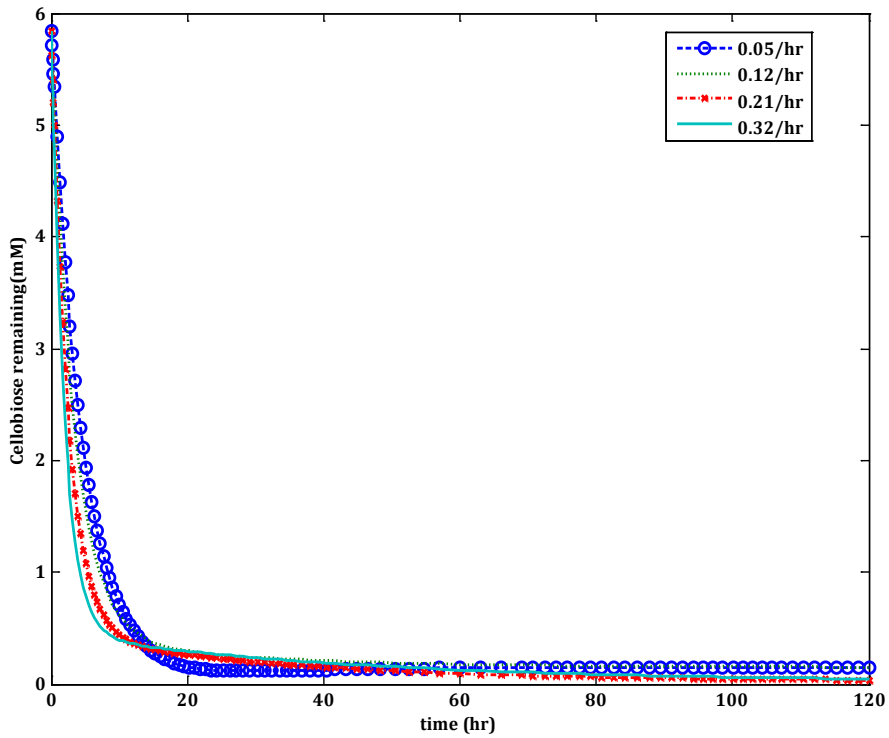


Figure 5-5: Amount of Cellobiose (mM) remaining over 120hr (input to model)

Observations from Figure 5-4 and Figure 5-5 indicate that cellobiose is consumed more quickly at higher dilution rates until steady state is reached. Cellobiose flux uptake at 0.05hr^{-1} and 0.32 hr^{-1} dilution rates were determined and compared over to time at each pressure of 0.1MPa, 7MPa, and 17.3MPa. Figure 5-6, Figure 5-7 and Figure 5-8 generally show similar patterns of cellobiose uptake (in terms of flux (mM/hr)) for the same dilution rate regardless of pressure conditions. That is, the cellobiose uptake at 0.1MPa, 7MPa and 17MPa followed similar patterns for 0.05hr^{-1} . This is also true for the 0.32 hr^{-1} dilution rate. However, it may be seen that more cellobiose was utilized at the 0.32 hr^{-1} for all pressures. At atmospheric conditions (0.1MPa) cellobiose uptake at 0.32 hr^{-1} dilution rate approximately increased by 5 times that of 0.05hr^{-1} at any given time during the transition. Cellobiose utilized at 0.32 hr^{-1} at both 7MPa and 17MPa pressures were approximately 4 times that of 0.05hr^{-1} .

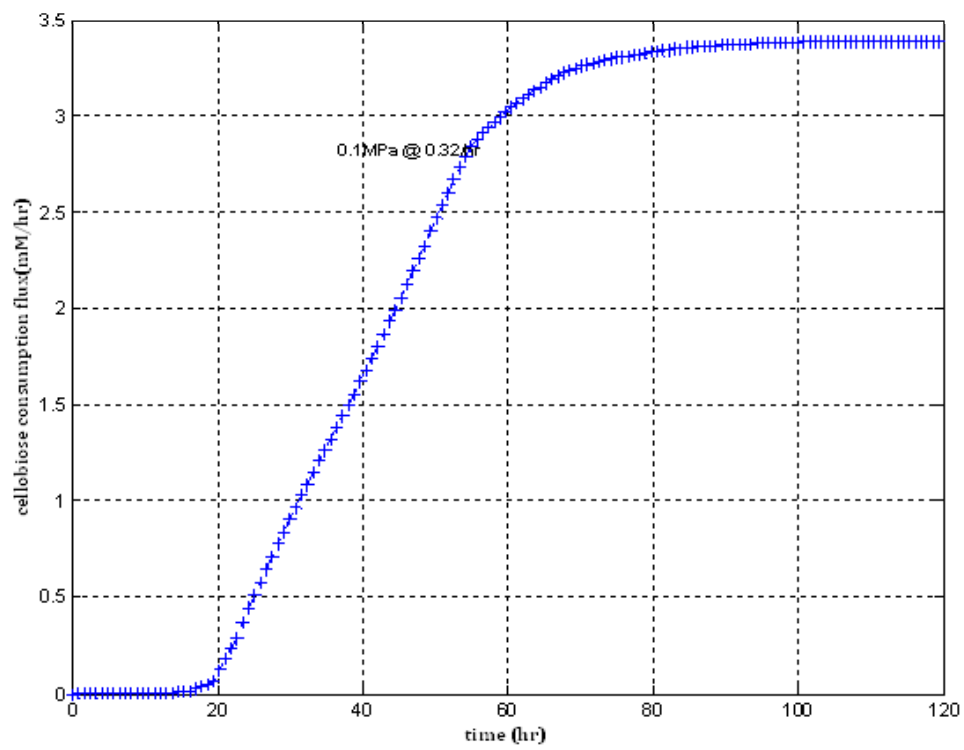
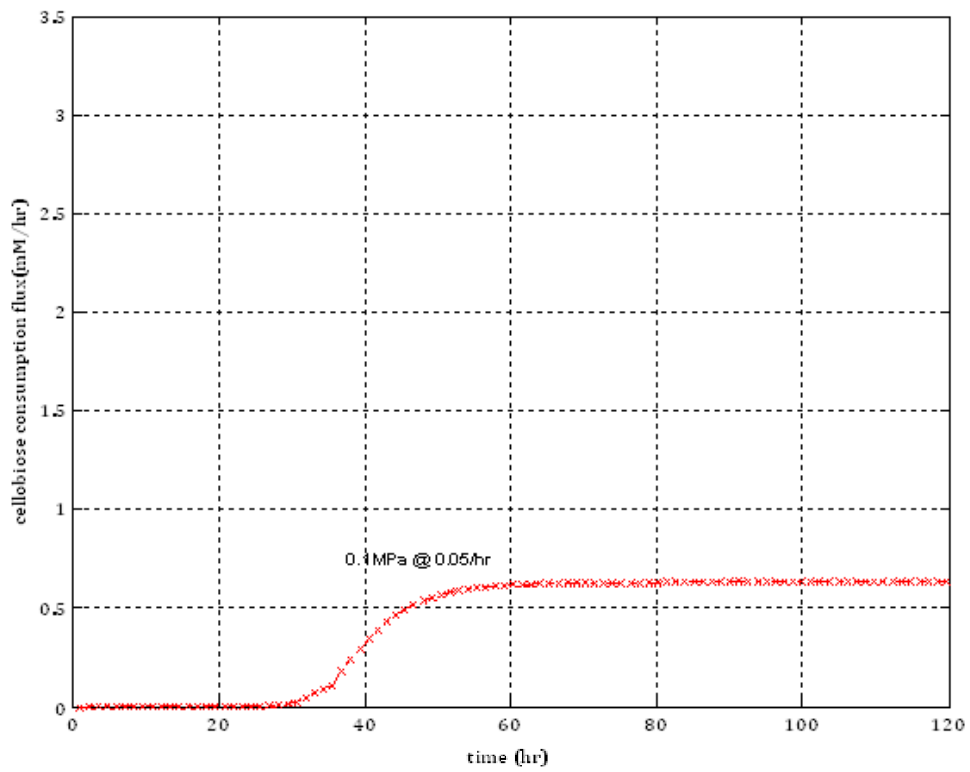


Figure 5-6: Cellobiose consumption fluxes for 0.05hr^{-1} (x) and 0.32hr^{-1} (+) at atmospheric pressure (predicted by model)

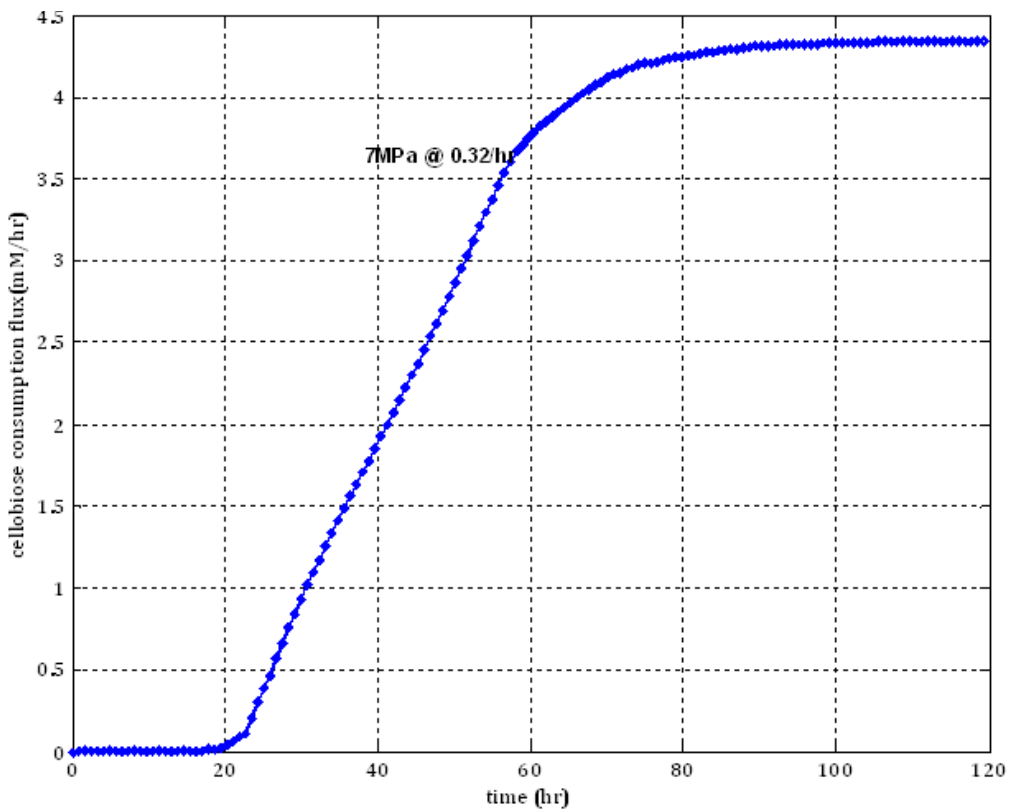
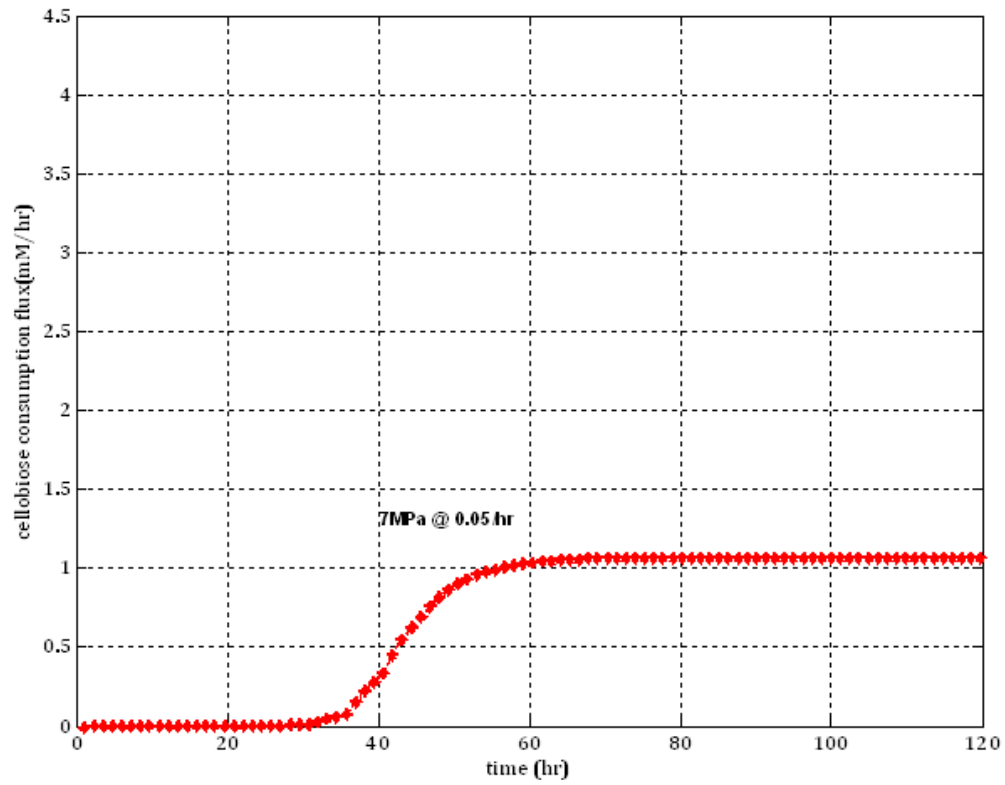


Figure 5-7: Cellobiose consumption fluxes for 0.05hr^{-1} (x) and 0.32hr^{-1} (x) at 7MPa pressure (predicted by model)

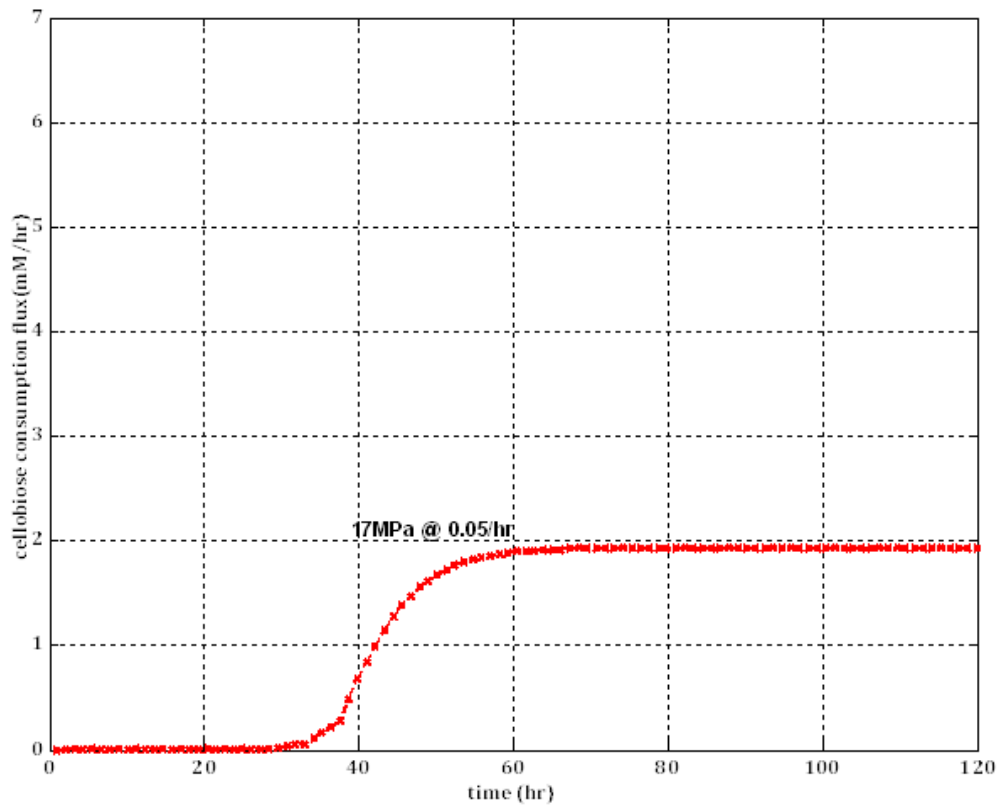


Figure 5-8: Cellobiose consumption fluxes for 0.05hr^{-1} (x) and 0.32hr^{-1} (+) at 17MPa pressure (predicted by model)

The relationship between predicted NADH and predicted hydrogen fluxes was examined at all pressures and compared to the predicted fluxes and yields of acetate and ethanol. Hydrogen fluxes increases correlated well with NADH fluxes and consequent influences on ethanol and acetate fluxes. Before the 80hr, NADH consumption decreased in response to elevated pressure (7MPa and 17MPa) as negligible amounts of hydrogen fluxes are produced. Under the same elevated pressure conditions at 80hr and beyond, hydrogen and NADH flux started increasing simultaneously (Figure 5-13 and Figure 5-14), which caused ethanol flux and the corresponding ethanol yields (Figure 5-9 and Figure 5-10) to increase while acetate and the corresponding acetate yields decreased (Figure 5-11 and Figure 5-12). This demonstrates the direct correlation between NADH/NAD and hydrogen and their effect on anaerobic metabolic end-products (acetate and ethanol) [38, 162, 176]. All plots are based on the maximum predicted flux distribution of metabolites. In this study, significance importance was attached to ethanol and acetate yields rather than ethanol to acetate ratios. Ethanol to acetate ratios may potentially mask the real picture.

The predicted ethanol and acetate flux pattern shown in Figure 5-9 and Figure 5-11 indicate that at atmospheric pressure (0.1MPa), both ethanol and acetate are produced at a fast rate from 0hr until 40hr, after which acetate begins to drop slightly while ethanol increased slightly. The ethanol and acetate yields followed similar patterns except for the near constant acetate yield observed throughout. Despite the observed increases in ethanol values the maximum yield and flux of 0.9 mol ethanol/mol cellobiose and 0.3mM/hr remained less than the corresponding acetate flux and yield (2.5 mol ace/mol cellobiose and 0.9mM/hr). Under elevated pressure ethanol flux begun to rise while acetate flux decreased over time. This can be seen at time of 80hr when ethanol started increasing as, acetate drops. Similar patterns were observed for their

corresponding yields. A maximum ethanol flux of 0.65mM/hr was reached as acetate flux minimized to as low as 0.1mM/hr. Ethanol yields improved to about 3 mol ethanol/ mol CB consumed. Yields of acetate decreased to 0.5mol acetate/mol CB consumed. Figure 5-11 and Figure 5-12 indicate that during the fermentation process, pressure takes effect on the cell's metabolism after a period of time. The pattern observed in predicted ethanol flux at 17MPa is similar to predicted ethanol flux at 7MPa (Figure 5-9). However, relative increases in ethanol yields and fluxes were observed at 17MPa compared to the corresponding values at 7MPa. Acetate fluxes and yields again followed the same pattern. Maximum ethanol yield of about 3.5 mol ethanol/mol CB consumed was obtained. Acetate yield went slightly below 0.5mol acetate/mol CB consumed. Based on the behavioral pattern shown by ethanol and acetate formation over time (Figure 5-9 and Figure 5-11), it is evident that during continuous culture growth of *C. thermocellum* under pressurized conditions (perturbation) coupled with hydrogen production, cell metabolism does not immediately shift end-products towards ethanol. The cell's metabolic profile adapts from one perturbation to another over a period of time before responding to the changes.

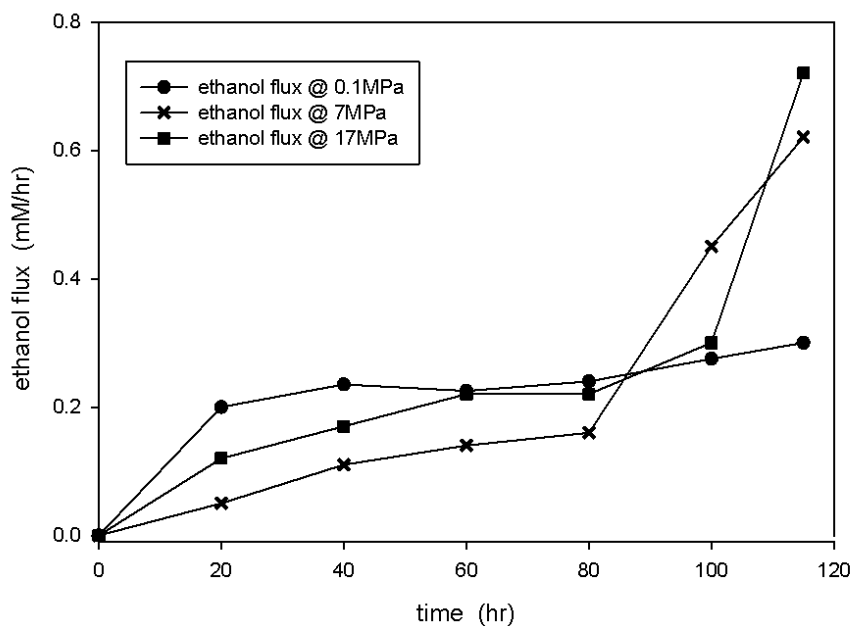


Figure 5-9: Predicted ethanol flux (mM/hr) over time @ 0.05hr^{-1} compared between 0.1MPa, 7MPa and 17.3MPa

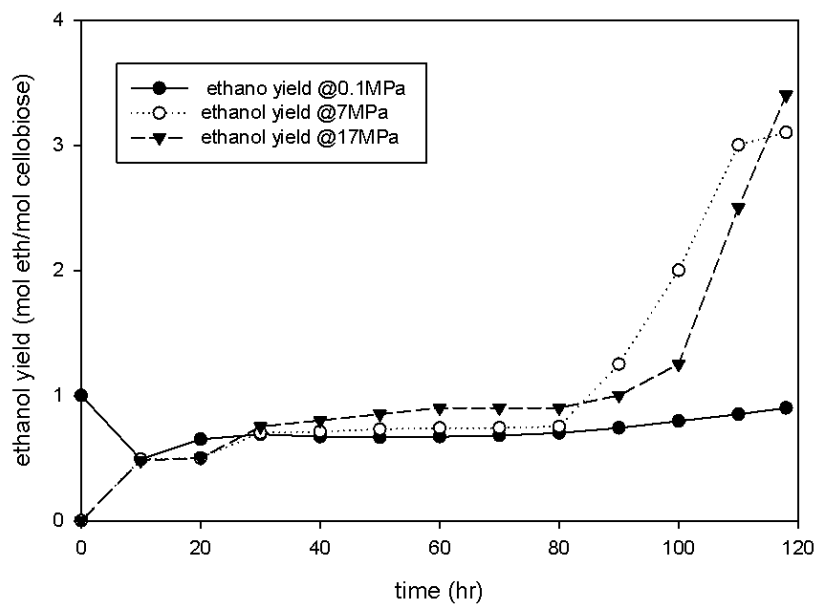


Figure 5-10: Predicted ethanol yield (mol ethanol/mol cellobiose consumed) over time @ 0.05hr^{-1} compared between 0.1MPa, 7MPa, and 17MPa.

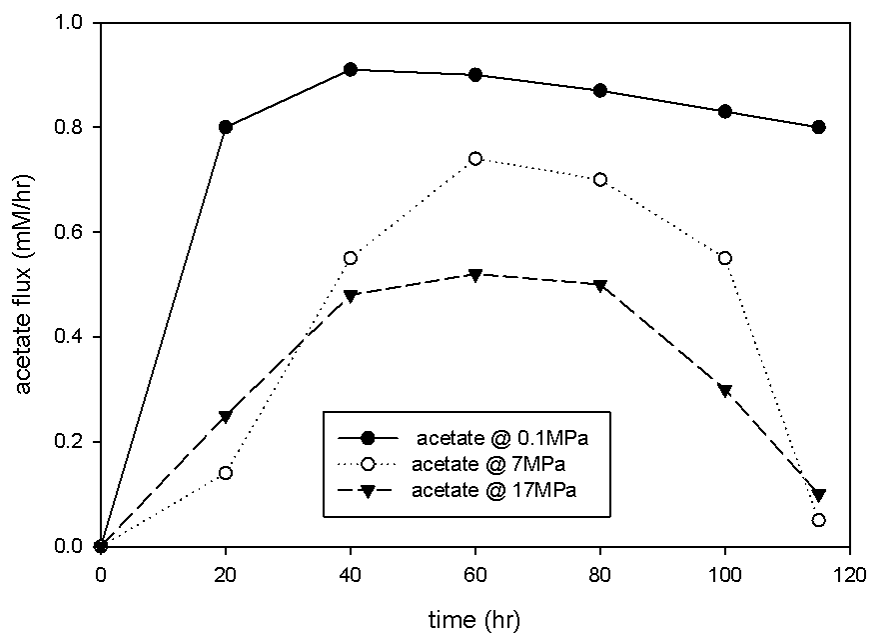


Figure 5-11: Predicted acetate flux (mM/hr) over time @ 0.05hr^{-1} compared between 0.1MPa, 7MPa and 17.3MPa

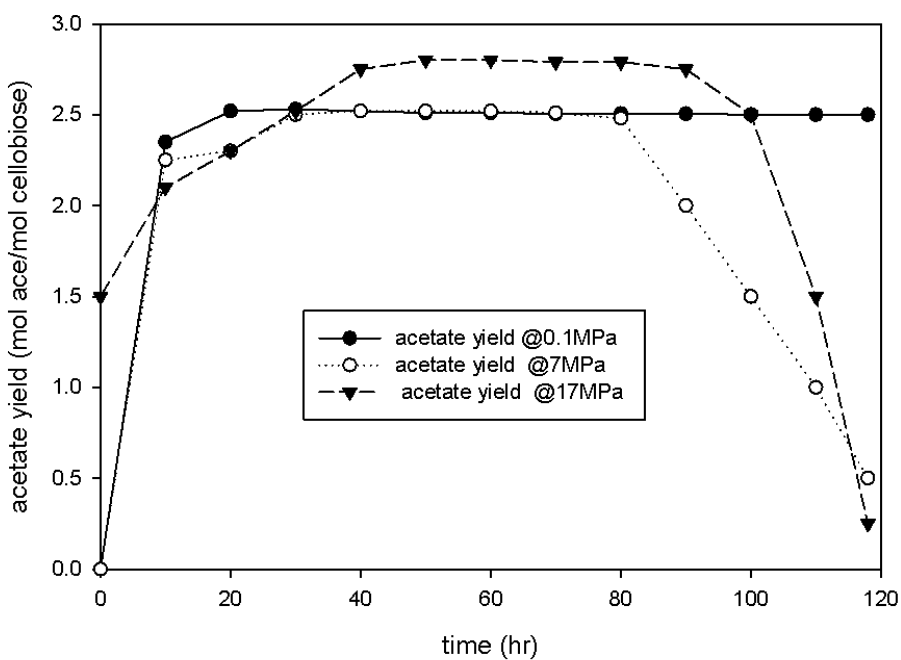


Figure 5-12: Predicted acetate yield (mol acetate/mol cellobiose consumed) over time @ 0.05hr^{-1} compared between 0.1MPa, 7MPa, and 17MPa.

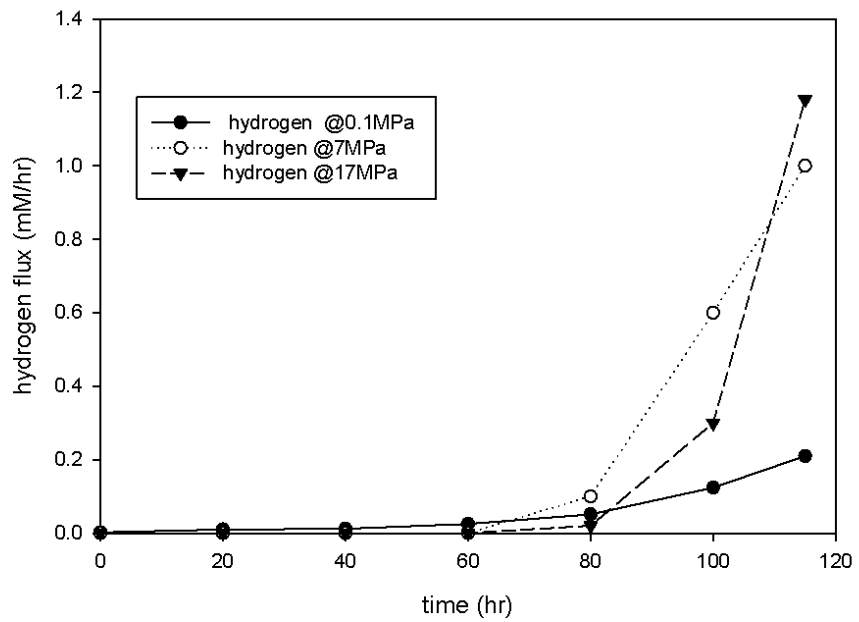


Figure 5-13: Predicted dissolved hydrogen gas flux (mM/hr) over time @ 0.05hr^{-1} compared between 0.1MPa, 7MPa and 17.3MPa

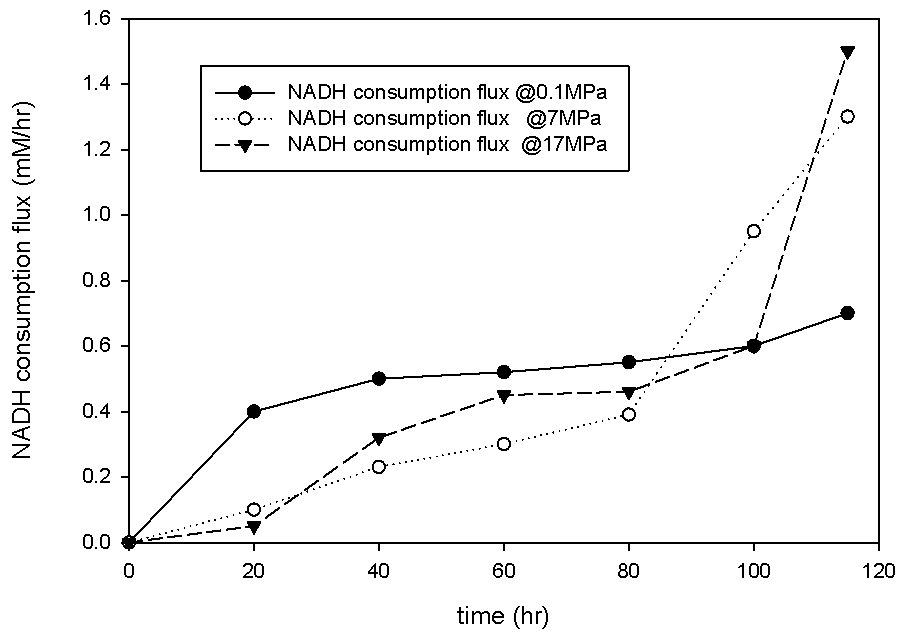


Figure 5-14: Predicted NADH consumption flux (mM/hr) over time @ 0.05hr^{-1} compared between 0.1MPa, 7MPa and 17.3MPa

The flux spectrum method was implemented with 20% variation in experimental measurements. The time profile estimates of metabolic flux distribution show great sensitivity of acetate and ethanol to hydrogen and pressure increases during the fermentation process. Cellobiose uptake was kept at a constant maximum under elevated pressures compared to atmospheric pressure conditions. Transient metabolic flux distribution of well studied NADH/NAD dependent pathways [162] supports the observed increases in ethanol flux and NADH consumption relative hydrogen flux increases over time. A maximum percentage increase (~ 300%) of ethanol yield corresponded to a maximum percentage decrease of 400% acetate yield at elevated pressure. This suggests that, in order for ethanol yields to improve significantly, the system should be subjected to relatively high pressures which will cause NADH to increase, thereby increasing ethanol production. At the same time, intracellular concentrations of acetate decrease and the thermodynamically feasible acetate production process which requires ADP and Pi will become infeasible and thus decrease acetate production [44, 45].

It has been demonstrated that Gibb's free energy of a metabolic reaction plays a significant role in describing the metabolic properties of the cell [44, 180, 191]. It was determined that the total Gibbs free energy of production (due to transport and glycolysis) for acetate was negative while that of ethanol was positive. This indicates that while acetate formation process in the forward direction, ethanol formation proceeds in the reverse direction, which means some ethanol, is retained inside the cell and requires more energy for it to be transported across the cell membrane. In that case, incorporating the Gibbs free energy of production due to transport and glycolysis into the model is recommended and expected to give more insight into the dynamics of the metabolic flux distribution.

5.5 CONCLUSION

The current study applied the FSA to quantify time-variant responses of *C. thermocellum* metabolism to pressure perturbations, given limited kinetic information. The results collectively suggest that ethanol production from *C. thermocellum* may be improved under conditions of elevated pressures in the presence of dissolved hydrogen concentration with a devised strategy to at least ensure that the reaction, $\text{NAD} + \text{H}_2 \leftrightarrow \text{NADH} + \text{H}^+$ is at equilibrium to maintain thermodynamic feasibility of increased hydrogen production.

In the absence of kinetic information, FSA effectively demonstrated significant time influence on metabolic flux distribution relative to steady state observations. Model predictions indicated that changes in acetate production and ethanol production respectively, do not happen immediately upon increases in hydrogen concentrations and pressures but occur after at least two-thirds of the time taken to reach steady state after the perturbation. However, a more sound approach (PMFA) to predict the metabolic flux distributions compared to FSA may be preferred. The improved version, PMFA subsequently provides more efficient and reliable estimates.

CHAPTER 6 FUTURE DEVELOPMENTS

Microbial activities resulting in metabolic product yield patterns are known to be greatly influenced by both phenotypic and genotypic profiling. Therefore, the absence of genome-scale information may affect the prediction of a true metabolic profile of the microorganism in the model [45, 192, 193]. It is desirable to produce a more comprehensive model to further improve the potential of the overall model. A constraint-based whole cell model involving metabolomic, genomic and thermodynamic components sensitive to pressure-controlled fermentation process of the microorganism is proposed for future developments. Existing conceptual whole cell modeling frameworks [6, 194-196] may serve as relevant pointers for further developing the proposed model.

Since the quality of model predictions may be affected by data scarcity, pairing labeling experiments (^{13}C , mass spectrometry (MS) or nuclear magnetic resonance spectroscopy (NMR)) with modeling/simulation is recommended as these methods would improve the prediction of flux distribution to provide more accurate physiological details of the biological system or metabolic network. For example, ^{13}C -MFA would provide measurable intracellular fluxes rather than just intracellular concentration, thereby increasing the accuracy of measured flux (as flux is measured directly). NMR and MS are interchangeable labeling measurement techniques for intracellular data except that the latter allows high quality data measurements at sensitive and high speed operating levels [193, 195, 197, 198]. Notwithstanding the above facts, our study involving *C. thermocellum* growth on cellobiose in a continuous culture fermentation process satisfied the quasi-steady state conditions assumption of MFA [197]. Also the future model should be able to deal with structural validation of the model and to predict a wider spectrum of products [44].

APPENDIX A - CHAPTER 2

A.1 EXAMPLE MATLAB CODE USED FOR MCA (WILD TYPE)

```
clear all
clc
m =6; n =6;           %number of matrix rows and columns
I = eye(m,n);        %Identity matrix
ContA = [m,n];       %dimension of control coefficient matrix (WT0)
ContB = [m,n];       %dimension of control coefficient matrix
(WT0.5)
ContC = [m,n];       %dimension of control coefficient matrix (WT1)

M = [m,n];           %matrix containing elasticities with respect
                    %to intracellular metabolites

ELG6P1 = 0.561;      % G6P elasticity with respect to enzyme 1
ELG6P2 = 0.067;      % G6P elasticity with respect to enzyme 2
ELPyr2 = 1.140;      % Pyruvate elasticity with respect to enzyme 2
ELPyr3 = -0.702;     % Pyruvate elasticity with respect to enzyme 3
ELPyr4 = 2.159;      % Pyruvate elasticity with respect to enzyme 4
ELAcCoA4 = 0.165;    % AcCoA elasticity with respect to enzyme 4
ELAcCoA5 = 0.811;    % AcCoA elasticity with respect to enzyme 5
ELAcCoA6 = 1.162;    % AcCoA elasticity with respect to enzyme 6

J2A = 5.20;          %Flux from G6P to Pyruvate      [A-WT0]
J3A = 0.27;          %Flux from Pyruvate to Lactate
J4A = 4.95*2/3;      %Flux from Pyruvate to AcCoA
J5A = 2.74;          %Flux from AcCoA to Ethanol
J6A = 0.56;          %Flux from AcCoA to Acetate

J2B = 6.54;          %Flux from G6P to Pyruvate      [B-WT0.5]
J3B = 0.24;          %Flux from Pyruvate to Lactate
J4B = 6.30*2/3;      %Flux from Pyruvate to AcCoA
J5B = 3.64;          %Flux from AcCoA to Ethanol
J6B = 0.56;          %Flux from AcCoA to Acetate
```

```

J2C = 7.62;           %Flux from G6P to Pyruvate      [C-WT1]
J3C = 0.50;           %Flux from Pyruvate to Lactate
J4C = 7.13*2/3;       %Flux from Pyruvate to AcCoA
J5C = 3.20;           %Flux from AcCoA to Ethanol
J6C = 1.55;           %Flux from AcCoA to Acetate

M1A= ones(1,n);      % Row1 of Ma
M2A= [ELG6P1,ELG6P2,zeros(1,n-2)]; % Row2 of Ma
M3A= [0,ELPyr2,ELPyr3,ELPyr4,0,0]; % Row3 of Ma
M4A= [0,0,0,ELAcCoA4,ELAcCoA5,ELAcCoA6]; % Row4 of Ma
M5A= [0,0,1-(J3A/J2A),-(J3A/J2A),0,0]; % Row5 of Ma
M6A= [zeros(1,n-2),-(J6A/J4A),1-(J6A/J4A)]; % Row6 of Ma

Ma=[M1A;M2A;M3A;M4A;M5A;M6A]; % Matrix Ma
Va=[1 -1 -1 -1 J4A/J2A J6A/J4A]';
ContA =inv(Ma)*diag(I*Va);
%ContA =inv(Ma)*eye(m,n);
%ContA = [ContA(:,1) (-1*ContA(:,2:n-2))];

M1B= ones(1,n);      % Row1 of Mb
M2B= [ELG6P1,ELG6P2,zeros(1,n-2)]; % Row2 of Mb
M3B= [0,ELPyr2,ELPyr3,ELPyr4,0,0]; % Row3 of Mb
M4B= [0,0,0,ELAcCoA4,ELAcCoA5,ELAcCoA6]; % Row4 of Mb
M5B= [0,0,1-(J3B/J2B),-(J3B/J2B),0,0]; % Row5 of Mb
M6B= [zeros(1,n-2),-(J6B/J4B),1-(J6B/J4B)]; % Row6 of Mb

Mb=[M1B;M2B;M3B;M4B;M5B;M6B]; % Matrix Mb
Vb=[1 -1 -1 -1 J4B/J2B J6B/J4B]';
ContB =inv(Mb)*diag(I*Vb);
%ContB =inv(Mb)*eye(m,n);
% ContB = [ContB(:,1) (-1*ContB(:,2:n-2))];

M1C= ones(1,n);      % Row1 of Mc
M2C= [ELG6P1,ELG6P2,zeros(1,n-2)]; % Row2 of Mc
M3C= [0,ELPyr2,ELPyr3,ELPyr4,0,0]; % Row3 of Mc
M4C= [0,0,0,ELAcCoA4,ELAcCoA5,ELAcCoA6]; % Row4 of Mc
M5C= [0,0,1-(J3C/J2C),-(J3C/J2C),0,0]; % Row5 of Mc

```

```

M6C= [zeros(1,n-2), -(J6C/J4C), 1-(J6C/J4C)]; % Row6 of Mc

Mc=[M1C;M2C;M3C;M4C;M5C;M6C]; % Matrix Mc
Vc=[1 -1 -1 -1 J4C/J2C J6C/J4C]';
ContC =inv(Mc)*diag(I*Vc);
%ContC =inv(Mc)*eye(m,n);
%ContC = [ContC(:,1) (-1*ContC(:,2:n-2))];

disp('Control Coefficients A')
disp(ContA)
disp('Control Coefficients B')
disp(ContB)
disp('Control Coefficients C')
disp(ContC)

```

APPENDIX B - CHAPTER 3

B.1 MFA AND MCA ESTIMATES FROM MODEL

Treatment	Statistics	Predicted fluxes from MFA model using experimental measurement inputs							
		Vcbp	Vemp	Vpdh	Vldh	Vadh	Vak	Vexteth	Vextco2
WT0	means	7.16	5.18	4.83	0.35	2.47	0.75	2.47	1.61
	variance	0.0010	0.0010	0.0027	0.0008	0.0716	0.0556	0.0715	0.0003
	stdev	0.0316	0.0316	0.0520	0.0283	0.2676	0.2358	0.2674	0.0173
WT05	means	8.52	6.54	6.27	0.27	3.36	0.83	3.36	2.09
	variance	0.0002	0.0002	0.0018	0.0025	0.1235	0.1431	0.1234	0.0002
	stdev	0.0141	0.0141	0.0424	0.0500	0.3514	0.3783	0.3513	0.0141
WT1	means	9.69	7.71	7.17	0.54	3.46	1.32	3.46	2.39
	variance	0.000008	0.000008	0.0006	0.0005	0.2970	0.3122	0.2967	0.00006
	stdev	0.0028	0.0028	0.0245	0.0224	0.5450	0.5587	0.5447	0.0077
EA0	means	10.58	8.60	7.64	0.96	3.99	1.11	3.98	2.54
	variance	0.0585	0.0585	0.0482	0.0215	0.0866	0.1460	0.0865	0.0053
	stdev	0.2419	0.2419	0.2195	0.1466	0.2943	0.3821	0.2941	0.0728
EA1	means	11.41	9.43	8.76	0.67	4.93	0.91	4.93	2.92
	variance	0.0030	0.0030	0.0014	0.0003	0.0073	0.0070	0.0073	0.0002
	stdev	0.0548	0.0548	0.0374	0.0173	0.0854	0.0837	0.0854	0.0141
EA5	means	11.01	9.03	8.24	0.79	4.08	1.42	4.07	2.74
	variance	0.4372	0.4372	0.4553	0.0011	0.2213	0.0085	0.2211	0.0505
	stdev	0.6612	0.6612	0.6748	0.0332	0.4704	0.0922	0.4702	0.2247

B.2 MFA AND MCA ESTIMATES FROM MONTE CARLO SIMULATION

Treatment	Statistics	Predicted fluxes from MFA model using Monte Carlo Simulation inputs							
		Vcbp	Vemp	Vpdh	Vldh	Vadh	Vak	Vexteth	Vextco2
WT0	means	6.96	4.98	4.62	0.36	2.24	0.84	2.24	1.54
	variance	0.0156	0.0156	0.0141	0.0001	0.0086	0.0044	0.0086	0.0016
	stdev	0.1249	0.1249	0.1187	0.0100	0.0927	0.0663	0.0927	0.0400
WT05	means	8.29	6.31	6.03	0.29	3.03	0.99	3.03	2.01
	variance	0.0173	0.0173	0.0164	0.0002	0.0163	0.0119	0.0163	0.0018
	stdev	0.1315	0.1315	0.1281	0.0141	0.1277	0.1091	0.1277	0.0424
WT1	means	9.40	7.42	6.89	0.53	3.04	1.56	3.04	2.29
	variance	0.0279	0.0279	0.0248	0.0001	0.0311	0.0258	0.0310	0.0028
	stdev	0.1670	0.1670	0.1575	0.0100	0.1764	0.1606	0.1761	0.0529
EA0	means	10.47	8.50	7.48	1.01	3.72	1.27	3.71	2.49
	variance	0.0212	0.0212	0.0197	0.0019	0.0188	0.0122	0.0188	0.0022
	stdev	0.1456	0.1456	0.1404	0.0436	0.1371	0.1105	0.1371	0.0469
EA1	means	11.18	9.20	8.54	0.66	4.77	0.93	4.76	2.85
	variance	0.0209	0.0209	0.0186	0.0001	0.0067	0.0007	0.0067	0.0021
	stdev	0.1446	0.1446	0.1364	0.0100	0.0819	0.0265	0.0819	0.0458
EA5	means	11.05	9.07	8.29	0.78	4.10	1.43	4.10	2.76
	variance	0.0661	0.0661	0.0621	0.0002	0.0233	0.0012	0.0233	0.0069
	stdev	0.2571	0.2571	0.2492	0.0141	0.1526	0.0346	0.1526	0.0831

APPENDIX C - CHAPTER 4

C.1 FLUX CALCULATIONS

$$\text{Extracellular metabolite flux (mmol/gdcwh)} = \frac{[\text{Extracellular metabolite}] \text{ (mM)}}{\text{cell density (g/L)}} \times \text{dilution rate (hr}^{-1}\text{)}$$

OR

$$\text{Extracellular metabolite flux (mM/hr)} = [\text{Extracellular metabolite}] \text{ (mM)} \times \text{dilution rate (hr}^{-1}\text{)}$$

$$\text{Biomass flux (mmol/gdcwh)} = \frac{[\text{Biomass}] \text{ (mg/l)}}{\text{cell density} \left(\frac{\text{g}}{\text{l}}\right) \times \text{molecular weight} \left(\frac{\text{g}}{\text{mol}}\right)} \times 1000 \times \text{dilution rate (hr}^{-1}\text{)}$$

OR

$$\text{Biomass flux (mM/hr)} =$$

$$\frac{[\text{Biomass}] \text{ (mg/l)}}{\text{molecular weight} \left(\frac{\text{g}}{\text{mol}}\right)} \times 1000 \times \text{dilution rate (hr}^{-1}\text{)}$$

$$\text{Hydrogen flux (mmol/gdcwh)} = \frac{2 \times D \left(\frac{\text{cm}^2}{\text{s}}\right)}{d \text{ (cm)}} \times A \left(\frac{\text{cm}^2}{\text{cell}}\right) \times n \text{ (cells/ml)} \times [\text{H}_2]^* \quad [199]$$

$[\text{H}_2]^*$ = maximum solubility of hydrogen gas (mM) at each pressure

A = cell surface area of contact

D = effective diffusion coefficient of hydrogen

d = representative diameter of cell

OR

$$\text{Hydrogen flux (mM/hr)} = ([\text{H}_2]_l - [\text{H}_2]^*) \times \text{dilution rate (hr}^{-1}\text{)}$$

$[\text{H}_2]^*$ = maximum solubility of hydrogen gas (mM) at each pressure

$[\text{H}_2]_l$ = dissolved hydrogen concentration in media

C.2 EXAMPLE MFA FOR GENERATING STOICHIOMETRIC MATRIX

```
clear all
clc
%% METABOLIC FLUX MODELING.....
% Created in 2005 by Bless Adotey.....
% Edited in 2005 by Tae Hoon Yang .....
% Revised by Bless Adotey (2009, 2010, 2011)
%%
```

```

%% STEP 01: involved fluxes as cell string
.....
% intracellular fluxes
intfluxcell = {'Jcbp';
'Jpgm';'Jemp';'Jpdh';'Jnadh';'Jnh3';'Jh20';'Jatp';'Jbio'; 'Jadh';'Jak';
              'Jldh';'Jextco2';'Jupt';'Jh2Dsolv'};

% extracellular fluxes
extfluxcell =
{'Jextace';'Jexteth';'Jextbio';'Jextlac';'Jgly';'Jh2press'};

% all fluxes participating in the network
fluxcell = [intfluxcell;extfluxcell];      % always intracellular
(immeasurable) followed by extracellular (measurable) fluxes

%%
%STEP 02: symbolize variables
.....
.....
for k = 1:length(fluxcell)
    flux = char(fluxcell(k));
    eval(['syms ',flux]);                %
symbolizing
    eval(['fluxvector(',num2str(k),',1) =',flux,'];']) % symbolized
fluxes as a vector notation
end

%% STEP 03: Steady state stoichiometric equations
.....
equation(1,1) = Jupt-Jcbp-1/3*Jbio;
% Cellobiose transport (Balance around CBin including biomass stoic)

equation(2,1) = Jcbp + Jpgm - Jemp;
% Balance around glucose G6P

equation(3,1) = Jcbp - Jpgm - Jgly;
% Balance around glucose 1P

```



```

equation(4,1) = 2*Jemp - Jldh - Jpdh;
% Balance around pyruvate
equation(5,1) = Jpdh - Jak - Jadh;
% Balance around acetyl CoA

equation(6,1) = Jldh - Jextlac;
% lactate transport out of cell membrane

equation(7,1) = Jak - Jextace;
% Acetate transport out of cell membrane

equation(8,1) = Jadh - Jexteth;
% Ethanol transport out of cell membrane

equation(9,1) = Jpdh - Jextco2;
% Carbon dioxide balance

equation(10,1) = Jbio - Jextbio;
% Biomass transport out of cell membrane

%% NADH, Hydrogen
% Reversible NAD + H2 reaction and nad consumption tied to H2.
equation(11,1)= Jnadh+Jemp-(Jldh+2*Jadh)- 0.58*Jbio;
equation(12,1) = -Jnadh+Jh2Dsolv+Jpdh-Jh2press;

%% Ammonia,ATP,H2O
equation(13,1)= Jnh3 - Jbio;
equation(14,1)= Jatp -7.93*Jbio;
equation(15,1)= Jh2o+ 1.67*Jbio-Jemp;

%%
% STEP 04: symbolic differentiation and its evaluation
.....
.....
Nsym = jacobian(equation, fluxvector);
N      = eval(Nsym);

```

```

disp(' ')
disp('>>> overall stoichiometric matrix
.....')
N
[row,col] = size(N);
%%
% STEP 05: system matrix partitioning and checking consistency
.....
disp(' ')
disp('>>> partial stoichiometric matrix: immeasurable
fluxes.....')
Nn      = N(:,1:length(intfluxcell));
Nnsym   = Nsym(:,1:length(intfluxcell)); % symbolic
nfluxsym = fluxvector(1:length(intfluxcell),1);

disp(' ')
disp('>>> partial stoichiometric matrix: measurable fluxes
.....')
Nb      = N(:,length(intfluxcell)+1:col);
Nbsym   = Nsym(:,length(intfluxcell)+1:col); % symbolic
bfluxsym = fluxvector(length(intfluxcell)+1:length(fluxvector),1);

disp(' ')
disp(['Rank of matrix Nn: ' num2str(rank(Nn))])
disp(['No. of unknown fluxes: ' num2str(length(intfluxcell))])
disp(['No. of equations: ' num2str(length(equation))])

% Matrix Sensitivity Analysis (Checking matrix singularity)
.....
RK = rcond(Nn'*Nn) % reciprocal condition number
if RK > 5*eps
    disp('')
    disp('>>> STOICHIOMETRIC MATRIX IS WELL-
CONDITIONED!.....')
else
    disp('')
    disp('>>> STOICHIOMETRIC MATRIX IS ILL-
CONDITIONED.....')

```

```

end

% Determinancy checking
.....

if rank(Nn) < length(intfluxcell)
    disp(' ')
    disp('>>> System is underdetermined')
else
    if rank(Nn)== length(intfluxcell)
        disp(' ')
        disp('>>> System is determined!')
    else
        disp(' ')
        disp('>>> System is overdetermined')
    end
end

end

% Implementing the following as given by Klamt et
al.(2002).....
% redundancy checking
% balanciability checking
% calculablity checking

% redundancy analysis
if rank(Nn) < length(equation)
    disp(' ')
    disp('..... System is redundant and can be inconsistent!')

% redundant matrix
REDmat = Nb-Nn*pinv(Nn)*Nb;

% degree of redundancy
DoRED = rank(REDmat);
disp(' ')
disp(['      Degree of Redundancy: ', num2str(DoRED)]);

% balanceablity analysis

```

```

[row, col] = size(REDmat)
nonbalancibleflux = {};
counter = 1;
for k = 1:col
    if sum(REDmat(:,k)) == 0
        nonbalancibleflux(counter,1) = extfluxcell(k);
        counter = counter + 1;
    end
end
if ~isempty(nonbalancibleflux)
    disp(' ')
    disp('..... Non-balanceable fluxes detected')
    nonbalancibleflux
end
else
    disp(' ')
    disp('..... System is not redundant and consistent')
    REDmat = [];
    DoRED = [];
    nonbalancibleflux = {};
end

% calculablity analysis
if rank(Nn) < length(intfluxcell)
    calculableflux = {};
    Kn = null(Nn, 'r');
    if isempty(Kn)
        disp(' ')
        disp('..... No degrees of freedom exist')
    else
        disp(' ')
        disp('..... Degrees of freedom exist')
        [row, col] = size(Kn);
        counter = 1;
        for k = 1:row
            nulls = find(Kn(k, :)==0);
            if length(nulls) == length(Kn(k, :))
                calculableflux(counter,1) = intfluxcell(k);
            end
        end
    end
end

```

```

        counter = counter + 1;
    end
    clear nulls
end
disp(' ')
disp(' Calculable fluxes using least-squares i.e. pseudo-
inverse method')
disp(' These fluxes can be used as additional constraints')
calculableflux
end
else
disp(' ')
disp('..... No calculable fluxes detected!')
calculableflux = {};
end

% STEP 06: Parametrization:
.....
% augmented matrix
[row,col] = size(N);
AUGmat = [N,zeros(row,1)];

% reduced row echelon matrix (Gauss Jordan elimination with partial
pivoting)
RREmat = rref(AUGmat);

% dependent flux identification by Gauss Jordan elimination
kk = 1;
[row, col] = size(RREmat);
for k = 1:row
    % find leading one
    a = find(RREmat(k,:) == 1);
    if length(a) >= 1
        leadingone = a(1);

        % identifying: dependent or independent
        if length(find(RREmat(:,leadingone) == 0)) == (row-1)
            flux_depend(kk,1) = fluxvector(leadingone);

```

```

        index_depend(kk,1) = leadingone;
        kk = kk + 1;
    end
end
clear a
end

% independent flux identification
kk = 1;
for k = 1:length(fluxvector)
    if any(index_depend == k) == 0
        flux_independ(kk,1) = fluxvector(k);
        kk = kk + 1;
    end
end

% symbolic solution
if length(flux_depend) == length(nfluxsym)
    if length(find(flux_depend-nfluxsym==0))==length(nfluxsym)
        disp(' ')
        disp('..... Dependent fluxes match with unknown intracellular
fluxes!')

        if length(find(fluxvector-
([nfluxsym;bfluxsym])==0))==length(fluxvector)
            fluxsolutionsym =inv(Nnsym)*(-Nbsym*bfluxsym);
        else
            for k = 1:length(equation)
                str1 = ['''',char(equation(k)), '=0'''];
                str2 = ['''',char(nfluxsym(k)), '''];

                if k == 1
                    equationstr = str1;
                    variablestr = str2;
                else
                    equationstr = [equationstr, ',', str1];
                    variablestr = [variablestr, ',', str2];
                end
            end
        end
    end
end

```

```

        end

        eqs = ['solve(',equationstr,',',',',variablestr,');'];
        Sflux = eval(eqs);
        for k = 1:length(nfluxsym)
            fluxsolutionsym(k,1) =
eval(['Sflux(',int2str(k),')',char(nfluxsym(k)),';']);
        end
    end

    fid = fopen('ResultantFluxEquation.m','w');
    for k = 1:length(nfluxsym)
        dependfluxcell(k,1) = cellstr(char(nfluxsym(k)));
        str2print          = [char(dependfluxcell(k,1)), ' =
',char(fluxsolutionsym(k)),';'];
        fluxsolutioncell(k,1) = cellstr(char(fluxsolutionsym(k)));
        str2print          = [str2print,'\n'];
        fprintf(fid,str2print);
    end
    fclose(fid);
else
    disp(' ');disp(' ');disp(' ');
    disp('WARNING: Inconsistency between...')
    disp('dependent fluxes chosen by system
.....')
    for k = 1:length(flux_depend)
        dependfluxes(k,1) = cellstr(char(flux_depend(k)));
    end
    dependfluxes'
    disp('dependent fluxes chosen by user
.....')
    intfluxcell'
    disp('Redefine "intfluxcell" & "extfluxcell" and try again!')
end
else
    disp(' ');disp(' ');disp(' ');
    disp('WARNING: Inconsistency between...')

```

```

disp('dependent fluxes chosen by system
.....')
for k = 1:length(flux_depend)
    dependfluxes(k,1) = cellstr(char(flux_depend(k)));
end
dependfluxes'
disp('dependent fluxes chosen by user
.....')
intfluxcell'
disp('Redefine "intfluxcell" & "extfluxcell" and try again!')
end

```

C.3 VSPECTRUMC_OPT FUNCTION TO CALCULATE THE FLUX SPECTRUM

```

% Francisco Llaneras
% Dept. of Systems Engineering and Control (DISA)
% Technical University of Valencia (UPV)
% e-mail: frallaes@doctor.upv.es and kikollan@gmail.com
% Web Page: http://science.ensilicio.com
function [Vmin,Vmax,Flag] =
vspectrumC_OptForIllustration(N,Q,irrev,Vm_mini,Vm_maxi,Options)

% N:      Stoichiometric matrix (N*v=0)
% Q:      Matrix of measured fluxes (Q*v=vm)
% irrev:  Vector with indexes of the irreversible fluxes
% Vm_mini: Vector with minimum values of the measured fluxes
% Vm_maxi: Vector with maximum values of the measured fluxes
% Options: Options for linprog
%
% Vmin:   'flux spectrum' minimums
% Vmax:   'flux spectrum' maximums
%
% Auxiliar
m=size(N,1);      % number of metabolite
n=size(N,2);      % number of fluxes
nvm=size(Vm_mini,1); %number of measured fluxes
Vmax=[];Vmin=[];Flag=[];

```



```

% for each flux...
for i=1:1:n
    ind=zeros(1,n);
    ind(i)=1;

    % calculate its minimum value with linear programming (minimize v)
    [min_i,a,flag_min]=linprog(ind,[-N;N;-Q;Q;-
diag(irrev)], [zeros(2*m,1);-
Vm_mini;Vm_maxi;zeros(n,1)], [], [], [], [], [], Options);
    Vmin=[Vmin;min_i(i)];
    ind=zeros(1,n);
    ind(i)=-1;

    % calculate its maximum value with linear programming (minimize -v)
    [max_i,a,flag_max]=linprog(ind,[-N;N;-Q;Q;-
diag(irrev)], [zeros(2*m,1);-
Vm_mini;Vm_maxi;zeros(n,1)], [], [], [], [], [], Options);
    Vmax=[Vmax;max_i(i)];
    Flag=[Flag;flag_min flag_max]; % Information about convergence
end

```

C.4 VSPECTRUMCB_OPT FUNCTION TO CALCULATE THE FLUX SPECTRUM

```

% Francisco Llaneras
% Dept. of Systems Engineering and Control (DISA)
% Technical University of Valencia (UPV)
% e-mail: frallaes@doctor.upv.es and kikollan@gmail.com
% Web Page: http://science.ensilicio.com

function [Vmin,Vmax,Flag] =
vspectrumCb_Opt(N,irrev,vm_ind,Vm_mini,Vm_maxi,Options)
% N: Stoichiometric matrix (N*v=0)
% irrev: Vector with indexes of the irreversible fluxes
% vm_ind: Vector with indexes of the measured fluxes
% Vm_mini: Vector with minimum values of the measured fluxes
% Vm_maxi: Vector with maximum values of the measured fluxes
% Options: Options for linprog
%

```

```

% Vmin:      'flux spectrum' minimums
% Vmax:      'flux spectrum' maximums
% Auxiliar
m=size(N,1);      % number of metabolite
n=size(N,2);      % number of fluxes
nvm=size(Vm_mini,1); %number of measured fluxes

% Compute matrix iQ      Q*v=vm
Q=zeros(nvm,n);
for i=1:1:nvm
    ind_vm=vm_ind(i);
    Q(i,ind_vm)=1;
end

% Compute the flux spectrum
[Vmin,Vmax,Flag] = vspectrumC_Opt(N,Q,irrev,Vm_mini,Vm_maxi,Options);

```

C.5 EXAMPLE STEADY STATE FSA CODE USING LLANERAS FUNCTION VSPECTRUMCb_OPT

```

%Stoichiometric Matrix
N;
% All fluxes assumed to be irreversible except 2,5
% irrev=[ones(1,6)];
irrev = ones(1,size(N,2));
irrev(2)=0;
irrev(5)=0;

% Index of measured fluxes
Jm_ind = [16,17,18,19,20,21];

% Example measured fluxes used as measured input with uncertainty
a=[1.01; 0.05; 0.22; 0.0.05; 0.005; 1.8];

% assuming +/- 5% uncertainty in measurements
% improved interval method
% max and min values per each fluxes
a_max=a*1.05;

```

```

a_min=min(0.001,a*0.95);
[a_min a_max]; % combining absolute and relative tolerances
Jm_max= [a_max ]';
Jm_min= [a_min ]';

% Computing flux spectrum solution using two Llaneras' matlab function
% vspectrumCb_opt

options=optimset('LargeScale','off', 'Simplex', 'on');

[Jm_min,Jm_max,flaga] =
vspectrumCb_opt(N,irrev,Jm_ind,Jm_min,Jm_max,options);

%% plotting results:
figure()
% Calculate center, up and down.
Jm=0.5*(Jm_min+Jm_max);
range_d=Jm-Jm_min;
range_u=Jm_max-Jm;
% Plot with errorbar function.
h1=errorbar([1:size(N,2)],Jm,range_d,range_u,'ok','LineWidth',2)
xlabel('Reaction (1-21)');
ylabel('Flux [mM/hr]');
set(gca,'XTick',[1:size(N,2)])
set(gca,'XLim',[0.5 21.5])
set(gca,'YLim',[0 5])
grid

```

APPENDIX D - CHAPTER 5

D.1 SAMPLE MATLAB CODE ODE FOR SOLUTION TO GIVEN DATA

```
clc
clear all
t=120;
% the initial guess for the parameters
global CBobs H2obs Ethobs Aceobs Lacobs CB01 CB02 CB03 H201 H202 H203
Eth01 Eth02 Eth03 Ace01 Ace02 Ace03 Lac01 Lac02 Lac03
global VeEthobs VeCBobs1 VeCBobs2 VeCBobs3 VeCBobs1b VeCBobs2b
VeCBobs3b VeAceobs VeLacobs D1 D2 X1 X2 X3 X1b X2b X3b theta;

% the initial conditions
CBobs=5.84;
VeCBobs1=0.65;
VeCBobs2=1.11;
VeCBobs3=1.95;
VeCBobs1b=3.40;
VeCBobs2b=4.38;
VeCBobs3b=11.68;
H2obs=0;
VeH2obs=0;
Ethobs=0;
VeEthobs=0;
Aceobs=0;
VeAceobs=0;
Lacobs=0;
VeLacobs=0;

X1=0.45;           %%0.05/hr 1atm
X2=0.2625;        %%0.05/hr 7Mpa
X3=0.15;          %%0.05/hr 17Mpa
X1b=0.55;         %%0.32/hr 1atm
X2b=0.4;          %%0.32/hr 7Mpa
X3b=0.125;        %%0.32/hr 7Mpa

D1=0.05;
D2=0.32;
```

```

% theta =0.11;      % unique adjustable parameter

CB01=0.15;  %residual cellobiose @0.05/hr 1atm
CB02=0.19;  %residual cellobiose @0.05/hr 7Mpa
CB03=0.042; %residual cellobiose @ 0.05/hr 17Mpa

CB01b=0.017; %residual cellobiose @0.32/hr 1atm
CB02b=0.042; %residual cellobiose @0.32/hr 7Mpa
CB03b=1.942; %residual cellobiose @ 0.32/hr 17Mpa

H201=0.7;           %@ 0.05/hr and 0.32/hr 1atm
H202=50.9;          %@ 0.05/hr and 0.32/hr 7Mpa
H203=130.4;         %@ 0.05/hr and 0.32/hr 17Mpa

Eth01=1;            %@0.05/hr 1atm
Eth02=12.8;         %@0.05/hr 7Mpa
Eth03=17.6;         %@0.05/hr 17Mpa

Eth01b=4.6;         %@0.32/hr 1atm
Eth02b =16.1;       %@0.32/hr 7Mpa
Eth03b =10.4;       %@0.32/hr 17Mpa

Ace01=20.2;         %@0.05/hr 1atm
Ace02=8.5;          %@0.05/hr 7Mpa
Ace03=7.4;          %@0.05/hr 17Mpa

Ace1b=12.6;         %@0.32/hr 1atm
Ace2b=10.1;         %@0.32/hr 7Mpa
Ace3b=7.4;          %@0.32/hr 17Mpa

Lac01=1;            %@0.05/hr 1atm
Lac02=2;            %@0.05/hr 7Mpa
Lac03=0.9;          %@0.05/hr 17Mpa

Lac01b=0.9;         %@0.32/hr 1atm
Lac02b=0.4;         %@0.32/hr 7Mpa

```

```

Lac03b=0.2;          %@0.32/hr 17Mpa

% ODE solution
% [T,Res] = ode45('ReUpdatedODEfunc',[0,t],
[CBobs;VeCBobs1;H2obs;VeH2obs;Ethobs;VeEthobs;Aceobs;VeAceobs;Lacobs;Ve
Lacobs]);
[T,Res] = ode45('ReUpdatedODEfunc',[0,t],
[CBobs;VeCBobs2;H2obs;VeH2obs;Ethobs;VeEthobs;Aceobs;VeAceobs;Lacobs;Ve
Lacobs]);
% [T,Res] = ode45('ReUpdatedODEfunc',[0,t],
[CBobs;VeCBobs3;H2obs;VeH2obs;Ethobs;VeEthobs;Aceobs;VeAceobs;Lacobs;Ve
Lacobs]);
%
% [T,Res] = ode45('ReUpdatedODEfunc',[0,t],
[CBobs;VeCBobs1b;H2obs;VeH2obs;Ethobs;VeEthobs;Aceobs;VeAceobs;Lacobs;V
eLacobs]);
% [T,Res] = ode45('ReUpdatedODEfunc',[0,t],
[CBobs;VeCBobs2b;H2obs;VeH2obs;Ethobs;VeEthobs;Aceobs;VeAceobs;Lacobs;V
eLacobs]);
% [T,Res] = ode45('ReUpdatedODEfunc',[0,t],
[CBobs;VeCBobs3b;H2obs;VeH2obs;Ethobs;VeEthobs;Aceobs;VeAceobs;Lacobs;V
eLacobs]); % you may solve for each metabolite individually or
together. NB: Acetate and Ethanol fluxes are compared to predictions
from model. Only lactate, cellobiose, hydrogen from here are used for
model inputs.

```

D.2 FUNCTION FSADYNAMICFUNC3

```

function y = FSAdynamicfunc3(t,x)
global CBobs H2obs Ethobs Aceobs Lacobs H201 H202 H203
global CB01 CB02 CB03 CB01b CB02b CB03b Eth01b Eth02b Eth03b
global Ace01 Ace02 Ace03 Ace01b Ace02b Ace03b
global Eth01 Eth02 Eth03Lac01 Lac02 Lac03 Lac01b Lac02b Lac03b
global X1 X2 X3 X1b X2b X3b D1 D2 theta
y=zeros(size(x));
% % All four measurements
%% transient @ 0.05 dilution rate for 0.1Mpa

```

```

% cellobiose @ atm pressure
% y(1)=((x(2).*X1-D1*x(1)-2*theta*(x(1)-CB01)));
% y(2)=-(((theta)^2).*x(1)-CB01))./X1;
% %Hydrogen @ atm pressure
% y(3)=((x(4).*X1-D1.*x(3)-2*theta*(x(3)-H201)));
% y(4)=-(((theta)^2).*x(3)-H201))./X1;
%
% %Ethanol @ atm pressure
% y(5)=((x(6)*X1-D1*x(5)-2*theta*(x(5)-Eth01)));
% y(6)=-(((theta)^2)*x(5)-Eth01)/X1;
%
% %Acetate @ atm pressure
% y(7)=((x(8)*X1-D1*x(7)-2*theta*(x(7)-Ace01)));
% y(8)=-(((theta)^2)*x(7)-Ace01)/X1;
%
% %Lactate @ atm pressure
% y(9)=((x(10)*X1-D1*x(9)-2*theta*(x(9)-Lac01)));
% y(10)=-(((theta)^2)*x(9)-Lac01)/X1;

%% transient @ 0.32 dilution rate for 0.1Mpa
% %cellobiose @ atm pressure
% y(1)=((x(2).*X1b-D2*x(1)-2*theta*(x(1)-CB01b)));
% y(2)=-(((theta)^2).*x(1)-CB01b))./X1b;
%
% %Hydrogen @ atm pressure
% y(3)=((x(4).*X1b-D2.*x(3)-2*theta*(x(3)-H201)));
% y(4)=-(((theta)^2).*x(3)-H201))./X1b;
%
% %Ethanol @ atm pressure
% y(5)=((x(6)*X1b-D2*x(5)-2*theta*(x(5)-Eth01b)));
% y(6)=-(((theta)^2)*x(5)-Eth01b)/X1b;
%
% %Acetate @ atm pressure
% y(7)=((x(8)*X1b-D2*x(7)-2*theta*(x(7)-Ace01b)));
% y(8)=-(((theta)^2)*x(7)-Ace01b)/X1b;
%
% %Lactate @ atm pressure

```

```

% y(9)=((x(10)*X1b-D2*x(9)-2*theta*(x(9)-Lac01b)));
% y(10)=-(((theta)^2)*(x(9)-Lac01b))/X1b;

%% transient @ 0.05 dilution rate for 7Mpa
%cellobiose @ 7Mpa pressure
y(1)=((x(2).*X2-D1*x(1)-2*theta*(x(1)-CB02))); % CBin= x(1)
y(2)=-(((theta)^2).*x(1)-CB02))./X2;

%Hydrogen @ 7Mpa pressure
y(3)=((x(4).*X2-D1.*x(3)-2*theta*(x(3)-H202))); % CBin= x(1)
y(4)=-(((theta)^2).*x(3)-H202))./X2;

%Ethanol @ 7Mpa pressure
y(5)=((x(6).*X2-D1*x(5)-2*theta*(x(5)-Eth02)));
y(6)=-(((theta)^2)*(x(5)-Eth02))/X2;

%Acetate @ 7Mpa pressure
y(7)=((x(8).*X2-D1*x(7)-2*theta*(x(7)-Ace02)));
y(8)=-(((theta)^2)*(x(7)-Ace02))/X2;

%Lactate @ 7Mpa pressure
y(9)=((x(10).*X2-D1*x(9)-2*theta*(x(9)-Lac02)));
y(10)=-(((theta)^2)*(x(9)-Lac02))/X2;
%

%% transient @ 0.32 dilution rate for 7Mpa
% cellobiose @ 7Mpa pressure
% y(1)=((x(2).*X2b-D2*x(1)-2*theta*(x(1)-CB02b)));
% y(2)=-(((theta)^2).*x(1)-CB02b))./X2b;

%Hydrogen @ 7Mpa pressure
% y(3)=((x(4).*X2b-D2.*x(3)-2*theta*(x(3)-H202)));
% y(4)=-(((theta)^2).*x(3)-H202b))./X2b;
%
% %Ethanol @ 7Mpa pressure
% y(5)=((x(6)*X2b-D2*x(5)-2*theta*(x(5)-Eth02b)));

```



```

% y(6)=-(((theta)^2)*(x(5)-Eth02b))/X2b;
%
% %Acetate @ 7Mpa pressure
% y(7)=((x(8)*X2b-D2*x(7)-2*theta*(x(7)-Ace02b)));
% y(8)=-(((theta)^2)*(x(7)-Ace02b))/X2b;
% %
% %Lactate @ 7Mpa pressure
% y(9)=((x(10)*X2b-D2*x(9)-2*theta*(x(9)-Lac02b)));
% y(10)=-(((theta)^2)*(x(9)-Lac02b))/X2b;

% %% transient @ 0.05 dilution rate for 17Mpa
% %cellobiose @ 17Mpa pressure
% y(1)=((x(2).*X3-D1*x(1)-2*theta*(x(1)-CB03)));
% y(2)=-(((theta)^2).*x(1)-CB03))./X3;
%
% %Hydrogen @ 17Mpa pressure
% y(3)=((x(4).*X3-D1.*x(3)-2*theta*(x(3)-H203)));
% y(4)=-(((theta)^2).*x(3)-H203))./X3;
%
% %Ethanol @ 17Mpa pressure
% y(5)=((x(6)*X3-D1*x(5)-2*theta*(x(5)-Eth03)));
% y(6)=-(((theta)^2)*(x(5)-Eth03))/X3;
%
% %Acetate @ 17Mpa pressure
% y(7)=((x(8)*X3-D1*x(7)-2*theta*(x(7)-Ace03)));
% y(8)=-(((theta)^2)*(x(7)-Ace03))/X3;
%
% %Lactate @ 17Mpa pressure
% y(9)=((x(10)*X3-D1*x(9)-2*theta*(x(9)-Lac03)));
% y(10)=-(((theta)^2)*(x(9)-Lac03))/X3;

% %% transient @ 0.32 dilution rate for 17Mpa
% %cellobiose @ 17Mpa pressure
% y(1)=((x(2).*X3b-D2*x(1)-2*theta*(x(1)-CB03b)));
% y(2)=-(((theta)^2).*x(1)-CB03b))./X3b;

%Hydrogen @ 17Mpa pressure

```

```

% y(3)=((x(4).*X3b-D2.*x(3)-2*theta*(x(3)-H203));
% y(4)=-(((theta)^2).*x(3)-H203)./X3b;
%
% %Ethanol @ 17Mpa pressure
% y(5)=((x(6)*X3b-D2*x(5)-2*theta*(x(5)-Eth03b));
% y(6)=-(((theta)^2)*x(5)-Eth03b)/X3b;
%
% %Acetate @ 17Mpa pressure
% y(7)=((x(8)*X3b-D2*x(7)-2*theta*(x(7)-Ace03b));
% y(8)=-(((theta)^2)*x(7)-Ace03b)/X3b;
%
% %Lactate @ 17Mpa pressure
% y(9)=((x(10)*X3b-D2*x(9)-2*theta*(x(9)-Lac03b));
% y(10)=-(((theta)^2)*x(9)-Lac03b)/X3b;

```

D.3 EXAMPLE DYNAMIC STATE FSA CODE USING FUNCTION VSPECTRUMCB_OPT

```

%Stoichiometric Matrix
N;
% All fluxes initialized into a vector as irreversible except 2,5
% irrev=[ones(1,6)];
irrev = ones(1,size(N,2));
irrev(2)=0;
irrev(5)=0;

% Measured fluxes used as measured input with uncertainty

Jm_ind = [16,17,18,19,20,21]; % index of measured fluxes

% max and min values per each fluxes
%% improved interval method
a=[] % vector of measurements for metabolite 16 obtained over time
b=[] % vector of measurements for metabolite 17 obtained over time
c=[] % vector of measurements for metabolite 18 obtained over time
d=[] % vector of measurements for metabolite 19 obtained over time
e=[] % vector of measurements for metabolite 20 obtained over time

```

```

f=[] % vector of measurements for metabolite 21 obtained over time

% assuming +/- 5% uncertainty in measurements
a_max=max(0.001,a*1.05);
a_min=a*0.95;
[a_min a_max]; % combining absolute and relative tolerances

b_max=max(0.001,b*1.05);
b_min=b*0.95;
[b_min b_max]; % combining absolute and relative tolerances

Jm_max= [a_max b_max]';
Jm_min= [a_min b_min]';

% Initializing resulting flux spectrum
Rmin=[];
Rmax=[];

for i=1:length(a)
    options=optimset('LargeScale','off','Simplex','on');
    [J_min,J_max,flag] =
vspectrumCb_opt(N,irrev,ind,Jm_min(:,i),Jm_max(:,i),options);
    if exist('Rmin','var')
        Rmin=[Rmin J_min];
        Rmax=[Rmax J_max];
    else
        Rmin=[];
        Rmin=[J_min];
        Rmax=[J_max];
    end

end

end

% Computing flux spectrum solution using defined function
% vspectrumCb_opt

```

```

options=optimset('LargeScale','off', 'Simplex', 'on');

[Jm_min, Jm_max, flaga] =
vspectrumCb_opt(N, irrev, Jm_ind, Jm_min, Jm_max, options);

```

D.4 LLANERAS' ET AL., 2007 FUNCTION VSPECTRUMCB_OPT

```

% Francisco Llaneras
% Dept. of Systems Engineering and Control (DISA)
% Technical University of Valencia (UPV)
% e-mail: frallaes@doctor.upv.es and kikollan@gmail.com
function [Vmin, Vmax, Flag] =
vspectrumCb_Opt(N, irrev, vm_ind, Vm_mini, Vm_maxi, Options)
% Calculate the flux spectrum
% N:      Stoichiometric matrix (N*v=0)
% irrev:  Vector with indexes of the irreversible fluxes
% vm_ind: Vector with indexes of the measured fluxes
% Vm_mini: Vector with minimum values of the measured fluxes
% Vm_maxi: Vector with maximum values of the measured fluxes
% Options: Options for linprog
%
% Vmin:   'flux spectrum' minimums
% Vmax:   'flux spectrum' maximums
%
%
m=size(N,1);      % number of metabolite
n=size(N,2);      % number of fluxes
nvm=size(Vm_mini,1); %number of measured fluxes

% Compute matrix iQ      Q*v=vm
Q=zeros(nvm,n);
for i=1:1:nvm
    ind_vm=vm_ind(i);
    Q(i,ind_vm)=1;
end

% Compute the flux spectrum
[Vmin, Vmax, Flag] = vspectrumC_Opt(N, Q, irrev, Vm_mini, Vm_maxi, Options);

```

D.5 LLANERAS' ET AL., 2007 FUNCTION VZPECTRUMC_OPT

```
% Francisco Llaneras
% Dept. of Systems Engineering and Control (DISA)
% Technical University of Valencia (UPV)
% e-mail: frallaes@doctor.upv.es and kikollan@gmail.com
function [Vmin,Vmax,Flag] =
vspectrumC_Opt(N,Q,irrev,Vm_mini,Vm_maxi,Options)
%
% Auxiliar
m=size(N,1);           % number of metabolite
n=size(N,2);           % number of fluxes
nvm=size(Vm_mini,1);   %number of measured fluxes
Vmax=[];Vmin=[];Flag=[];

% for each flux...
for i=1:1:n
    ind=zeros(1,n);
    ind(i)=1;

    % calculate its minimum value with linear programming (minimize v)
    [min_i,a,flag_min]=linprog(ind,[-N;N;-Q;Q;-
diag(irrev)], [zeros(2*m,1);-
Vm_mini;Vm_maxi;zeros(n,1)], [], [], [], [], Options);
    Vmin=[Vmin;min_i(i)];
    ind=zeros(1,n);
    ind(i)=-1;

    % calculate its maximum value with linear programming (minimize -v)
    [max_i,a,flag_max]=linprog(ind,[-N;N;-Q;Q;-
diag(irrev)], [zeros(2*m,1);-
Vm_mini;Vm_maxi;zeros(n,1)], [], [], [], [], Options);
    Vmax=[Vmax;max_i(i)];
    Flag=[Flag;flag_min flag_max]; % Information about convergence
end
```


BIBLIOGRAPHY

- [1] C. N. Hamelinck, G. v. Hooijdonk, and A. P. C. Faaij, "Ethanol from lignocellulosic biomass: techno-economic performance in short-, middle- and long-term," *Biomass and Bioenergy*, vol. 28, pp. 384-410, 2005.
- [2] M. E. Himmel, "Biomass recalcitrance: engineering plants and enzymes for biofuels production (vol 315, pg 804, 2007)," *Science*, vol. 316, pp. 982-982, May 2007.
- [3] M. E. Himmel, S. Y. Ding, D. K. Johnson, W. S. Adney, M. R. Nimlos, J. W. Brady, and T. D. Foust, "Biomass recalcitrance: Engineering plants and enzymes for biofuels production," *Science*, vol. 315, pp. 804-807, Feb 2007.
- [4] S. W. Kang, Y. S. Park, J. S. Lee, S. I. Hong, and S. W. Kim, "Production of cellulases and hemicellulases by *Aspergillus niger* KK2 from lignocellulosic biomass," *Bioresource Technology*, vol. 91, pp. 153-156, 2004.
- [5] J. Lee, "Biological conversion of lignocellulosic biomass to ethanol," *Journal of Biotechnology*, vol. 56, pp. 1-24, 1997.
- [6] M. Tomita, "Whole-cell simulation: a grand challenge of the 21st century," *Trends in Biotechnology*, vol. 19, pp. 205-210, 2001.
- [7] J. J. Morgan, I. V. Surovtsev, and P. A. Lindahl, "A framework for whole-cell mathematical modeling," *Journal of Theoretical Biology*, vol. 231, pp. 581-596, Dec 2004.
- [8] A. L. Demain, M. Newcomb, and J. H. D. Wu, "Cellulase, clostridia, and ethanol," *Microbiology and Molecular Biology Reviews*, vol. 69, pp. 124+, Mar 2005.
- [9] W. Wiechert, "Modeling and simulation: tools for metabolic engineering," *Journal of Biotechnology*, vol. 94, pp. 37-63, Mar 2002.
- [10] N. D. Price, J. L. Reed, J. A. Papin, I. Famili, and B. O. Palsson, "Analysis of metabolic capabilities using singular value decomposition of extreme pathway matrices," *Biophysical Journal*, vol. 84, pp. 794-804, Feb 2003.
- [11] Horton HR, Moran LA, Scrimgeour KG, Perry MD, and R. JD, *Principles of Biochemistry*: Pearson Education Inc., 2006.
- [12] Stephanopoulos GN, Aristidou AA, and N. J., *Metabolic Engineering: Principles and Methodologies*: San Diego, California: Academic Press, 1998.
- [13] A. K. Agarwal, "Biofuels (alcohols and biodiesel) applications as fuels for internal combustion engines," *Process in Energy and Combustion Science*, vol. 33, pp. 233 - 271, 2007.
- [14] O. Zuhail and O. H. Kemal, "Turkish sugar production potential and use of waste of sugar beet as energy source," *International Journal of Green Energy*, vol. 1, pp. 381 - 392, Aug 2004 2004.
- [15] S. Kim and B. E. Dale, "Global potential bioethanol production from wasted crops and crop residues," *Biomass and Bioenergy*, vol. 26, pp. 361 - 375, 2004.
- [16] C. A. C. Alzate and O. J. S. Toro, "Energy consumption analysis of integrated flowsheets for production of fuel ethanol from lignocellulosic biomass," *Energy*, vol. 31, pp. 2447 - 2459, Oct 2006 2006.
- [17] Z. Kadar, S. F. Maltha, Z. Szengyel, K. Reczey, and W. De Laat, "Ethanol Fermentation of various pretreated and hydrolyzed substrates at low initial pH," *Applied Biochemistry and Biotechnology*, pp. 847 - 858, 2007.
- [18] K. A. Gray, L. S. Zhao, and M. Emptage, "Bioethanol," *Current Opinion in Chemical Biology*, vol. 10, pp. 141 - 146, Apr 2006 2006.

- [19] K. A. Gray, "Cellulosic ethanol - state of the technology," *International Sugar Journal* vol. 109, pp. 145 -, Mar 2007 2007.
- [20] B. S. Dien, M. A. Cotta, and T. W. Jeffries, "Bacteria engineered for fuel ethanol production: current status," *Applied Biochemistry and Biotechnology*, vol. 63, pp. 258 - 266, Dec 2003 2003.
- [21] P. Claassen, J. van Lier, C. AML, E. van Niel, L. Sijtsma, A. Stams, S. de Vries, and R. Weusthuis, "Utilisation of biomass for the supply of energy carriers," *Applied Microbiology and Biotechnology*, vol. 52, pp. 741-755, 1999.
- [22] E. Palmqvist and B. Hahn-Hägerdal, "Fermentation of lignocellulosic hydrolysates. I: inhibition and detoxification," *Bioresource Technology*, vol. 74, pp. 17-24, 2000.
- [23] C. A. Cardona and O. J. Sanchez, "Fuel ethanol production: Process design trends and integration opportunities," *Bioresource Technology*, vol. 98, pp. 2415 - 2457, Sept 2007 2007.
- [24] M. A. Das Neves, N. Shimizu, T. Kimura, and K. Shiiba, "Kinetics of bioethanol production from wheat milling by-products," *Journal of Food Process Engineering* vol. 30, pp. 338-356, Jun 2007 2007.
- [25] L. Larsen, P. Nielsen, and B. K. Ahring, "Thermoanaerobacter mathranii sp nov, an ethanol-producing, extremely thermophilic anaerobic bacterium from a hot spring in Iceland," *ARCHIVES OF MICROBIOLOGY* vol. 168 pp. 114-119 1997.
- [26] L. R. Lynd, H. W. van Zyl, J. E. McBride, and M. Laser, "Consolidated bioprocessing of cellulosic biomass: an update," *Current Opinion in Biotechnology* vol. 16, pp. 577-583, 2005.
- [27] J. Wiegel and L. G. Ljungdahl, "Thermoanaerobacter ethanolicus gen. nov., spec. nov., a New, Extreme Thermophilic, Anaerobic Bacterium," *Arch Microbiol* vol. 128, pp. 343-348, 1981.
- [28] D. Karakashev, A. B. Thomsen, and I. Angelidaki, "Anaerobic biotechnological approaches for production of liquid energy carriers from biomass," *Biotechnology Letters*, vol. 29, pp. 1005-1012, July 2007 2007.
- [29] J. McMillan, "Bioethanol production: Status and prospects," *Renewal Energy*, vol. 10, pp. 295-302, Feb-Mar 1997 1997.
- [30] L. R. Lynd, " Production of Ethanol from Lignocellulosic Material Using Thermophilic Bacteria: Critical Evaluation of Potential and Review," *Adv. Biochem. Eng. Biotechnol* vol. 38, pp. 1-52, 1989.
- [31] A. Demain, M. Newcomb, and J. H. D. Wu, "Cellulase, clostridia, and ethanol," *Microbiology and Molecular Biology Reviews* vol. 69, pp. 124-145, 2005
- [32] C. E. Wyman and N. D. Hinman, "Ethanol - Fundamentals of Production from Renewable Feedstocks and Use As A Transportation Fuel," *Applied Biochemistry and Biotechnology* vol. 24, pp. 735-753, 1990.
- [33] C. E. Wyman, "What is (and is not) vital to advancing cellulosic ethanol," *Trends in Biotechnology*, vol. 25, pp. 153-157, 2007.
- [34] J. A. Berberich, B. L. Knutson, H. J. Strobel, S. Tarhan, S. E. Nokes, and K. A. Dawson, "Product selectivity shifts in *Clostridium thermocellum* in the presence of compressed solvents.," *Ind Eng Chem Res* vol. 39, pp. 4500-4505, 2000.
- [35] G. D. Bothun, B. L. Knutson, J. A. Berberich, H. J. Strobel, and S. E. Nokes, "Metabolic selectivity and growth of *Clostridium thermocellum* in continuous culture under elevated hydrostatic pressure," *Appl Microbiol Biotechnol* vol. 65, pp. 149-157, 2004.

- [36] C. R. Felix and L. G. Ljungdahl, "The cellulosome: the exocellular organelle of *Clostridium*," *Annu Rev Microbiol* vol. 47, pp. 791–819, 1993.
- [37] R. J. Lamad, J. H. Lobos, and T. M. Su, "Effects of stirring and hydrogen on fermentation products of *Clostridium thermocellum*," *Appl Environ Microbiol*, vol. 54, pp. 1216–1221, 1988.
- [38] G. D. Bothun, B. L. Knutson, J. A. Berberich, H. J. Strobel, and S. E. Nokes, "Metabolic selectivity and growth of *Clostridium thermocellum* in continuous culture under elevated hydrostatic pressure," *Applied Microbiology and Biotechnology*, vol. 65, pp. 149-157, Aug 2004.
- [39] N. D. Price, J. A. Papin, C. H. Schilling, and B. O. Palsson, "Genome-scale microbial *in silico* models: the constraints-based approach," *TRENDS in Biotechnology* vol. 21, pp. 162-169, 2003.
- [40] M. O'Malley and J. Dupre', "Fundamental issues in systems biology," *BioEssays* vol. 27, pp. 1270-1276, 2005.
- [41] J. Varner and D. Ramkrishna, "Mathematical models of metabolic pathways," *Current Opinion in Biotechnology* vol. 10, pp. 146-150, 1999.
- [42] J. Stelling, "Mathematical models in microbial systems biology," *Current Opinion in Microbiology* vol. 7, pp. 513 - 518, 2004.
- [43] S. E. Lowe, M. K. Jain, and J. G. Zeikus, "BIOLOGY, ECOLOGY, AND BIOTECHNOLOGICAL APPLICATIONS OF ANAEROBIC-BACTERIA ADAPTED TO ENVIRONMENTAL STRESSES IN TEMPERATURE, PH, SALINITY, OR SUBSTRATES," *Microbiological Reviews*, vol. 57, pp. 451-509, Jun 1993.
- [44] J. Rodriguez, R. Kleerebezem, J. M. Lema, and M. C. M. van Loosdrecht, "Modeling product formation in anaerobic mixed culture fermentations," *Biotechnology and Bioengineering*, vol. 93, pp. 592-606, Feb 2006.
- [45] T. Rydzak, D. B. Levin, N. Cicek, and R. Sparling, "Growth phase-dependant enzyme profile of pyruvate catabolism and end-product formation in *Clostridium thermocellum* ATCC 27405," *Journal of Biotechnology*, vol. 140, pp. 169-175, Mar 2009.
- [46] Y. H. P. Zhang and L. R. Lynd, "Cellulose utilization by *Clostridium thermocellum*: Bioenergetics and hydrolysis product assimilation," *Proceedings of the National Academy of Sciences of the United States of America*, vol. 102, pp. 7321-7325, May 2005.
- [47] H. J. Strobel, "GROWTH OF THE THERMOPHILIC BACTERIUM *CLOSTRIDIUM-THERMOCELLUM* IN CONTINUOUS-CULTURE," *Current Microbiology*, vol. 31, pp. 210-214, 1995.
- [48] R. Islam, N. Cicek, R. Sparling, and D. Levin, "Effect of substrate loading on hydrogen production during anaerobic fermentation by *Clostridium thermocellum* 27405," *Applied Microbiology and Biotechnology*, vol. 72, pp. 576-583, Sep 2006.
- [49] D. B. Levin, L. Pitt, and M. Love, "Biohydrogen production: prospects and limitations to practical application," *International Journal of Hydrogen Energy*, vol. 29, pp. 173-185, Feb 2004.
- [50] D. M. Stevenson and P. J. Weimer, "Expression of 17 genes in *Clostridium thermocellum* ATCC 27405 during fermentation of cellulose or cellobiose in continuous culture," *Applied and Environmental Microbiology*, vol. 71, pp. 4672-4678, Aug 2005.
- [51] L. R. Lynd, P. J. Weimer, W. H. van Zyl, and I. S. Pretorius, "Microbial cellulose utilization: Fundamentals and biotechnology," *Microbiology and Molecular Biology Reviews*, vol. 66, pp. 506-+, Sep 2002.

- [52] P. Tailliez, H. Girard, J. Millet, and P. Beguin, "ENHANCED CELLULOSE FERMENTATION BY AN ASPOROGENOUS AND ETHANOL-TOLERANT MUTANT OF CLOSTRIDIUM-THERMOCELLUM," *Applied and Environmental Microbiology*, vol. 55, pp. 207-211, Jan 1989.
- [53] G. D. Bothun, B. L. Knutson, H. J. Strobel, and S. E. Nokes, "Liposome fluidization and melting point depression by pressurized CO₂ determined by fluorescence anisotropy," *Langmuir*, vol. 21, pp. 530-536, Jan 2005.
- [54] E. A. Bayer, E. Setter, and R. Lamed, "ORGANIZATION AND DISTRIBUTION OF THE CELLULOSE IN CLOSTRIDIUM-THERMOCELLUM," *Journal of Bacteriology*, vol. 163, pp. 552-559, 1985.
- [55] E. A. Bayer and R. Lamed, "ULTRASTRUCTURE OF THE CELL-SURFACE CELLULOSE OF CLOSTRIDIUM-THERMOCELLUM AND ITS INTERACTION WITH CELLULOSE," *Journal of Bacteriology*, vol. 167, pp. 828-836, Sep 1986.
- [56] A. A. Herrero and R. F. Gomez, "Development of ethanol tolerance in *Clostridium thermocellum*: effect of growth temperature," *Appl. Environ. Microbiol.*, vol. 40, pp. 571-577, September 1, 1980 1980.
- [57] M. Timmons, B. Knutson, S. Nokes, H. Strobel, and B. Lynn, "Analysis of composition and structure of *Clostridium thermocellum* membranes from wild-type and ethanol-adapted strains," *Applied Microbiology and Biotechnology*, vol. 82, pp. 929-939, 2009.
- [58] T. I. Williams, J. C. Combs, B. C. Lynn, and H. J. Strobel, "Proteomic profile changes in membranes of ethanol-tolerant *Clostridium thermocellum*," *Applied Microbiology and Biotechnology*, vol. 74, pp. 422-432, Feb 2007.
- [59] Y. T. Zheng and G. Sriram, "Mathematical Modeling: Bridging the Gap between Concept and Realization in Synthetic Biology," *Journal of Biomedicine and Biotechnology*, 2010.
- [60] M. W. Covert, C. H. Schilling, I. Famili, J. S. Edwards, Goryanin, II, E. Selkov, and B. O. Palsson, "Metabolic modeling of microbial strains in silico," *Trends in Biochemical Sciences*, vol. 26, pp. 179-186, Mar 2001.
- [61] T. Tryfona and M. T. Bustard, "Fermentative production of lysine by *Corynebacterium glutamicum*: transmembrane transport and metabolic flux analysis," *Process Biochemistry*, vol. 40, pp. 499-508, Feb 2005.
- [62] Y. Matsuoka and K. Shimizu, "Current status of C-13-metabolic flux analysis and future perspectives," *Process Biochemistry*, vol. 45, pp. 1873-1881, Dec 2010.
- [63] A. Varma and B. O. Palsson, "METABOLIC FLUX BALANCING - BASIC CONCEPTS, SCIENTIFIC AND PRACTICAL USE," *Bio-Technology*, vol. 12, pp. 994-998, Oct 1994.
- [64] B. Adotey, "Metabolic Flux Analysis of Carbon Flow through *Clostridium thermocellum*," in *Biosystems & Agricultural Engineering*. vol. MS Lexington: University of Kentucky, 2006, p. 172.
- [65] C. Herwig and U. von Stockar, "A small metabolic flux model to identify transient metabolic regulations in *Saccharomyces cerevisiae*," *Bioprocess and Biosystems Engineering*, vol. 24, pp. 395-403, Mar 2002.
- [66] A. Varma and B. O. Palsson, "STOICHIOMETRIC FLUX BALANCE MODELS QUANTITATIVELY PREDICT GROWTH AND METABOLIC BY-PRODUCT SECRETION IN WILD-TYPE *ESCHERICHIA-COLI* W3110," *Applied and Environmental Microbiology*, vol. 60, pp. 3724-3731, Oct 1994.
- [67] P. Duboc and U. Vonstockar, "ENERGETIC INVESTIGATION OF *SACCHAROMYCES-CEREVISIAE* DURING TRANSITIONS .1. MASS BALANCES," *Thermochimica Acta*, vol. 251, pp. 119-130, Mar 1995.

- [68] F. Llaneras and J. Pico, "A procedure for the estimation over time of metabolic fluxes in scenarios where measurements are uncertain and/or insufficient," *Bmc Bioinformatics*, vol. 8, Oct 2007.
- [69] G. Lequeux, J. Beauprez, J. Maertens, E. Van Horen, W. Soetaert, E. Vandamme, and P. A. Vanrolleghem, "Dynamic Metabolic Flux Analysis Demonstrated on Cultures Where the Limiting Substrate Is Changed from Carbon to Nitrogen and Vice Versa," *Journal of Biomedicine and Biotechnology*, 2010.
- [70] M. De Mey, G. J. Lequeux, J. J. Beauprez, J. Maertens, H. J. Waegeman, I. N. Van Bogaert, M. R. Foulquie-Moreno, D. Charlier, W. K. Soetaert, P. A. Vanrolleghem, and E. J. Vandamme, "Transient metabolic modeling of Escherichia coli MG1655 and MG1655 Delta ackA-pta, Delta poxB Delta pppc ppc-p37 for recombinant beta-galactosidase production," *Journal of Industrial Microbiology & Biotechnology*, vol. 37, pp. 793-803, Aug 2010.
- [71] D. A. Fell and H. M. Sauro, "METABOLIC CONTROL AND ITS ANALYSIS - ADDITIONAL RELATIONSHIPS BETWEEN ELASTICITIES AND CONTROL COEFFICIENTS," *European Journal of Biochemistry*, vol. 148, pp. 555-561, 1985.
- [72] V. Hatzimanikatis and J. E. Bailey, "MCA has more to say," *Journal of Theoretical Biology*, vol. 182, pp. 233-242, Oct 1996.
- [73] H. V. Westerhoff and D. B. Kell, "What biotechnologists knew all along ...?," *Journal of Theoretical Biology*, vol. 182, pp. 411-420, Oct 1996.
- [74] L. Q. Wang, I. Birol, and V. Hatzimanikatis, "Metabolic control analysis under uncertainty: Framework development and case studies," *Biophysical Journal*, vol. 87, pp. 3750-3763, Dec 2004.
- [75] H. Kacser, J. A. Burns, and D. A. Fell, "THE CONTROL OF FLUX," *Biochemical Society Transactions*, vol. 23, pp. 341-366, May 1995.
- [76] V. Hatzimanikatis and J. E. Bailey, "Effects of spatiotemporal variations on metabolic control: Approximate analysis using (log)linear kinetic models," *Biotechnology and Bioengineering*, vol. 54, pp. 91-104, Apr 1997.
- [77] J. H. S. Hofmeyr, H. Kacser, and K. J. Vandermerwe, "METABOLIC CONTROL ANALYSIS OF MOIETY-CONSERVED CYCLES," *European Journal of Biochemistry*, vol. 155, pp. 631-641, Mar 1986.
- [78] L. Acerenza, H. M. Sauro, and H. Kacser, "CONTROL ANALYSIS OF TIME-DEPENDENT METABOLIC SYSTEMS," *Journal of Theoretical Biology*, vol. 137, pp. 423-444, Apr 1989.
- [79] S. M. Allison, J. R. Small, H. Kacser, and J. I. Prosser, "CONTROL ANALYSIS OF MICROBIAL INTERACTIONS IN CONTINUOUS-CULTURE - A SIMULATION STUDY," *Journal of General Microbiology*, vol. 139, pp. 2309-2317, Oct 1993.
- [80] D. A. Fell, "METABOLIC CONTROL ANALYSIS - A SURVEY OF ITS THEORETICAL AND EXPERIMENTAL DEVELOPMENT," *Biochemical Journal*, vol. 286, pp. 313-330, Sep 1992.
- [81] D. A. Fell, "Enzymes, metabolites and fluxes," *Journal of Experimental Botany*, vol. 56, pp. 267-272, Jan 2005.
- [82] M. Tomita, "Whole-cell simulation: a grand challenge of the 21st century," *TRENDS in Biotechnology*, vol. 19, pp. 205 - 210, 2001.
- [83] M. Tomita, K. Hashimoto, K. Takahashi, M. T. Shimizu, F. Miyoshi, K. Saito, S. Tanida, K. Yugi, J. C. Venter, and C. A. Hutchison, "E-CELL: software environment for whole-cell simulation," *Bioinformatics*, vol. 15, pp. 72 - 84, 1999.
- [84] J. J. Morgan, I. V. Surovtsev, and P. A. Lindhal, "A framework for whole-cell mathematical modeling," *Journal of Theoretical Biology* vol. 231, pp. 581 - 596, 2004.

- [85] K. Takahashi, K. Kaizu, B. Hu, and M. Tomita, "A multi-algorithm, multi-timescale method for cell simulation," *Bioinformatics*, vol. 20, pp. 538 - 546, 2004.
- [86] I. Goryanin, T. C. Hodgman, and E. Selkov, "Mathematical simulation and analysis of cellular metabolism," *Bioinformatics*, vol. 15, pp. 749 - 758, 1999.
- [87] S. T. Browning and M. L. Shuler, "Towards the development of a minimal cell model by generalization of a model of Escherichia coli: use of dimensionless rate parameters," *Biotechnology and Bioengineering*, vol. 76, pp. 187-92, 2001.
- [88] S. T. Browning and M. L. Shuler, "Towards the Development of a Minimal Cell Model by Generalization of a Model of Escherichia coli: Use of Dimensionless Rate Parameters," *Blotechnology and Bioengineering*, vol. 76, pp. 187 - 192, 2001.
- [89] M. Altman, J. Gill, and M. P. McDonald, "accuracy: Tools for accurate and reliable statistical computing," *Journal of Statistical Software*, vol. 21, Jul 2007.
- [90] R. R. Kitchen, M. Kubista, and A. Tichopad, "Statistical aspects of quantitative real-time PCR experiment design," *Methods*, vol. 50, pp. 231-236, Apr 2010.
- [91] N. S. Wang and G. Stephanopoulos, "APPLICATION OF MACROSCOPIC BALANCES TO THE IDENTIFICATION OF GROSS MEASUREMENT ERRORS," *Biotechnology and Bioengineering*, vol. 25, pp. 2177-2208, 1983.
- [92] M. Altman, J. Gill, and M. McDonald, "R Modules for Accurate and Reliable Statistical Computing," 2003, p. 35.
- [93] F. Llaneras, A. Sala, and J. Pico, "A possibilistic framework for constraint-based metabolic flux analysis," *Bmc Systems Biology*, vol. 3, Jul 2009.
- [94] R. Vanderheijden, B. Romein, J. J. Heijnen, C. Hellinga, and K. Luyben, "LINEAR CONSTRAINT RELATIONS IN BIOCHEMICAL REACTION SYSTEMS .3. SEQUENTIAL APPLICATION OF DATA RECONCILIATION FOR SENSITIVE DETECTION OF SYSTEMATIC-ERRORS," *Biotechnology and Bioengineering*, vol. 44, pp. 781-791, Sep 1994.
- [95] W. Skolpap, S. Nuchprayoon, J. M. Scharer, and M. Moo-Young, "Parametric analysis of metabolic fluxes of alpha-amylase and protease-producing *Bacillus subtilis*," *Bioprocess and Biosystems Engineering*, vol. 30, pp. 337-348, Sep 2007.
- [96] G. Pettersson, "Errors associated with experimental determinations of enzyme flux control coefficients," *Journal of Theoretical Biology*, vol. 179, pp. 191-197, Apr 1996.
- [97] H. J. Noorman, B. Romein, K. Luyben, and J. J. Heijnen, "Classification, error detection, and reconciliation of process information in complex biochemical systems," *Biotechnology and Bioengineering*, vol. 49, pp. 364-376, Feb 1996.
- [98] H. P. J. Bonarius, J. H. M. Houtman, G. Schmid, C. D. de Gooijer, and J. Tramper, "Error analysis of metabolic-rate measurements in mammalian-cell culture by carbon and nitrogen balances," *Cytotechnology*, vol. 29, pp. 167-175, 1999.
- [99] E. K. Ainscow and M. D. Brand, "Errors associated with metabolic control analysis. Application of Monte-Carlo simulation of experimental data," *Journal of Theoretical Biology*, vol. 194, pp. 223-233, Sep 1998.
- [100] M. Dauner, J. E. Bailey, and U. Sauer, "Metabolic flux analysis with a comprehensive isotopomer model in *Bacillus subtilis*," *Biotechnology and Bioengineering*, vol. 76, pp. 144-156, Sep 2001.
- [101] R. J. Kleijn, J. M. Buescher, L. Le Chat, M. Jules, S. Aymerich, and U. Sauer, "Metabolic Fluxes during Strong Carbon Catabolite Repression by Malate in *Bacillus subtilis*," *Journal of Biological Chemistry*, vol. 285, pp. 1587-1596, Jan 2010.
- [102] T. H. Yang, C. J. Bolten, M. V. Coppi, J. Sun, and E. Heinzle, "Numerical bias estimation for mass spectrometric mass isotopomer analysis," *Analytical Biochemistry*, vol. 388, pp. 192-203, May 2009.

- [103] A. Saltelli, S. Tarantola, and F. Campolongo, "Sensitivity analysis as an ingredient of modeling," *Statistical Science*, vol. 15, pp. 377-395, Nov 2000.
- [104] USDA and DOE, "Biomass Research and Development Board: Leading the Federal Interagency Biomass Research and Development Initiative," 2008.
- [105] C. R. Felix and L. G. Ljungdahl, "THE CELLULOSOME - THE EXOCELLULAR ORGANELLE OF CLOSTRIDIUM," *Annual Review of Microbiology*, vol. 47, pp. 791-819, 1993.
- [106] Y.-H. P. Zhang and L. R. Lynd, "Cellulose utilization by *Clostridium thermocellum*: Bioenergetics and hydrolysis product assimilation," *Proceedings of the National Academy of Science*, vol. 102, pp. 7321-7325, 2005.
- [107] R. Islam, N. Cicek, R. Sparling, and D. Levin, "Influence of initial cellulose concentration on the carbon flow distribution during batch fermentation by *Clostridium thermocellum* ATCC 27405," *Applied Microbiology and Biotechnology*, vol. 82, pp. 141-148, Feb 2009.
- [108] Y. H. P. Zhang and L. R. Lynd, "Kinetics and relative importance of phosphorolytic and hydrolytic cleavage of cellodextrins and cellobiose in cell extracts of *Clostridium thermocellum*," *Applied and Environmental Microbiology*, vol. 70, pp. 1563-1569, Mar 2004.
- [109] G. D. Bothun, B. L. Knutson, H. J. Strobel, and S. E. Nokes, "Molecular and phase toxicity of compressed and supercritical fluids in biphasic continuous cultures of *Clostridium thermocellum*," *Biotechnology and Bioengineering*, vol. 89, pp. 32-41, Jan 2005.
- [110] P. Tailliez, H. Girard, R. Longin, P. Beguin, and J. Millet, "CELLULOSE FERMENTATION BY AN ASPOROGENOUS MUTANT AND AN ETHANOL-TOLERANT MUTANT OF CLOSTRIDIUM-THERMOCELLUM," *Applied and Environmental Microbiology*, vol. 55, pp. 203-206, Jan 1989.
- [111] M. D. Timmons, B. L. Knutson, S. E. Nokes, H. J. Strobel, and B. C. Lynn, "Analysis of composition and structure of *Clostridium thermocellum* membranes from wild-type and ethanol-adapted strains," *Applied Microbiology and Biotechnology*, vol. 82, pp. 929-939, Apr 2009.
- [112] J. A. Berberich, B. L. Knutson, H. J. Strobel, S. Tarhan, S. E. Nokes, and K. A. Dawson, "Product selectivity shifts in *Clostridium thermocellum* in the presence of compressed solvents," *Industrial & Engineering Chemistry Research*, vol. 39, pp. 4500-4505, Dec 2000.
- [113] D. S. Burdette, S. H. Jung, G. J. Shen, R. I. Hollingsworth, and J. G. Zeikus, "Physiological function of alcohol dehydrogenases and long-chain (C-30) fatty acids in alcohol tolerance of *Thermoanaerobacter ethanolicus*," *Applied and Environmental Microbiology*, vol. 68, pp. 1914-1918, Apr 2002.
- [114] Q. Z. Wang, M. S. Ou, Y. Kim, L. O. Ingram, and K. T. Shanmugam, "Metabolic Flux Control at the Pyruvate Node in an Anaerobic *Escherichia coli* Strain with an Active Pyruvate Dehydrogenase," *Applied and Environmental Microbiology*, vol. 76, pp. 2107-2114, Apr 2010.
- [115] S. B. Roberts, C. M. Gowen, J. P. Brooks, and S. S. Fong, "Genome-scale metabolic analysis of *Clostridium thermocellum* for bioethanol production," *Bmc Systems Biology*, vol. 4, Mar 2010.
- [116] A. A. Herrero, R. F. Gomez, and M. F. Roberts, "Ethanol-induced changes in the membrane lipid composition of *Clostridium thermocellum*," *Biochimica et Biophysica Acta (BBA) - Biomembranes*, vol. 693, pp. 195-204, 1982.
- [117] D. C. Thomas, "The need for a systematic approach to complex pathways in molecular epidemiology," *Cander Epidemiology, Biomarkers & Prevention*, vol. 14, pp. 557-559, 2005.

- [118] A. P. Thakur, "Metabolite analysis of *Clostridium Thermocellum* using capillary electrophoresis based techniques," in *Chemistry*. vol. PhD Lexington: Univerisity of Kentucky, 2008, p. 149.
- [119] A. Varma and B. O. Palsson, "Metabolic Flux Balancing: Basic Concepts, Scientific and Practical Use," *Bio/Technology*, vol. 12, pp. 994-998, October 1994 1994.
- [120] A. Gombert and J. Nielsen, "Mathematical modeling of metabolism. ," *Current Opinion in Biotechnology* vol. 11, pp. 180-186, 2000.
- [121] G. N. Stephanopoulos, A. A. Aristidou, and J. Nielsen, *Metabolic Engineering: Principles and Methodologies*. San Diego, California: Academic Press, 1998.
- [122] H. Kacser and J. A. Burns, "The Control of Flux," *Biochem. Soc. Trans.*, vol. 23, pp. 341 - 366, 1995.
- [123] K. Snell and D. A. Fell, "METABOLIC CONTROL ANALYSIS OF MAMMALIAN SERINE METABOLISM," *Advances in Enzyme Regulation*, vol. 30, pp. 13-32, 1990.
- [124] H. Kacser and J. Burns, "Control of enzyme flux," *Symp Soc Exp Biol*, vol. 27, pp. 65-104, 1973.
- [125] R. Heinrich and T. A. Rapoport, "LINEAR STEADY-STATE TREATMENT OF ENZYMATIC CHAINS - GENERAL PROPERTIES, CONTROL AND EFFECTOR STRENGTH," *European Journal of Biochemistry*, vol. 42, pp. 89-95, 1974.
- [126] M. Wildermuth, "Metabolic control analysis: biological applications and insights," *Genome Biology*, vol. 1, pp. reviews1031.1 - reviews1031.5, 2000.
- [127] J. D. Varner, "Large-scale prediction of phenotype: Concept," *Biotechnology and Bioengineering*, vol. 69, pp. 664-678, Sep 2000.
- [128] H. Holms, "Flux Analysis and Control of the Central Metabolic Pathways in *Escherichia coli*," *FEMS Microbiology Reviews*, vol. 19, pp. 85 - 116, 1996.
- [129] D. Fell and H. Sauro, "Metabolic control analysis: additional relationships between elasticities and control coefficients. European," *Journal of Biochemistry* vol. 148, pp. 555-561, 1985
- [130] J. H. S. Hofmeyr and A. Cornishbowden, "QUANTITATIVE ASSESSMENT OF REGULATION IN METABOLIC SYSTEMS," *European Journal of Biochemistry*, vol. 200, pp. 223-236, Aug 1991.
- [131] D. B. Kell and H. V. Westerhoff, "Metabolic Control Theory: Its Role in Microbiology and Biotechnology," *FEMS Microbiology Reviews* vol. 3, pp. 305 - 320, 1986.
- [132] D. A. Fell, "Metabolic Control Analysis: a survey of its theoretical and experimental development," *Journal of Biochemistry* vol. 286, pp. 313 - 330, 1992.
- [133] C. P. Cartwright, J. R. Juroszek, M. J. Beavan, F. M. S. Ruby, S. M. F. Demorais, and A. H. Rose, "ETHANOL DISSIPATES THE PROTON-MOTIVE FORCE ACROSS THE PLASMA-MEMBRANE OF *SACCHAROMYCES-CEREVISIAE*," *Journal of General Microbiology*, vol. 132, pp. 369-377, Feb 1986.
- [134] V. Meyrial, J. P. Delgenes, J. Davison, J. M. Salmon, R. Moletta, and A. M. Gounot, "Relationship between effect of ethanol on proton flux across plasma membrane and ethanol tolerance, in *Pichia stipitis*," *Anaerobe*, vol. 3, pp. 423-429, Dec 1997.
- [135] C. K. Son, R. Tourdot-Marechal, P. A. Marechal, and J. Guzzo, "Combined, cold, acid, ethanol shocks in *Oenococcus oeni*: Effects on membrane fluidity and cell viability," *Biochimica Et Biophysica Acta-Biomembranes*, vol. 1717, pp. 118-124, Nov 2005.
- [136] L. M. Blank and L. Kuepfer, "Metabolic flux distributions: genetic information, computational predictions, and experimental validation," *Applied Microbiology and Biotechnology*, vol. 86, pp. 1243-1255, May 2010.

- [137] M. El-Mansi, E. M. T. El-Mansi, B. C. F. A., A. L. Demain, and A. R. Allman, *Fermentation Microbiology and Biotechnology*: CRC Press, 2006.
- [138] H. V. Westerhoff and D. B. Kell, "Matrix Method for Determining Steps Most Rate-Limiting to Metabolic Fluxes in Biotechnological Processes," *Biotechnology and Bioengineering*, vol. 104, pp. 3-9, Sep 2009.
- [139] J. L. Galazzo and J. E. Bailey, "FERMENTATION PATHWAY KINETICS AND METABOLIC FLUX CONTROL IN SUSPENDED AND IMMOBILIZED SACCHAROMYCES-CEREVISIAE," *Enzyme and Microbial Technology*, vol. 12, pp. 162-172, Mar 1990.
- [140] D. A. Fell, "Enzymes, metabolites and fluxes," 2005, pp. 267-272.
- [141] D. B. Kell and H. V. Westerhoff, "METABOLIC CONTROL-THEORY - ITS ROLE IN MICROBIOLOGY AND BIOTECHNOLOGY," *Fems Microbiology Reviews*, vol. 39, pp. 305-320, Oct 1986.
- [142] K. Schmidt, J. Nielsen, and J. Villadsen, "Quantitative analysis of metabolic fluxes in Escherichia coli, using two-dimensional NMR spectroscopy and complete isotopomer models," *Journal of Biotechnology*, vol. 71, pp. 175-189, May 1999.
- [143] J. E. Bailey, "TOWARD A SCIENCE OF METABOLIC ENGINEERING," *Science*, vol. 252, pp. 1668-1675, Jun 1991.
- [144] T. W. Simpson, B. D. Follstad, and G. Stephanopoulos, "Analysis of the pathway structure of metabolic networks," *Journal of Biotechnology*, vol. 71, pp. 207-223, May 1999.
- [145] C. T. Goudar, R. Biener, K. B. Konstantinov, and J. M. Piret, "Error Propagation from Prime Variables into Specific Rates and Metabolic Fluxes for Mammalian Cells in Perfusion Culture," *Biotechnology Progress*, vol. 25, pp. 986-998, Jul-Aug 2009.
- [146] W. A. van Winden, J. C. van Dam, C. Ras, R. J. Kleijn, J. L. Vinke, W. M. van Gulik, and J. J. Heijnen, "Metabolic-flux analysis of Saccharomyces cerevisiae CEN.PK113-7D based on mass isotopomer measurements of C-13-labeled primary metabolites," *Fems Yeast Research*, vol. 5, pp. 559-568, Apr 2005.
- [147] V. R. Vasquez, W. B. Whiting, and M. M. Meerschaert, "Confidence interval estimation under the presence of non-Gaussian random errors: Applications to uncertainty analysis of chemical processes and simulation," *Computers & Chemical Engineering*, vol. 34, pp. 298-305, Mar 2010.
- [148] H. J. Noorman, J. J. Heijnen, and K. Luyben, "LINEAR RELATIONS IN MICROBIAL REACTION SYSTEMS - A GENERAL OVERVIEW OF THEIR ORIGIN, FORM, AND USE," *Biotechnology and Bioengineering*, vol. 38, pp. 603-618, Sep 1991.
- [149] U. von Stockar and L. A. M. van der Wielen, "Thermodynamics in biochemical engineering," *Journal of Biotechnology*, vol. 59, pp. 25-37, Dec 1997.
- [150] S. Klamt and S. Schuster, "Calculating as many fluxes as possible in underdetermined metabolic networks," *Molecular Biology Reports*, vol. 29, pp. 243-248, 2002.
- [151] H. Kurata, Q. Y. Zhao, R. Okuda, and K. Shimizu, "Integration of enzyme activities into metabolic flux distributions by elementary mode analysis," *Bmc Systems Biology*, vol. 1, Jul 2007.
- [152] F. Llaneras and J. Pico, "An interval approach for dealing with flux distributions and elementary modes activity patterns," *Journal of Theoretical Biology*, vol. 246, pp. 290-308, 2007.
- [153] S. Conti, J. P. Gosling, J. E. Oakley, and A. O'Hagan, "Gaussian process emulation of dynamic computer codes," *Biometrika*, vol. 96, pp. 663-676, Sep 2009.
- [154] D. S. Parker, B. Pierce, and P. R. Eggert, "Monte Carlo arithmetic: How to gamble with floating point and win," *Computing in Science & Engineering*, vol. 2, pp. 58-68, Jul-Aug 2000.

- [155] J. Schellenberger and B. O. Palsson, "Use of Randomized Sampling for Analysis of Metabolic Networks," *Journal of Biological Chemistry*, vol. 284, pp. 5457-5461, Feb 2009.
- [156] S. Klamt, J. Stelling, M. Ginkel, and E. D. Gilles, "FluxAnalyzer: exploring structure, pathways, and flux distributions in metabolic networks on interactive flux maps," *Bioinformatics*, vol. 19, pp. 261-269, Jan 2003.
- [157] M. Bayram, "Application of computer algebra matrix operation techniques to the control of metabolic networks," *Applied Mathematics and Computation*, vol. 152, pp. 289-297, Apr 2004.
- [158] U. S. Ramli, J. J. Salas, P. A. Quant, and J. L. Harwood, "Use of metabolic control analysis to give quantitative information on control of lipid biosynthesis in the important oil crop, *Elaeis guineensis* (oilpalm)," *New Phytologist*, vol. 184, pp. 330-339, 2009.
- [159] J. Pico, H. De Battista, and F. Garelli, "Smooth sliding-mode observers for specific growth rate and substrate from biomass measurement," *Journal of Process Control*, vol. 19, pp. 1314-1323, Sep 2009.
- [160] G. Jud, K. Schneider, and R. Bachofen, "The role of hydrogen mass transfer for the growth kinetics of *Methanobacterium thermoautotrophicum* in batch and chemostat cultures," *Journal of Industrial Microbiology & Biotechnology*, vol. 19, pp. 246-251, Oct 1997.
- [161] R. Kleerebezem and A. J. M. Stams, "Kinetics of syntrophic cultures: A theoretical treatise on butyrate fermentation," *Biotechnology and Bioengineering*, vol. 67, pp. 529-543, 2000.
- [162] S. J. Berrios- Rivera, K. Y. San, and G. N. Bennett, "The effect of NAPRTase overexpression on the total levels of NAD, the NADH/NAD(+) ratio, and the distribution of metabolites in *Escherichia coli*," *Metabolic Engineering*, vol. 4, pp. 238-247, Jul 2002.
- [163] M. Desvaux, "Unravelling carbon metabolism in anaerobic cellulolytic bacteria," *Biotechnology Progress*, vol. 22, pp. 1229-1238, Oct 2006.
- [164] M. Desvaux, "Clostridium cellulolyticum: model organism of mesophilic cellulolytic clostridia," *FEMS Microbiology Reviews*, vol. 29, pp. 741 - 764, 2005.
- [165] M. Ruzicka, "The effect of hydrogen on acidogenic glucose cleavage," *Water Research*, vol. 30, pp. 2447-2451, Oct 1996.
- [166] D. B. Archer, "THE MICROBIOLOGICAL BASIS OF PROCESS-CONTROL IN METHANOGENIC FERMENTATION OF SOLUBLE WASTES," *Enzyme and Microbial Technology*, vol. 5, pp. 162-170, 1983.
- [167] A. J. Guwy, F. R. Hawkes, D. L. Hawkes, and A. G. Rozzi, "Hydrogen production in a high rate fluidised bed anaerobic digester," *Water Research*, vol. 31, pp. 1291-1298, Jun 1997.
- [168] R. J. Lamed, J. H. Lobos, and T. M. Su, " Effects of stirring and hydrogen on fermentation products of *Clostridium thermocellum*," *Appl Environ Microbiol*, vol. 54, pp. 1216-1221, 1988.
- [169] R. P. Jones and P. F. Greenfield, "EFFECT OF CARBON-DIOXIDE ON YEAST GROWTH AND FERMENTATION," *Enzyme and Microbial Technology*, vol. 4, pp. 210-222, 1982.
- [170] B. K. S. Chung and D.-Y. Lee, "Flux-sum analysis: a metabolite-centric approach for understanding the metabolic network," *Bmc Systems Biology*, vol. 3, 2009.
- [171] S. Payot, E. Guedon, C. Cailliez, E. Gelhaye, and H. Petitdemange, "Metabolism of cellobiose by *Clostridium cellulolyticum* growing continuous culture: evidence for decreased NADH reoxidation as a factor limiting growth," *Microbiology*, vol. 144, pp. 375 - 384, 1998.

- [172] E. Guedon, S. Payot, M. Desvaux, and H. Petitdemange, "Carbon and electron flow in *Clostridium cellulolyticum* grown in chemostat culture on synthetic medium," *Journal of Bacteriology*, vol. 181, pp. 3262-3269, May 1999.
- [173] A. Paus, G. Andre, M. Perrier, and S. R. Guiot, "LIQUID-TO-GAS MASS-TRANSFER IN ANAEROBIC PROCESSES - INEVITABLE TRANSFER LIMITATIONS OF METHANE AND HYDROGEN IN THE BIOMETHANATION PROCESS," *Applied and Environmental Microbiology*, vol. 56, pp. 1636-1644, Jun 1990.
- [174] R. Thauer, "ENERGY-CONSERVATION IN CHEMOTROPIC ANAEROBIC BACTERIA," *Bacteriological reviews*, vol. 41, pp. 100-180, 1977.
- [175] F. E. Mosey, "MATHEMATICAL-MODELING OF THE ANAEROBIC-DIGESTION PROCESS - REGULATORY MECHANISMS FOR THE FORMATION OF SHORT-CHAIN VOLATILE ACIDS FROM GLUCOSE," *Water Science and Technology*, vol. 15, pp. 209-232, 1983.
- [176] S. J. Berrios-Rivera, G. N. Bennett, and K. Y. San, "The effect of increasing NADH availability on the redistribution of metabolic fluxes in *Escherichia coli* chemostat cultures," *Metabolic Engineering*, vol. 4, pp. 230-237, Jul 2002.
- [177] W. A. Cramer and D. B. Knaff, *Energy Transduction in Biological Membranes: A Textbook of Bioenergetics*. New York: Springer-Verlag, 1991.
- [178] M. J. McInerney and P. S. Beaty, "ANAEROBIC COMMUNITY STRUCTURE FROM A NONEQUILIBRIUM THERMODYNAMIC PERSPECTIVE," *Canadian Journal of Microbiology*, vol. 34, pp. 487-493, 1988.
- [179] M. J. McInerney, J. R. Sieber, and R. P. Gunsalus, "Syntrophy in anaerobic global carbon cycles," *Current Opinion in Biotechnology*, vol. 20, pp. 623-632, 2009.
- [180] J. Rodriguez, J. M. Lema, and R. Kleerebezem, "Energy-based models for environmental biotechnology," *Trends in Biotechnology*, vol. 26, pp. 366-374, Jul 2008.
- [181] D. A. Beard, S. C. Liang, and H. Qian, "Energy balance for analysis of complex metabolic networks," *Biophysical Journal*, vol. 83, pp. 79-86, Jul 2002.
- [182] F. Llaneras and J. Pico, "Stoichiometric modelling of cell metabolism," *Journal of Bioscience and Bioengineering*, vol. 105, pp. 1-11, 2008.
- [183] L. K. Ju and C. S. Ho, "CORRELATION OF CELL-VOLUME FRACTIONS WITH CELL CONCENTRATIONS IN FERMENTATION MEDIA," *Biotechnology and Bioengineering*, vol. 32, pp. 95-99, Jun 1988.
- [184] A. Provost and G. Bastin, "Dynamic metabolic modelling under the balanced growth condition," *Journal of Process Control*, vol. 14, pp. 717-728, 2004.
- [185] A. Varma and B. O. Palsson, "PARAMETRIC SENSITIVITY OF STOICHIOMETRIC FLUX BALANCE MODELS APPLIED TO WILD-TYPE *ESCHERICHIA-COLI* METABOLISM," *Biotechnology and Bioengineering*, vol. 45, pp. 69-79, Jan 1995.
- [186] C. S. Henry, L. J. Broadbelt, and V. Hatzimanikatis, "Thermodynamics-based metabolic flux analysis," *Biophysical Journal*, vol. 92, pp. 1792-1805, Mar 2007.
- [187] D. A. Beard and H. Qian, "Thermodynamic-based computational profiling of cellular regulatory control in hepatocyte metabolism," *American Journal of Physiology-Endocrinology and Metabolism*, vol. 288, pp. E633-E644, Mar 2005.
- [188] D. A. Beard, E. Babson, E. Curtis, and H. Qian, "Thermodynamic constraints for biochemical networks," *Journal of Theoretical Biology*, vol. 228, pp. 327-333, Jun 2004.
- [189] M. Farza, K. Busawon, and H. Hammouri, "Simple nonlinear observers for on-line estimation of kinetic rates in bioreactors," *Automatica*, vol. 34, pp. 301-318, 1998.
- [190] D. R. Lide, "Handbook of Chemistry and Physics," 91st ed, W. M. Haynes, Ed.: Taylor and Francis Group, LLC, 2011.

- [191] C. J. Adams, M. C. Redmond, and D. L. Valentine, "Pure-culture growth of fermentative bacteria, facilitated by H₂ removal: Bioenergetics and H₂ production," *Applied and Environmental Microbiology*, vol. 72, pp. 1079-1085, Feb 2006.
- [192] C. M. Gowen and S. S. Fong, "Exploring Biodiversity for Cellulosic Biofuel Production," *Chemistry & Biodiversity*, vol. 7, pp. 1086-1097, 2010.
- [193] M. Kohlstedt, J. Becker, and C. Wittmann, "Metabolic fluxes and beyond-systems biology understanding and engineering of microbial metabolism," *Applied Microbiology and Biotechnology*, vol. 88, pp. 1065-1075, Nov 2010.
- [194] M. L. Shuler, "Single-cell models: promise and limitations," *Journal of Biotechnology*, vol. 71, pp. 225-228, 1999.
- [195] M. Terzer, N. D. Maynard, M. W. Covert, and J. Stelling, "Genome-scale metabolic networks," *Wiley Interdisciplinary Reviews-Systems Biology and Medicine*, vol. 1, pp. 285-297, Nov-Dec 2009.
- [196] M. L. Shuler and F. Kargi, *Bioprocess Engineering: Basic Concepts*, Second Edition ed.: Prentice Hall PTR, 2002.
- [197] W. Wiechert "13C Metabolic Flux Analysis," *Metabolic Engineering*, vol. 3, pp. 195 - 206, May 31 2001.
- [198] C. Wittmann, "Metabolic Flux Analysis using mass spectrometry," *Advances in Biochemical engineering and Biotechnology*, vol. 74, pp. 39 - 64, 2002.
- [199] S. Aiba, A. E. Humphery, and N. F. Millis, *Biochemical Engineering*, Second ed.: Academic Press Incorporated, 1973.

VITA

Bless Adotey

- Date/Place of Birth** July 15, 1978
Accra, Ghana
- Education**
- **MS in Biosystems & Agricultural Engineering (GPA : 3.52) 2006**
University of Kentucky-Lexington, KY
Thesis: “Metabolic Flux Analysis of Carbon Flow through *Clostridium thermocellum*.”
 - **BSc (Honors) in Agricultural Engineering 2002**
Kwame Nkrumah University of Science and Technology (KNUST),
Ghana
- Professional experience**
- **Department of Biosystems and Agricultural Engineering,
University of Kentucky, Lexington, KY**
Research Assistant
August 2004-present
 - **Food Crops Development Project
Kumasi, Ghana**
Consulting Service
October 2002-March 2004
 - **KNUST
Kumasi, Ghana**
Teaching/Research Assistant
October 2002-October 2003
 - **Regional Technology Transfer Center
Sunyani, Ghana**
Intern
August 2000-October 2000
 - **Ghana Water Company Limited
Kumasi, Ghana**
Intern
August 1999-October 1999

- **Rapid Preparatory School**
Sunyani, Ghana
Student Teacher

September 1997-July 1998

Professional memberships and activities

- American Society of Agricultural and Biological Engineers (ASABE)
- National Society of Black Engineers (NSBE)
- Alpha Epsilon

Conference presentations and publications

- Adotey, B., S.E. Nokes. **Mathematical Modeling of *Clostridium thermocellum*'s Response to Dissolved Hydrogen Gas Concentration.** ASABE, August 7-10, 2011. Louisville, Kentucky. Oral presentation.
- Adotey, B., S.E. Nokes. **Metabolic Flux and Control Analyses of Wild Type and Ethanol Adapted *Clostridium thermocellum*.** ASABE, June 20-23, 2010. Pittsburg, Pennsylvania. Oral presentation.
- Adotey, B., S.E. Nokes., Strobel, H.J., B. Lynn., and B.L. Knutson. **Metabolic flux analysis of *Clostridium thermocellum* wild type and ethanol adapted.** ASABE, Minneapolis, Minnesota, June 17-20, 2007.
- Adotey, B., and S.E. Nokes. **Modeling *Clostridium thermocellum*, ("Metabolic Model Development for *Clostridium thermocellum*: a Thermophilic Anaerobe capable of converting Lignocellulose to ethanol.")** ASABE, Portland Oregon, July 9-12, 2006.
- Adotey, B. 2006. **Metabolic Flux Analysis of Carbon Flow through *Clostridium thermocellum*.** MS Thesis. University of Kentucky, Lexington, KY.